

**PREPARATION OF HIGH DENSITY POLYETHYLENE
COMPOSITES FROM EGGSHELL POWDER AND
HEAT-TREATED EGGSHELL POWDER**

Panuwat Pakdeechote



**A Thesis Submitted in Partial Fulfillment of the Requirements for the
Degree of Master of Engineering in Polymer Engineering
Suranaree University of Technology
Academic Year 2010**

การเตรียมวัสดุเชิงประกอบพอลิเอทีลีนความหนาแน่นสูงจากผงเปลือกไข่และ
ผงเปลือกไข่ที่ตัดแปรด้วยความร้อน



นายภาณุวัฒน์ ภัคดีโชติ

วิทยานิพนธ์นี้เป็นส่วนหนึ่งของการศึกษาตามหลักสูตรปริญญาวิศวกรรมศาสตรมหาบัณฑิต
สาขาวิชาวิศวกรรมพอลิเมอร์
มหาวิทยาลัยเทคโนโลยีสุรนารี
ปีการศึกษา 2553

**PREPARATION OF HIGH DENSITY POLYETHYLENE
COMPOSITES FROM EGGSHELL POWDER AND
HEAT-TREATED EGGSHELL POWDER**

Suranaree University of Technology has approved this thesis submitted in partial fulfillments of the requirements for a Master's Degree.

Thesis Examining Committee

(Asst. Prof. Dr. Chantima Deeprasertkul)

Chairperson

(Asst. Prof. Dr. Wimonlak Sutapun)

Member (Thesis Advisor)

(Asst. Prof. Dr. Nitinat Suppakarn)

Member

(Asst. Prof. Dr. Yupaporn Ruksakulpiwat)

Member

(Asst. Prof. Dr. Kasama Jarukumjorn)

Member

(Assoc. Prof. Dr. Jatuporn Wittayakun)

Member

(Dr. Wut Dankittikul)

(Assoc. Prof. Dr. Vorapot Khompis)

Acting Vice Rector for Academic Affairs Dean of Institute of Engineering

ภาณุวัฒน์ ภัคดีโชติ : การเตรียมวัสดุเชิงประกอบพอลิเอทิลีนความหนาแน่นสูงจาก
ผงเปลือกไข่และผงเปลือกไข่ที่ดัดแปรด้วยความร้อน (PREPARATION OF HIGH
DENSITY POLYETHYLENE COMPOSITES FROM EGGSHELL POWDER
AND HEAT-TREATED EGGSHELL POWDER) อาจารย์ที่ปรึกษา :
ผู้ช่วยศาสตราจารย์ ดร.วิมลลักษณ์ สุตะพันธ์, 139 หน้า

วิทยานิพนธ์นี้เป็นการศึกษาการเตรียมผงเปลือกไข่ เปลือกไข่ที่ดัดแปรด้วยความร้อน และ
พอลิเอทิลีนความหนาแน่นสูงที่ถูกเติมด้วยผงเปลือกไข่ และผงเปลือกไข่ที่ดัดแปรด้วยความร้อน
สำหรับการเตรียมเปลือกไข่ที่ดัดแปรด้วยความร้อน อิทธิพลของเวลา และอุณหภูมิในการดัดแปรได้
ถูกศึกษา เปลือกไข่ที่ดัดแปรด้วยความร้อนถูกเตรียมที่อุณหภูมิ 650 670 770 และ 800 องศา
เซลเซียส ที่เวลาดัดแปรต่าง ๆ สำหรับพอลิเอทิลีนความหนาแน่นสูงที่ถูกเติมด้วยผงเปลือกไข่
อิทธิพลของปริมาณและขนาดอนุภาคของผงเปลือกไข่ และการเติมสารช่วยให้เข้ากันต่อสมบัติ
การไหล สมบัติทางความร้อน และสมบัติทางกลของวัสดุเชิงประกอบพอลิเอทิลีน
ความหนาแน่นสูงได้ถูกศึกษา สำหรับพอลิเอทิลีนความหนาแน่นสูงที่ถูกเติมด้วยผงเปลือกไข่ที่
ดัดแปรด้วยความร้อน อิทธิพลของปริมาณผงเปลือกไข่ที่ดัดแปรด้วยความร้อน และการเติมสาร
ช่วยให้เข้ากันต่อสมบัติการไหล สมบัติทางความร้อน และสมบัติทางกลของวัสดุเชิงประกอบ
พอลิเอทิลีนความหนาแน่นสูงได้ถูกศึกษา วัสดุเชิงประกอบพอลิเอทิลีนความหนาแน่นสูงถูกเตรียม
ที่ปริมาณสารตัวเติม 10 20 30 และ 40 เปอร์เซ็นต์โดยน้ำหนัก ขนาดอนุภาค (D_{50}) ของผงเปลือกไข่
คือ 17.1 ไมโครเมตร และ 14.4 ไมโครเมตร D_{50} ของผงเปลือกไข่ที่ดัดแปรด้วยความร้อน คือ 4.6
ไมโครเมตร ผงเปลือกไข่ที่มี D_{50} เท่ากับ 14.4 ไมโครเมตร ถูกใช้สำหรับการเตรียมวัสดุเชิงประกอบ
พอลิเอทิลีนความหนาแน่นสูงทั้งที่ไม่เติม และเติมสารช่วยให้เข้ากันที่ 40 เปอร์เซ็นต์โดยน้ำหนัก
ผงเปลือกไข่ วัสดุเชิงประกอบพอลิเอทิลีนความหนาแน่นสูงที่มีการเติมสารช่วยให้เข้ากันที่ 40
เปอร์เซ็นต์โดยน้ำหนักผงเปลือกไข่ที่ดัดแปรด้วยความร้อนถูกเตรียมด้วยเช่นกันพอลิเอทิลีน
ความหนาแน่นสูงกราฟต์ด้วยมาเลอิกแอนไฮไดรด์ในปริมาณ 2 เปอร์เซ็นต์โดยน้ำหนัก
พอลิเอทิลีนความหนาแน่นสูงถูกใช้เป็นสารช่วยให้เข้ากัน

จากการศึกษาพบว่า เปลือกไข่ที่ใช้ในงานวิจัยนี้ ประกอบด้วยแคลเซียมคาร์บอเนต
ประมาณ 95 เปอร์เซ็นต์โดยน้ำหนักในรูปผลึกแคลไซต์ เมื่อเพิ่มเวลา และอุณหภูมิในการดัดแปร
แคลเซียมคาร์บอเนตในเปลือกไข่ถูกเปลี่ยนไปเป็นแคลเซียมออกไซด์มากขึ้น และในที่สุด
ก็เปลี่ยนไปเป็นแคลเซียมไฮดรอกไซด์เมื่อสัมผัสกับอากาศ เปลือกไข่ที่ดัดแปรด้วยอุณหภูมิ 800
องศาเซลเซียส เป็นเวลา 3 ชั่วโมงถูกใช้เป็นสารตัวเติมสำหรับวัสดุเชิงประกอบพอลิเอทิลีน

ความหนาแน่นสูง ผงเปลือกไข่ที่ตัดแปรด้วยความร้อนประกอบด้วยแคลเซียมไฮดรอกไซด์เป็นองค์ประกอบหลัก

ความหนืดเนียนปรากฏของวัสดุเชิงประกอบพอลิเอทิลีนความหนาแน่นสูงมีค่าเพิ่มขึ้นเมื่อเพิ่มปริมาณผงเปลือกไข่ เสถียรภาพทางความร้อนของพอลิเอทิลีนความหนาแน่นสูงไม่ได้รับผลกระทบจากการเพิ่มปริมาณผงเปลือกไข่ มอดูลัสของยังค์ มอดูลัสของการโค้งงอ และอุณหภูมิการโค้งงอด้วยความร้อนของวัสดุเชิงประกอบมีค่าเพิ่มขึ้น แต่ความทนทานต่อแรงดึง ณ จุดคราก เปอร์เซ็นต์การยืด ณ จุดขาด และความทนทานต่อแรงกระทำของวัสดุเชิงประกอบมีค่าลดลงเมื่อเพิ่มปริมาณผงเปลือกไข่ ความทนทานต่อแรงดึง ณ จุดขาด และความทนทานต่อการโค้งงอของวัสดุเชิงประกอบไม่ได้รับผลกระทบอย่างมีนัยสำคัญเมื่อเพิ่มปริมาณผงเปลือกไข่ ความแข็งของวัสดุเชิงประกอบมีค่าเพิ่มขึ้นเล็กน้อยเมื่อเพิ่มปริมาณผงเปลือกไข่

การลดขนาดอนุภาคผงเปลือกไข่จาก D_{50} เท่ากับ 17.1 ไมโครเมตรเป็น D_{50} เท่ากับ 14.4 ไมโครเมตร ไม่มีผลต่อความหนืดเนียนปรากฏ เสถียรภาพทางความร้อน และสมบัติทางกลต่าง ๆ ของวัสดุเชิงประกอบ

สมบัติการไหล สมบัติทางความร้อน และสมบัติทางกลต่าง ๆ ของวัสดุเชิงประกอบพอลิเอทิลีนความหนาแน่นสูงที่มีการเติมพอลิเอทิลีนความหนาแน่นสูงกราฟต์ด้วยมาเลอิกแอนไฮไดรด์ในปริมาณ 2 เปอร์เซ็นต์โดยน้ำหนักไม่ได้แตกต่างอย่างมีนัยสำคัญจากวัสดุเชิงประกอบพอลิเอทิลีนความหนาแน่นสูงที่ไม่มีการเติมสารช่วยให้เข้ากัน

ความหนืดเนียนปรากฏของพอลิเอทิลีนความหนาแน่นสูงที่ถูกเติมด้วยผงเปลือกไข่ที่ตัดแปรด้วยความร้อน มีค่าเพิ่มขึ้นเมื่อเพิ่มปริมาณผงเปลือกไข่ที่ตัดแปรด้วยความร้อน เสถียรภาพทางความร้อนของพอลิเอทิลีนความหนาแน่นสูงมีค่าเพิ่มขึ้นอย่างไม่มีนัยสำคัญเมื่อเพิ่มปริมาณผงเปลือกไข่ที่ตัดแปรด้วยความร้อน มอดูลัสของยังค์ ความทนทานต่อแรงดึง ณ จุดขาด มอดูลัสของการโค้งงอ ความทนทานต่อการโค้งงอ และอุณหภูมิการโค้งงอด้วยความร้อนของวัสดุเชิงประกอบมีค่าเพิ่มขึ้นเมื่อเพิ่มปริมาณผงเปลือกไข่ที่ตัดแปรด้วยความร้อน ความแข็งของวัสดุเชิงประกอบมีค่าเพิ่มขึ้นเล็กน้อย เมื่อเพิ่มปริมาณผงเปลือกไข่ที่ตัดแปรด้วยความร้อน เปอร์เซ็นต์การยืด ณ จุดขาด และความทนทานต่อแรงกระทำของวัสดุเชิงประกอบมีค่าลดลง แต่ความทนทานต่อแรงดึง ณ จุดครากของวัสดุเชิงประกอบไม่ได้รับผลกระทบ เมื่อเพิ่มปริมาณผงเปลือกไข่ที่ตัดแปรด้วยความร้อน

สมบัติการไหล สมบัติทางความร้อน สมบัติการดึง สมบัติการโค้งงอ และความแข็งของวัสดุเชิงประกอบพอลิเอทิลีนความหนาแน่นสูงเปลี่ยนแปลงอย่างไม่มีนัยสำคัญเมื่อเทียบกับวัสดุเชิงประกอบพอลิเอทิลีนความหนาแน่นสูงที่ไม่มีการเติมสารช่วยให้เข้ากัน แต่ความทนทานต่อ

แรงกระแทกของวัสดุเชิงประกอบถูกปรับปรุงให้ดีขึ้นด้วยการเติมพอลิเอทิลีนความหนาแน่นสูง
กราฟต์ด้วยมาเลอิกแอนไฮไดรด์



สาขาวิชาวิศวกรรมพอลิเมอร์

ปีการศึกษา 2553

ลายมือชื่อนักศึกษา _____

ลายมือชื่ออาจารย์ที่ปรึกษา _____

ลายมือชื่ออาจารย์ที่ปรึกษาร่วม _____

ลายมือชื่ออาจารย์ที่ปรึกษาร่วม _____

PANUWAT PAKDEECHOTE : PREPARATION OF HIGH DENSITY
POLYETHYLENE COMPOSITES FROM EGGSHELL POWDER AND
HEAT-TREATED EGGSHELL POWDER. THESIS ADVISOR :
ASST. PROF. WIMONLAK SUTAPUN, Ph.D., 139 PP.

CHICKEN EGGSHELL/HIGH DENSITY POLYETHYLENE/HDPE/EGGSHELL
POWDER/ESP/HEAT-TREATED EGGSHELL POWDER/
COMPATIBILIZATION

In this thesis, eggshell powder, heat-treated eggshell and high density polyethylene filled with eggshell powder and heat-treated eggshell powder were prepared. For preparing heat-treated eggshell, the effect of treatment time and temperature was investigated. The heat-treated eggshell was prepared at temperature of 650°C, 670°C, 770°C, and 800°C at various treatment times. For eggshell powder filled high density polyethylene, the effect of eggshell powder content and particle size, and compatibilization on rheological, thermal, and mechanical properties of high density polyethylene composites were studied. For heat-treated eggshell powder filled high density polyethylene, the effect of heat-treated eggshell powder content and compatibilization on those properties were investigated. The filled high density polyethylene was prepared at filler contents of 10, 20, 30, and 40 wt%. The particle size (D_{50}) of eggshell powder was 17.1 μm and 14.4 μm . The D_{50} of heat-treated eggshell powder was 4.6 μm . The eggshell powder with D_{50} of 14.4 μm was employed for preparing the uncompatibilized and compatibilized high density polyethylene composites at 40 wt% eggshell powder. The compatibilized high density

polyethylene composites at 40 wt% heat-treated eggshell powder were also prepared. Maleic anhydride grafted high density polyethylene (HDPE-g-MAH) at 2 wt% high density polyethylene was used as compatibilizer.

It was found that the eggshell used in this study comprised calcium carbonate about 95 wt% in calcite crystal form. With increasing treatment time and temperature, calcium carbonate deposited in eggshell was increasingly transformed to calcium oxide and finally turned into calcium hydroxide after atmospheric exposure. The eggshell treated at 800°C for 3 h was used to prepared high density polyethylene composite. The heat-treated eggshell powder consisted of calcium hydroxide as main component.

For high density polyethylene composite, the apparent shear viscosity was increased with increasing eggshell powder content. The thermal stability of high density polyethylene was not affected by increasing eggshell powder content. Young's modulus, flexural modulus, and heat distortion temperature of composites were increased but yield strength, elongation at break, and impact strength of the composites were decreased with increasing eggshell powder content. Tensile stress at break and flexural strength of the composites were not significantly affected by increasing eggshell powder content. Hardness of the composites was slightly increased with increasing ESP content.

The reduction of particle size of eggshell powder from D_{50} of 17.1 μm to D_{50} of 14.4 μm did not much affect apparent shear viscosity, thermal stability, and mechanical properties of composites.

The rheological, thermal, and mechanical properties of compatibilized high density polyethylene composites with 2 wt% HDPE-g-MAH were not much different from uncompatibilized HDPE composites.

For high density polyethylene filled with heat-treated eggshell powder, the apparent shear viscosity was increased with increasing heat-treated eggshell powder content. The thermal stability of high density polyethylene insignificantly increased with increasing heat-treated eggshell powder content. Young's modulus, tensile stress at break, flexural modulus, flexural strength, and heat distortion temperature of composites were increased with increasing heat-treated eggshell powder content. The hardness of the composites was slightly increased with increasing heat-treated eggshell powder. Elongation at break and impact strength of the composites were decreased but yield strength of the composites was not affected with increasing heat-treated eggshell powder content.

The rheological, thermal, tensile, flexural, and hardness of compatibilized high density polyethylene composites were insignificant change comparing to those of uncompatibilized high density polyethylene composites. However, impact strength of the composites was improved by compatibilization with HDPE-g-MAH.

School of Polymer Engineering

Academic Year 2010

Student's Signature _____

Advisor's Signature _____

Co-advisor's Signature _____

Co-advisor's Signature _____

ACKNOWLEDGEMENTS

I would like to express my grateful thanks to Asst. Prof. Dr. Wimonlak Sutapun, my advisor, for her advice, guidance, and any support throughout this thesis. Special thanks are also extended to Asst. Prof. Dr. Nitinat Suppakarn, Asst. Prof. Dr. Yupaporn Ruksakulpiwat, and Asst. Prof. Dr. Sutham Srilomsak for their valuable suggestion.

I wish to acknowledge all the faculty and staff members of the School of Polymer Engineering and the Center for Scientific and Technology Equipment of Suranaree University of Technology for their help and supporting during my study for master degree. I also thanks SUT farm, Suranaree University of Technology for kindly supplying chicken eggshell waste, Chemical Innovation Co., Ltd. for kindly supplying maleic anhydride grafted high density polyethylene, HDPE-g-MAH, (Fusabond[®] MB100D, DuPont[™]), Sand and Soil Co., Ltd. for kindly supplying commercial calcium carbonate, and Mettler-Toledo (Thailand) Co., Ltd. for their kind supporting and providing TGA instrument.

Finally, I appreciate my beloved parents for their supporting and continuous encouragement. In addition, I would like to thank MAXXIS International (Thailand) Co., Ltd. for giving me the opportunity to experience work in polymer practice, especially rubber compound for radial tire.

Panuwat Pakdeechote

TABLE OF CONTENTS

	Page
ABSTRACT (THAI)	I
ABSTRACT (ENGLISH)	IV
ACKNOWLEDGEMENTS	VII
TABLE OF CONTENTS	VIII
LIST OF TABLES	XII
LIST OF FIGURES	XV
SYMBOLS AND ABBREVIATIONS	XX
CHAPTER	
I INTRODUCTION	1
1.1 Introduction	1
1.2 Statement of motivation	3
1.3 Research objectives	4
1.4 Scope and limitation of the research	5
II LITERATURE REVIEW	7
2.1 Calcium carbonate (CaCO ₃)	7
2.1.1 Crystalline forms	7
2.1.2 Types of CaCO ₃	8
2.1.3 Cost and availability	9
2.1.4 Surface modification of CaCO ₃	10

TABLE OF CONTENTS (Continued)

	Page
2.2 HDPE filled with CaCO ₃	11
2.2.1 Effect of CaCO ₃ content on mechanical properties of HDPE composites	11
2.2.2 Effect of particle size of CaCO ₃ on mechanical properties of HDPE composites	15
2.2.3 Effect of compatibilization on mechanical properties of HDPE composites	17
2.3 Avian egg	23
2.3.1 Component of egg	23
2.3.2 Structure of eggshell (ES)	23
2.3.3 Chemical composition of eggshell	25
2.3.4 Application of eggshell	29
2.3.5 Preparation of eggshell powder (ESP)	30
2.3.6 Properties of eggshell	33
2.4 Polymer filled with eggshell powder (ESP).....	35
2.4.1 Polyethylene filled with ESP.....	35
2.4.2 Polypropylene filled with ESP	36
2.4.3 Epoxy filled with ESP	36
2.4.4 Poly (styrene-b-ethylene/butylenes-b-styrene) tri block copolymer filled with ESP	37

TABLE OF CONTENTS (Continued)

	Page
III EXPERIMENTAL	38
3.1 Materials	38
3.2 Preparation of eggshell powder (ESP)	38
3.3 Preparation of heat-treated eggshell (HT-ES)	39
3.4 Preparation of CaCO ₃ powder	40
3.5 Preparation of HDPE composites	41
3.5.1 Mixing process	41
3.5.2 Molding process	42
3.6 Material characterizations	44
3.6.1 Characterizations for ESP, HT-ES, and CaCO ₃	44
3.6.2 Characterization of HDPE composites	45
IV RESULTS AND DISCUSSION	49
4.1 Characterization of ESP and HT-ES	49
4.1.1 Crystal form of ESP and HT-ES by XRD	49
4.1.2 Chemical composition of ESP and HT-ES by XRF	54
4.1.3 Thermal properties	55
4.1.4 Particle size and size distribution	66
4.1.5 Morphology of ESP and HT-ESP	67

TABLE OF CONTENTS (Continued)

	Page
4.2 Characterization of HDPE composites from ESP	69
4.2.1 Effect of ESP content on physical properties of HDPE composites	69
4.2.2 Effect of particle size and compatibilization of ESP on physical properties of 40 wt% ESP/HDPE composites	86
4.3 Characterization of HDPE composites from HT-ESP.....	98
4.3.1 Effect of HT-ESP content and compatibilization on physical properties of HT-ESP/HDPE composites.....	101
V CONCLUSIONS.....	115
REFERENCES.....	118
APPENDIX A. LIST OF PUBLICATIONS.....	130
BIOGRAPHY.....	140

LIST OF TABLES

Table	Page
1.1 Worldwide and Thailand usage of the most common types of polymer	2
2.1 Different types of proteins localizing in eggshell membrane and eggshell matrix.....	27
2.2 Types and compositions of fatty acid of eggshell matrix	28
3.1 Heat treatment conditions for preparing HT-ES in a chamber furnace	40
3.2 All compositions of material for preparing HDPE composites.....	43
4.1 Elemental analysis of ESP and HT-ES at 800°C for 3 h.....	55
4.2 Peak temperature (T_{peak}) and weight loss of ES, ESP, commercial $CaCO_3$, and HT-ES at various treatment temperatures and times.....	65
4.3 The particle size and size distribution of ESP before and after sieving, HT-ESP (800°C for 3 h), and commercial $CaCO_3$	68
4.4 MFI of neat HDPE, ESP1/HDPE composites, and $CaCO_3$ /HDPE composites	71
4.5 Decomposition temperatures and weight residue of ESP1/HDPE, $CaCO_3$ /HDPE composites, and neat HDPE.....	76

LIST OF TABLES (Continued)

Table	Page
4.6 Tensile properties of ESP1/HDPE and CaCO ₃ /HDPE composites at various contents of ESP1 and CaCO ₃	81
4.7 Flexural modulus and strength of ESP1/HDPE and CaCO ₃ /HDPE composites	82
4.8 Unnotched Izod impact strength of ESP1/HDPE and CaCO ₃ /HDPE composites	83
4.9 Hardness and HDT of neat HDPE, ESP1/HDPE composites, and CaCO ₃ /HDPE composites at various filler contents.....	84
4.10 MFI of ESP1/HDPE, ESP2/HDPE, and compatibilized ESP2/HDPE composites with ESP content of 40 wt%	88
4.11 Decomposition temperatures of ESP1/HDPE, ESP2/HDPE, and compatibilized ESP2/HDPE composites at ESP content of 40 wt%	90
4.12 Tensile properties of ESP1/HDPE, ESP2/HDPE, and compatibilized ESP2/HDPE composites with ESP content of 40 wt%	93
4.13 Flexural properties of ESP1/HDPE, ESP2/HDPE, and compatibilized ESP2/HDPE composites with ESP content of 40 wt%	95
4.14 Impact strength, hardness, and HDT of ESP1/HDPE, ESP2/HDPE, and compatibilized ESP2/HDPE composites with ESP content of 40 wt%	96

LIST OF TABLES (Continued)

Table	Page
4.15 MFI of HT-ESP1/HDPE and compatibilized HT-ESP1/HDPE composites	99
4.16 Decomposition temperature of HT-ESP1/HDPE composites and compatibilized HT-ESP1/HDPE composites	102
4.17 Young's modulus, elongation at break, yield strength, and tensile stress at break of HT-ESP1/HDPE composites with and without compatibilization.....	108
4.18 Flexural modulus and flexural strength of HT-ESP1/HDPE composites with and without compatibilization.....	110
4.19 Unnotched Izod impact strength of HT-ESP1/HDPE composites with and without compatibilization.....	111
4.20 Hardness and HDT of HT-ESP1/HDPE composites with and without compatibilization.....	112

LIST OF FIGURES

Figure	Page
2.1 Crystal form of calcite (a) and aragonite (b)	8
2.2 Schematic representing the mechanism of surface modification with maleic anhydride grafted polyethylene (PE-g-MAH) in CaCO ₃ /PE composites.....	18
2.3 Schematic of different parts of egg structure	23
2.4 SEM micrograph of a fractured eggshell	24
3.1 Images of ES after cleaning and drying (a), broken eggshell for preparing ESP and HT-ES (b), ESP (c), and HT-ES (d).....	39
3.2 Images of test specimens for tensile test (a) and flexural test (b) of HDPE and HDPE composites	46
3.3 Images of test specimens for impact test of HDPE and HDPE composites	47
4.1 XRD patterns of ESP and commercial CaCO ₃	50
4.2 XRD patterns of HT-ES prepared at 650°C for 16, 20, and 24 h.....	51
4.3 XRD patterns of HT-ES prepared at 670°C for 12 and 16 h.....	52
4.4 XRD patterns of HT-ES prepared at 770°C for 4 and 6 h	53
4.5 XRD patterns of HT-ES prepared at 800°C for 3, 4 and 5 h	53

LIST OF FIGURES (Continued)

Figure	Page
4.6 TGA (a) and DTGA (b) curves of ES, ESP, ESM, and commercial CaCO ₃	57
4.7 TGA (a) and DTGA (b) curves of HT-ES prepared at 650°C for 16, 20, and 24 h	60
4.8 TGA (a) and DTGA (b) curves of HT-ES prepared at 670°C for 12 and 16 h.	61
4.9 TGA (a) and DTGA (b) curves of HT-ES prepared at 770°C for 4 and 6 h.	62
4.10 TGA (a) and DTGA (b) curves of HT-ES prepared at 800°C for 3, 4 and 5 h	64
4.11 SEM micrographs (x200) and particle size distribution curves of commercial CaCO ₃ (a), ESP1 (b), ESP2 (c), and HT-ESP1 (d).....	68
4.12 Plot of apparent shear viscosity as a function of apparent shear rate of ESP1/HDPE composites (a) and CaCO ₃ /HDPE composites (b) at various contents of ESP1 and CaCO ₃	70
4.13 TGA (a) and DTGA (b) thermograms of HDPE and ESP1/HDPE composites with various contents of ESP1	74
4.14 TGA (a) and DTGA (b) thermograms of HDPE and CaCO ₃ /HDPE composites with various contents of CaCO ₃	75

LIST OF FIGURES (Continued)

Figure	Page
4.15 Tensile stress-strain curves of ESP1/HDPE (a) and CaCO ₃ /HDPE (b) composites at various contents of ESP1 and CaCO ₃	77
4.16 Plot of Young's modulus (—) and elongation at break (— —) of ESP1/HDPE and CaCO ₃ /HDPE composites vs. filler contents.....	78
4.17 Plot of yield strength (—) and tensile stress at break (— —) of ESP1/HDPE and CaCO ₃ /HDPE composites vs. filler contents	80
4.18 SEM micrographs (x300) of ESP1/HDPE (a) CaCO ₃ /HDPE (b) composites: 10 wt% (1), 20 wt% (2), 30 wt% (3), 40 wt% (4).....	85
4.19 Plot of apparent shear viscosity of ESP1/HDPE, ESP2/HDPE, and compatibilized ESP2/HDPE composites at ESP content of 40 wt% versus apparent shear rate	87
4.20 TGA (a) and DTGA (b) thermograms of ESP1/HDPE, ESP2/HDPE, and compatibilized ESP2/HDPE composites with ESP content of 40 wt%.....	89
4.21 Plot of Young's modulus and elongation at break of ESP1/HDPE, ESP2/HDPE, and compatibilized ESP2/HDPE composites with ESP content of 40 wt%.....	92

LIST OF FIGURES (Continued)

Figure	Page
4.22 Plot of yield strength and tensile stress at break of ESP1/HDPE, ESP2/HDPE, and compatibilized ESP2/HDPE composites with ESP content of 40 wt%	93
4.23 Plot of flexural modulus and strength of ESP1/HDPE, ESP2/HDPE, and compatibilized ESP2/HDPE composites with ESP content of 40 wt%	95
4.24 SEM micrographs at magnification of x300 (1), and x1000 (2) of ESP1/HDPE (a), ESP2/HDPE (b), and compatibilized ESP2/HDPE (c) composites with ESP content of 40 wt%	97
4.25 Plot of the apparent shear viscosity of HT-ESP1/HDPE and compatibilized HT-ESP1/HDPE composites against the apparent shear rate	99
4.26 TGA (a) and DTGA (b) thermograms of HDPE, HT-ESP1/HDPE composites, and compatibilized HT-ESP1/HDPE composites	101
4.27 Tensile stress-strain curves of HT-ESP1/HDPE composites and compatibilized HT-ESP1/HDPE composite	103
4.28 Plot of Young's modulus of HT-ESP1/HDPE composites against HT- ESP1 content	104

LIST OF FIGURES (Continued)

Figure	Page
4.29 Plot of elongation at break of HT-ESP1/HDPE composites against HT-ESP1 content	105
4.30 Plot of yield strength of HT-ESP1/HDPE composites against HT-ESP1 content	106
4.31 Plot of tensile stress at break of HT-ESP1/HDPE composites against HT-ESP1 content	107
4.32 Plot of flexural modulus of HT-ESP1/HDPE composites as a function of HT-ESP1 content	109
4.33 Plot of flexural strength of HT-ESP1/HDPE composites as a function of HT-ESP1 content	110
4.34 SEM micrographs (x1000) of HT-ESP1/HDPE composites: 10 wt% HT-ESP1 (a), 20 wt% HT-ESP1 (b), 30 wt% HT-ESP1 (c), 40 wt% HT-ESP1 (d), 40 wt% HT-ESP1(x300) (e), and 40 wt% HT-ESP1+HDPE-g-MAH (f)	114

SYMBOLS AND ABBREVIATIONS

°	=	Degree
%	=	Percent
°C	=	Degree Celsius
cm ³	=	Cubic centimeter
µm	=	Micrometer
cm ²	=	Square centimeter
g	=	Gram
Pa	=	Pascal
h	=	Hour
kV	=	Kilovolt
kg	=	Kilogram
mg	=	Milligram
kJ	=	Kilojoule
kN	=	Kilo Newton
kPa	=	Kilopascal
m ²	=	Square meter
min	=	Minute
mA	=	Milliampere
mm	=	Millimeter
nm	=	Nanometer
vol%	=	Percent by volume

SYMBOLS AND ABBREVIATIONS (Continued)

s	=	Second
MPa	=	Megapascal
wt%	=	Percent by weight
ton	=	Tonne
rpm	=	Revolution per minute
Deriv.	=	Derivative
D ₁₀	=	10 vol% less than or equal to a given diameter
D ₅₀	=	50 vol% less than or equal to a given diameter
D ₉₀	=	90 vol% less than or equal to a given diameter
D _[4,3]	=	Mean diameter by volume
D _[3,2]	=	Mean diameter by surface area
Span	=	Width of size distribution $[(D_{90}-D_{10})/ D_{50}]$
ES	=	Eggshell
ESM	=	Eggshell membrane
ESP	=	Eggshell powder
HT-ES	=	Heat-treated eggshell
HT-ESP	=	Heat-treated eggshell powder
HDPE	=	High density polyethylene
HDPE-g-MAH	=	Maleic anhydride grafted high density polyethylene

CHAPTER I

INTRODUCTION

1.1 Introduction

Nowadays, plastic materials play an important role in daily life as packaging for food, bottles, grocery sacks, pails, tight-head pails, toys, crates, pallets, wire and cable insulation, pipe (diameter more than 1 cm), and tubing (diameter less than 1 cm) (Benham and McDaniel, 2003; Peacock, 2000). Many plastics are usually composed of at least one or more of the other substances such as fillers and additives (Rosen, 1993; Saravari, 2003).

Fillers have been used since the early times of plastic industry. However, fillers have been significantly developed just in the last 30 years (Houssa, 2003). They might be either organic or inorganic compounds. The fillers for plastics were divided into two groups according to their functionality : inactive (extender) fillers and active (functional) fillers (Hohenberger, 2001). The inactive fillers are used mainly for cost reduction whereas the active fillers cause specific improvements in certain degree of mechanical properties or other physical properties (Silva et al., 2002; Hohenberger, 2001). The functional fillers causing an increase of tensile strength of polymer were often referred to as reinforcing fillers (Saravari, 2003). The commonly used fillers in plastic industry are calcium carbonate, mica, talc, kaolin, wollastonite, asbestos, silica, zinc oxide, aluminium hydroxide, alumina trihydrate, carbon black, wood flour, wood pulp, and starch (Saravari, 2003). Over 90 wt% of plastic fillers are employed in the following polymer : polyvinyl chloride (PVC), polyethylene (PE),

polypropylene (PP), rubber, and unsaturated polyester (UP) (Hohenberger, 2001; Houssa, 2003; Saravari, 2003).

High density polyethylene (HDPE), semi-crystalline, is the most important commodity polymers widely used throughout the world (Benham and McDaniel, 2003). The major commercial plastic of the world and Thailand is illustrated in Table 1.1. Polyethylene (PE) is consumed more than other types are. In Thailand, the consumption of PE is in the same trend as the worldwide consumption. For HDPE, it is used as packaging and transportation equipments such as food containers, crates, pallets and tight-head pails owing to its superior stiffness and low permeability (Peacock, 2000).

Table 1.1 Worldwide and Thailand usage of the most common types of polymer (Benham and McDaniel, 2003; Petroleum Institute of Thailand, 2009).

Polymer type	World usage (wt%)	Thailand usage (wt%)
PE (LDPE, EVA, LLDPE, and HDPE)	40.3	25
polypropylene	21.9	21
Polyvinyl chloride	21.1	10
Polystyrene	11.6	5
ABS/SAN	5.1	3
Others	-	36
Total	100	100

Among mineral fillers, calcium carbonate (CaCO_3) plays an important role as reinforcing filler for thermoplastic. There are two types of CaCO_3 : ground CaCO_3 (GCC) and precipitated CaCO_3 (PCC). Fine GCC is consumed as six times of PCC (Carr and Frederick, 2004). It was one of the fillers mostly used for HDPE (Phueakbuakhao, Prissanaroon-Ouajai, and Kreua-Ongarjnuakool, 2008). The commercial CaCO_3 is normally derived from sedimentary rocks. These sedimentary rocks are not easily renewable. Therefore, new source for CaCO_3 is essential in the near future. One of the alternative sources of CaCO_3 is eggshell (ES) which normally contains CaCO_3 of 95 wt%.

1.2 Statement of motivation

Chicken eggshell has been reported that its major component, as much as 95%, is CaCO_3 with crystal form of calcite and an organic of 3.5 wt% (Hincke et al, 2000). The chicken ES is not extensively utilized even though it is a calcium carbonate-rich material. It is always discarded as a waste material. In general, the waste ES is mainly produced from food processing and hatchery industries. In Thailand, Ministry of Agricultural and Cooperatives, Center for Agricultural Information reported that 9,786,808,273 chicken eggs were produced in 2010. They accounts for 587,208 tons of eggshell based on 10% of the total weight (ca. 60 g) of egg (Stadelman, 2000; Tsai et al., 2006). It is a good CaCO_3 source because it contains 95 wt% calcite which is closed to the purity of CaCO_3 used as filler for HDPE. In present, the awareness of enviromental impact and environmental sustainability has an extensive increase from several sectors. The utilization of chicken eggshell in polymer industry may provide a great benefit of environmental

sustaining due to its renewable resource and reduction of energy consumed for waste disposal. In this work, two methods was used to prepare filler from eggshell. First, it was prepared as eggshell powder (ESP) without any treatment. Secondly, the eggshell was thermally treated for removing organic substances. The ESP and heat-treated eggshell powder (HT-ESP) were then further used to prepare ESP/HDPE and HT-ESP/HDPE composites.

1.3 Research objectives

The main purposes of this research are as follows :

- (i) To prepare ESP and HT-ESP from chicken eggshell.
- (ii) To study the effect of time and temperature of heat treatment on chemical composition of heat-treated eggshell (HT-ES).
- (ii) To study the effect of ESP and HT-ESP contents on rheological, thermal, mechanical, and morphological properties of the HDPE composites.
- (iii) To study the effect of particle size of ESP on rheological, thermal, mechanical, and morphological properties of ESP/HDPE composites.
- (iv) To investigate the effect of a compatibilizer on rheological, thermal, mechanical, and morphological properties of the HDPE composites.

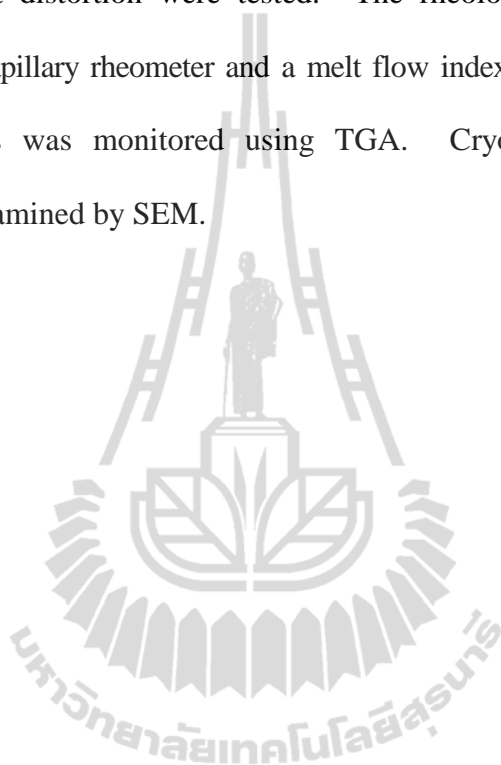
1.4 Scope and limitation of the research

Chicken ES was prepared into two forms : ESP and HT-ESP. In order to obtain HT-ESP, the ES was treated at 650°C for 16, 20, and 24 h, at 670°C for 12 and 16 h, at 770°C for 4 and 6 h, and at 800°C for 3, 4, and 5 h.

The chemical compositions of ESP and HT-ESP were determined using X-ray fluorescence (XRF) spectrometer. The crystal form of ESP and HT-ESP were determined using the X-ray diffractometer (XRD). The decomposition temperature and weight loss of eggshell, ESP, HT-ESP, and commercial CaCO₃, were monitored by thermogravimetric analyzer (TGA). Particle size and size distribution of ESP, HT-ESP, and commercial CaCO₃ were measured using particle size analyzer. In addition, particle morphology of ESP, HT-ESP, and commercial CaCO₃ was investigated by scanning electron microscope (SEM).

The composites of HDPE were prepared with various contents of ESP, HT-ESP, and CaCO₃, 10, 20, 30, and 40 wt%. Two different particle ranges of ESP were used for preparing the HDPE composites. ESP, HT-ESP, and commercial CaCO₃ were sieved using mesh no 325 sieve (ϕ 45 μ m) and mesh no. sieve 230 (ϕ 63 μ m). Furthermore, ESP was sieved using mesh no 500 sieve (ϕ 25 μ m) and mesh no 450 sieve (ϕ 32 μ m). The effect of particle size was studied only on ESP/HDPE composites at the content of ESP having the best mechanical properties. HDPE-g-MAH of 2 wt% of HDPE was used to prepare compatibilized ESP/HDPE and HT-ESP/HDPE composites.

Rheological, mechanical, thermal, and morphological properties of ESP/HDPE, HT-ESP/HDPE, and compatibilized ESP/HDPE and HT-ESP/HDPE composites were determined. For mechanical properties, tensile, flexural, impact, hardness, and heat distortion were tested. The rheology of the composites was determined via a capillary rheometer and a melt flow indexer. Thermal decomposition of the composites was monitored using TGA. Cryo-fractured surface of the composites was examined by SEM.



CHAPTER II

LITERATURE REVIEW

2.1 Calcium carbonate (CaCO_3)

2.1.1 Crystalline forms

Three crystalline forms of CaCO_3 occurring in nature are calcite, aragonite, and vaterite (Kitamura, Konno, Yasui, and Masuoka, 2002; Montes-Hernandez, Renard, Geoffroy, Charlet, and Pironon, 2007; Tai and Chen, 2008). Aragonite and vaterite are less stable than calcite, under ambient temperature and atmospheric pressure (Kitamura et al., 2002; Tai and Chen, 2008) whereas vaterite is least stable (Tai and Chen, 2008). Vaterite is rarely found under geological conditions but it is found during high temperature precipitation of CaCO_3 (Carr and Frederick, 2004). Aragonite and vaterite readily transform into calcite by heating (Montes-Hernandez et al., 2007; Wypych, 2000). Calcite has a specific gravity of 2.60-2.75 and a hardness of 3.0 on the Mohs' scale with rhombohedral form as the most widespread crystal system. Aragonite is orthorhombic crystal system having a specific gravity of 2.92-2.94 and a hardness of 3.5-4.0 on the Mohs' scale (Carr and Frederick, 2004). Figure 2.1 shows the crystal form of calcite and aragonite.

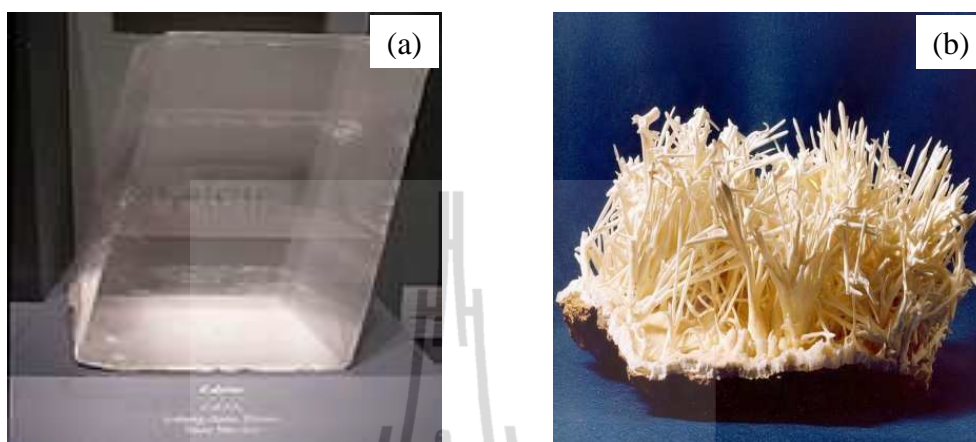


Figure 2.1 Crystal forms of calcite (a) and aragonite (b)

(http://en.wikipedia.org/wiki/Calcium_carbonate).

2.1.2 Types of CaCO_3

CaCO_3 is the most common deposit formed in sedimentary rocks, which compose primarily of calcite crystal (Wypych, 2000; Xanthos, 2005). The sedimentary rocks are, for instance, chalk and limestone. There are two types of CaCO_3 used as filler for polymeric material : ground CaCO_3 (GCC) and precipitated CaCO_3 (PCC).

2.1.2.1 Ground calcium carbonate (GCC)

The commercial grades of GCC are commonly produced from chalk, limestone, or marble (metamorphic rocks) (Carr and Frederick, 2004; Hohenberger, 2001; Xanthos, 2005). More than 90% of the CaCO_3 used in plastics industry is GCC (Xanthos, 2005). Calcite is the most common crystal system for GCC. Chemical composition of commercial GCC grades comprises CaCO_3 as the major composition (94-99%), MgCO_3 as major impurity, and alumina, iron oxide,

silica, or manganese oxide as the minor impurity (Xanthos, 2005). GCC has a density of 2.7 g/cm^3 with a hardness of 3 mohs which means less abrasive to processing equipments (Hohenberger, 2001; Houssa, 2003). GCC with a particle size (D_{50}) range of $0.8\text{-}5 \text{ }\mu\text{m}$ and whiteness of 85-95% (Saravari, 2003) is normally used as filler in plastic industry (Houssa, 2003).

2.1.2.2 Precipitated calcium carbonate (PCC)

PCC can be produced in three crystal forms, calcite, aragonite, and vaterite (Lazzeri et al., 2005). In most PCC, aragonite is the crystal system predominantly produced (Carr and Frederick, 2004; Hohenberger, 2001). However, the calcite crystal form is most commonly used in plastic industry (Lazzeri et al., 2005). Chemical composition of PCC is roughly the same as of GCC (Hohenberger, 2001). However, PCC has CaCO_3 content of 98-99%, is purer than GCC, and is lower in silica and lead content (Xanthos, 2005). Its other properties are very similar to GCC (Hohenberger, 2001; Xanthos, 2005). The particle size of PCC is in a range of $1\text{-}10 \text{ }\mu\text{m}$ for using in plastics industry (<http://www.specialtyminerals.com/our-minerals/what-is-pcc/>; Hohenberger, 2001). The PCC has high purity, very fine particles, regular in shape, a narrow particle size distribution, and high surface area (Xanthos, 2005). The PCC is widely used as functional fillers in the polymer composites (Shi, Rosa, and Lazzeri, 2010).

2.1.3 Cost and availability

Price of commercial CaCO_3 commonly depends on particle size and surface treatment, and quantity. For GCC, the price was \$110 – \$160 per ton for $5\text{-}7 \text{ }\mu\text{m}$ and \$140-\$290 per ton for $0.5\text{-}2 \text{ }\mu\text{m}$. For PCC, the price was \$250-\$270 per ton for fine grade ($0.4\text{-}1\mu\text{m}$) and \$375-\$750 per ton for ultrafine grade ($0.02\text{-}0.36 \text{ }\mu\text{m}$)

(Xanthos, 2005). In Thailand, most CaCO_3 is commercially produced as GCC of total annual capacity about 800,000-1,000,000 metric tons while PCC is produced by 40,000-60,000 metric tons/year (Ministry of Industry, 2004).

2.1.4 Surface modification of CaCO_3

The presence of CaCO_3 in polymer matrix often makes it difficult to disperse uniformly as a result of hydrophilic and lipophobic properties of CaCO_3 . CaCO_3 usually tends to form agglomerates, which weaken the interfacial interaction (Shui, Yue, and Xu, 2004). With poor adhesion between filler particle and polymer matrix, the agglomeration is most often observed (Wang, Zeng, Wang, and Chen, 2007). The poor interfacial adhesion of composite components is responsible for discontinuity in stress transfer from polymer matrix to particles; therefore, mechanical properties, especially tensile and impact strengths of composites are not promoted (Fu et al., 2008). To solve this problem, the interfacial modification must be done.

It is known that CaCO_3 has no functional groups on its surface, inert surface. For this reason, the interfacial adhesion between CaCO_3 and polymer matrix can only be improved by chemical modification (Wypych, 2000). Generally, the most widely used surface modifiers to enhance the interaction between CaCO_3 and HDPE are stearic acid, titanates, maleic derivative, phosphates, and acrylamide (Mihajlović et al., 2009; Wypych, 2000).

2.2 HDPE filled with CaCO₃

As a general rule, the end-use product made of thermoplastic is commonly altered the existing polymer properties to meet the customer requirements (Silva et al., 2002). Particulate fillers normally adjust the mechanical properties of polymers such as Young's modulus, yield strength, tensile stress at break, and toughness. The mechanical properties of particulate-polymer composites depend strongly on the particle size, particle size distribution, particle content, particle shape (aspect ratio), degree of particle dispersion, and particle-matrix interfacial adhesion (Albano and Perera, 2008; Bartczak, Argon, Cohen, and Weinberg, 1999; Fu, Feng, Lauke, and Mai, 2008). In this work, the effect of particle size, particle content, and particle-matrix interfacial adhesion on CaCO₃/HDPE composites was reviewed.

2.2.1 Effect of CaCO₃ content on mechanical properties of HDPE composites

2.2.1.1 Young's modulus

Bartczak et al. (1999) studied the effect of CaCO₃ content on mechanical properties of HDPE composites. Two types of CaCO₃ were used as filler, GCC and PCC. Content of CaCO₃ was 10, 20, 25, and 30 vol% for GCC and 5, 10, 15, 20, 25, and 30 vol% for PCC. The particle size of CaCO₃ was 3.50 μm for GCC and 0.70 μm for PCC. Both types of CaCO₃ were surface treated with calcium stearate by manufacturer. They reported that Young's modulus of HDPE filled with either GCC or PCC was higher than that of neat HDPE and increased with increasing content of CaCO₃.

Misra, Nerikar, Bertrand, and Murphy (2004) studied the effect of CaCO₃ content of 5, 10, and 20 wt% on Young's modulus of HDPE composites. The particle size of CaCO₃ was 1.2 μm. They reported that the addition of CaCO₃ into HDPE matrix caused an increase of Young's modulus of HDPE composites with increasing content of CaCO₃. This was due to the increase in rigidity and stiffness by the addition of CaCO₃.

Tanniru, Misra, Berbrand, and Murphy (2005) investigated the Young's modulus of CaCO₃/HDPE composites at 5, 10, and 20 wt% CaCO₃. The particle size of CaCO₃ was about 1.2 μm. The Young's modulus of the composites was higher than that of neat HDPE and increased as CaCO₃ content was increased. This was because the crystallinity was increased as increasing CaCO₃ content.

Yang, Bai, G'Sell, and Hiver (2006) studied the effect of adding 10, 20, 30, 40, and 50 wt% of CaCO₃ on the tensile properties of the HDPE composites. The CaCO₃ with particle size of 0.70 μm was treated with 2 wt% amino acid based on weight of calcium carbonate. The Young's modulus of the HDPE composites was significant increase as the amount of CaCO₃ increased.

Deshmane, Yuan, and Misra (2007) evaluated the effect of addition of nano-PCC (50-60 nm) with the content of 5 and 10 wt% on the mechanical properties of HDPE composites. Surface of PCC was treated with stearic acid of 8 wt%. HDPE-g-MAH of 5 wt% was used as a compatibilizer. The results indicated that the Young's modulus of the composites was higher than that of neat HDPE. However, the Young's modulus of the composites at 10 wt% CaCO₃ was 10 MPa lower than that at 5 wt% CaCO₃. This was explained that the reinforcement and nucleating effects of CaCO₃ were opposed to each other on the Young's modulus.

Since, the reinforcement effect was positive on Young's modulus, while the nucleating effect was negative on the Young's modulus.

2.2.1.2 Yield stress

Bartczak et al. (1999) studied tensile properties of CaCO₃-filled HDPE at various contents of GCC (10-30 vol%) and PCC (5-30 vol%). Yield stress of the composites gradually decreased with increasing CaCO₃ content. They explained that it was caused by low interfacial adhesion between CaCO₃ and HDPE matrix.

Misra et al. (2004) studied the mechanical properties of CaCO₃/HDPE composites with different CaCO₃ contents (5-20 wt%). They found that the yield stress of the HDPE composites at 5 and 10 wt% CaCO₃ was about 2 MPa higher than that of neat HDPE. Further increasing CaCO₃ to 20 wt%, the yield stress of the composites was decreased and equal to that of neat HDPE. It was commented that increasing CaCO₃ content was not apparently influenced on the yield stress of HDPE composites.

Tanniru and Misra (2006) studied the tensile properties of HDPE filled with CaCO₃ with particle size of 1.2 μm. They observed that the addition of CaCO₃ at 5-20 wt% caused insignificant difference in the yield stress of the HDPE composites. They suggested that, in general, the reinforcement with minerals increased the yield stress of the composites. However, this was not expected by the reinforcement effect. This was attributed to the nucleating effect of CaCO₃. The nucleating effect was responsible for decreasing spherulite size and negative effect on yield stress. Hence, the incorporation of CaCO₃ into HDPE matrix was simultaneously encounter effect between reinforcement effect and nucleating effect.

Yang et al. (2006) observed the tensile properties of CaCO₃/HDPE composites. CaCO₃ contents were 10-50 wt%. It was revealed that as the content of CaCO₃ increased, the yield stress of the composites was considerably decreased due to poor interfacial adhesion between CaCO₃ and HDPE matrix.

Deshmane et al. (2007) investigated the effect of CaCO₃ content of 5-10 wt% on the yield stress of the HDPE composites. From the observation, it indicated that there were insignificant differences in the yield stress of the composites. They explained that the larger spherulite size led to the presence of voids at the spherulite boundaries as a result of the contraction of the spherulite during cooling. These spherulite boundaries were the weak region and caused a decrease in the yield stress of the composites. In addition, the increase in crystallinity made an improvement of yield stress. They reported that there was an increase in crystallinity and decrease in spherulite size by reinforcing with CaCO₃. Therefore, it should lead to an increasing in the yield stress of the composites. Thus, they concluded that the yield stress of the composites might be related to lamellar thickness and crystalline long period. The lamellar thickness was an important parameter dominating the activation of yield, and the yield stress of neat HDPE was proportional to the lamellar thickness.

2.2.1.3 Impact strength

Bartczak et al. (1999) studied the notched Izod impact strength of the HDPE composites as a function of PCC content of 5-30 vol%. The results showed that the impact strength of the HDPE composites prepared from PCC was strongly increased at 10 vol% CaCO₃. Further increasing the content of CaCO₃ gave rise to the insignificant improvement of impact strength. As the CaCO₃ reaching 30

vol%, the impact strength of the composites was intensively decreased. This was because the dispersion of the CaCO_3 became much poorer with increasing content of CaCO_3 comparing to the composites at lower content of filler. In addition, the presence of agglomerates was the cause of decreasing in the impact strength of the composites.

Surampadi, Pesacreta, and Misra (2007) and Tanniru et al. (2005) investigated the effect of content of CaCO_3 with a particle size of $1.2 \mu\text{m}$ at a range of 5-20 wt% on the Izod impact strength of the HDPE composites. The impact strength of the composites was gradually increased with increasing content of CaCO_3 . This was attributed to the particle-induced cavitation and fibrillation of the composites.

2.2.2 Effect of particle size of CaCO_3 on mechanical properties of HDPE composites

2.2.2.1 Young's modulus

Mlecnik and La Mantai (1997) studied the effect of particle size of CaCO_3 on the Young's modulus of the HDPE composites. The 10 and $30 \mu\text{m}$ particle size of CaCO_3 was employed. The CaCO_3 /HDPE composites were prepared at 20 wt% CaCO_3 . It was reported that the smaller particle size of CaCO_3 improved the Young's modulus of the composites, while the larger one slightly lowered Young's modulus of the composites.

Bartczak et al. (1999) investigated the effect of particle size of GCC on the Young's modulus of the HDPE composites. This was conducted on GCC with particle size of $3.50 \mu\text{m}$ and PCC with particle size of $0.70 \mu\text{m}$. It was reported

that the composites with larger particle, GCC, had slightly higher Young's modulus than those prepared with smaller particles, PCC.

González, Albano, Ichazo, and Díaz (2002) studied the effect of particle size of CaCO_3 on the Young's modulus of CaCO_3 /PP/HDPE composites at 30 wt% CaCO_3 . The particle size of CaCO_3 was 3.0 and 1.8 μm . They reported that the Young's modulus of the composites with smaller particle size was higher than that of the composites with the larger particle size. This was because CaCO_3 with smaller size had better filler particle dispersion than that with larger particle size. In addition, the agglomerate sizes of 1.8 μm CaCO_3 were smaller than those of 3.0 μm CaCO_3 .

2.2.2.2 Yield stress

Mlecnik and La Mantai (1997) studied the effect of particle size of CaCO_3 on yield stress of the HDPE composites at 20 wt% CaCO_3 . They found that the yield stress of the HDPE composites prepared from CaCO_3 with 10 μm was exactly similar to that of the HDPE composites prepared from CaCO_3 with 30 μm . It was indicated that the yield stress of the composites was not influenced by the particle sizes of CaCO_3 .

Bartczak et al. (1999) investigated the effect of particle size of CaCO_3 on yield stress of the HDPE composites. The yield stress of the composites with the smaller particle size of CaCO_3 (0.70 μm) was higher than that of the composites with the larger one (3.50 μm). This observation was more clearly observed at high filler content. This was caused by the interior imperfection of structure within the composites due to a large particle size.

2.2.2.3 Impact strength

Bartczak et al. (1999) investigated the effect of two particle size (3.50 and 0.70 μm) of CaCO_3 on notched Izod impact strength of the HDPE composites. Izod impact strength of the HDPE composites increased with decreasing particle size of CaCO_3 . This was due to the decreased ligament thickness with lowering particle size of CaCO_3 .

2.2.3 Effect of compatibilization on mechanical properties of HDPE composites

Maleic anhydride grafted polyethylene (PE-g-MAH) such as HDPE-g-MAH and LDPE-g-MAH has been the most common approach for improvement the interfacial adhesion between calcium carbonate and non-polar polyethylene (Phueakbuakhao et al., 2008; Wang, Chen, and Liu, 2002). The PE-g-MAH becomes chemical bridge to link with the hydrophilic calcium carbonate on one side and the hydrophobic polyethylene chain on the other side. In other words, the PE-g-MAH has both the hydrophilic and hydrophobic properties required for it to attach well with the calcium carbonate and polyethylene matrix. The mechanism of compatibilization of PE-g-MAH between polyethylene and calcium carbonate is shown in Figure 2.2.

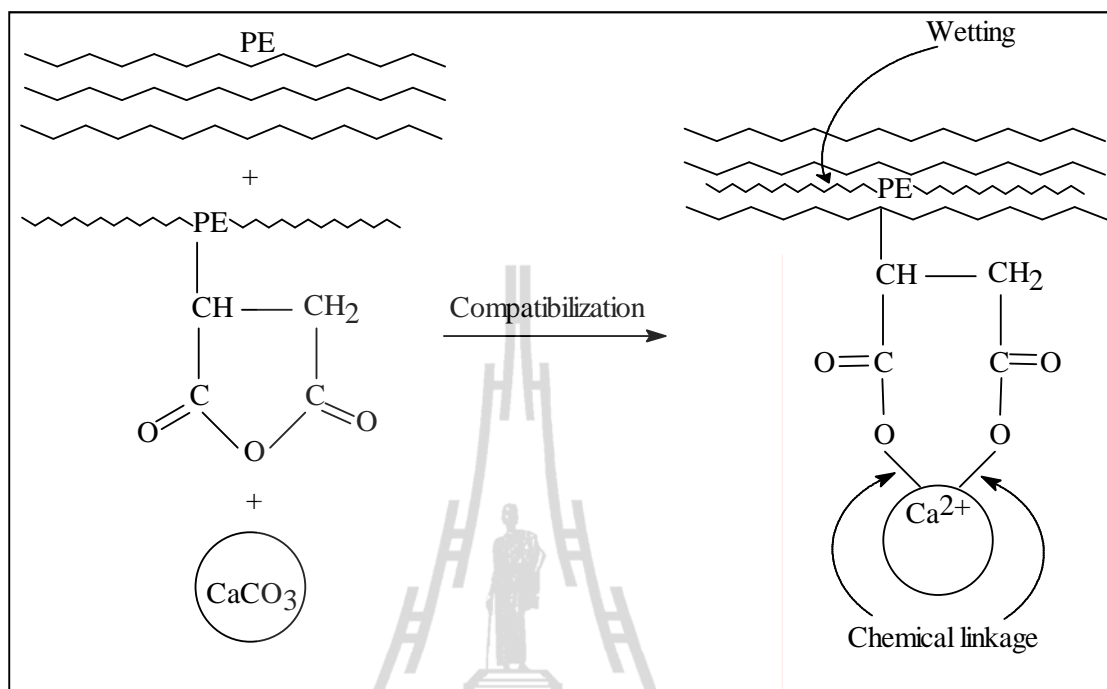


Figure 2.2 Schematic representing the mechanism of surface modification with maleic anhydride grafted polyethylene (PE-g-MAH) in CaCO₃/PE composites (adapted from Zhang et al., 2006).

2.2.3.1 Young's modulus

Bartczak et al. (1999) investigated the effect of surface treatment of CaCO₃ by calcium stearate on Young's modulus of the HDPE composites with 25 vol% CaCO₃. The Young's modulus of the composites with treated and untreated CaCO₃ was not improved. This was because the interfacial modification with calcium stearate did not improve the interfacial adhesion between CaCO₃ and HDPE.

Lazzeri et al. (2005) studied the influence of content of stearic acid (SA) for surface treatment of CaCO₃ on Young's modulus of 10 vol% CaCO₃/HDPE composites. It was observed that the Young's modulus of the

composites decreased with increasing content of SA. This was due to a softer interphase when increasing the content of SA.

2.2.3.2 Yield stress

Bartczak et al. (1999) investigated the effect of surface treatment of CaCO_3 by calcium stearate on yield stress of the HDPE composites with 25 vol% CaCO_3 . The yield stress of the composites prepared with treated and untreated CaCO_3 was similar. This was attributed to no improvement of interfacial adhesion between CaCO_3 and HDPE by calcium stearate.

Lazzeri et al. (2005) studied the influence of content of SA for surface treatment of CaCO_3 on yield stress of 10 vol% CaCO_3 /HDPE composites. They found that the yield stress of the composites decreased with increasing SA content. This was attributed to a decreasing interfacial strength and stress transfer ability from matrix to filler particles by increasing SA content.

2.2.3.3 Tensile strength

Bartczak et al. (1999) investigated the effect of surface treatment of CaCO_3 by calcium stearate on tensile strength of the HDPE composites with 25 vol% CaCO_3 . They found that tensile strength of the composites with CaCO_3 treated with calcium stearate slightly higher than that of the composites with untreated CaCO_3 . This was because surface treatment with calcium stearate did not improve the interfacial adhesion between the two components but it merely promoted the random dispersion of particles.

Wang et al. (2002) observed the effect of LDPE-g-MAH content on tensile strength of CaCO_3 /HDPE composites with 30 wt% CaCO_3 . The influence of grafting ratio of MAH on LDPE on tensile strength of CaCO_3 /HDPE

composites with 0.6 wt% LDPE-g-MAH was investigated as well. The contents of LDPE-g-MAH were 16.7, 33.3, 50.0, 66.7, 83.3, and 100 wt% based on total weight of the system. The grafting ratios were 0.60, 0.92, and 1.38 wt%. They found that the highest tensile strength of the composites was obtained. However, with increasing content of LDPE-g-MAH, the tensile strength of the composites declined. This was probably due to the degradation of LDPE during solid-phase mechanochemical grafting process. In addition, the tensile strength of the composites increased with increasing grafting rate.

Phueakbuakhao et al. (2008) investigated the effect of adding CaCO_3 treated with various coupling agent including SA, 3-aminopropyltriethoxysilane (AMPTES), 3-glycidoxy propyltrimethoxy silane (GPTMS), and HDPE-g-MAH on the tensile strength of CaCO_3 -filled recycled HDPE with 10 wt% CaCO_3 . With 1 wt% of different coupling agents, it was found that the addition of CaCO_3 treated with SA exhibited the greatest tensile strength of CaCO_3 -filled recycled HDPE. This was because a strong chemical bonding between the polar group of the SA and CaCO_3 in a form of calcium stearate enhanced the compatibility of the polymer matrix and CaCO_3 . For other coupling agents (AMPTES, GPTMS, and HDPE-g-MAH), the interfacial interaction between CaCO_3 and recycled HDPE matrix was a weak physical bond or van der waals forces.

2.2.3.4 Impact strength

Liu, Kwok, Li, and Choy (2002) studied the effect of isopropyltriisostearoyl titanate as a coupling agent on notched Izod impact strength of CaCO_3 /HDPE composites. The particle size of CaCO_3 was 0.6 μm and CaCO_3 content was 0-35 vol%. It was observed that the addition of small content of coupling

agent (2.5 wt%) gave rise to good dispersion of CaCO_3 . In addition, the toughening efficiency increased as coupling agent content increased from 2.5-5 wt%. This was probably due to better dispersion of the particles. However, the toughening efficiency decreased with adding coupling agent of 7.5 and 10 wt%. This was due to the agglomeration of CaCO_3 particles.

Wang et al. (2002) studied the effect of content of LDPE-g-MAH on notched Izod impact strength of CaCO_3 /HDPE composites with 30 wt% CaCO_3 . The contents of LDPE-g-MAH were 0, 16.7, 33.3, 50.0, 66.7, 83.3, and 100 wt% based on total weight of the system. The influence of grafting ratio of MAH on LDPE on impact strength of 30 wt% CaCO_3 /HDPE composites with 5 wt% LDPE-g-MAH was also investigated. The grafting ratio was 0, 0.60, 0.92, and 1.38 wt%. The impact strength of the composites was increased from 185.4 J/m to 319.8 J/m by addition LDPE-g-MAH at content of 16.7 wt%. However, the impact strength of composites decreased with increasing content of LDPE-g-MAH. This was possible due to the degradation of LDPE during solid-phase mechanochemical grafting process. In addition, the impact strength of the composites increased with increasing grafting ratio.

Lazzeri et al. (2005) studied the influence of SA content for surface treatment of CaCO_3 on Charpy impact strength of 10 vol% CaCO_3 /HDPE composites. It was observed that the impact strength of the composites almost linearly increased with increasing SA content. This was because the main effect of SA is to effectively reduce agglomerate size of CaCO_3 thus the composites was more ductile as increasing SA content.

Phueakbuakhao et al. (2008) investigated the effect of adding CaCO_3 treated with various coupling agent including SA, AMPTES, GPTMS, and HDPE-g-MAH on the impact strength of CaCO_3 -filled recycled HDPE with 10 wt% CaCO_3 . CaCO_3 was treated with different coupling agents at a content of 1 wt% with respect to CaCO_3 . They found that the addition of CaCO_3 treated with SA exhibited the highest impact strength of CaCO_3 -filled recycled HDPE. This was because a strong chemical bonding between the polar group of the SA and CaCO_3 in a form of calcium stearate enhanced the compatibility of the polymer matrix and CaCO_3 by changing hydrophilic surface of CaCO_3 to hydrophobic one. For other coupling agents (AMPTES, GPTMS, and HDPE-g-MAH), the interfacial adhesion between CaCO_3 and recycled HDPE matrix was a weak physical bond or van der Waals forces. In addition, it was found that as increasing coupling agents content the impact strength was improved. This was explained by based on the fact that when increasing the content of coupling agent, the interfacial adhesion between CaCO_3 and HDPE was improved. Furthermore, it was reported that the optimum content of SA, AMPTES, GPTMS, and HDPE-g-MAH was 1, 2, 3, and 4 wt%, respectively, with respect to CaCO_3 .

2.3 Avian egg

2.3.1 Component of egg

The avian egg consists of three main parts : eggshell with eggshell membrane (ESM), albumen or white, and yolk. The egg comprises approximately 10 wt% shell, 30 wt% yolk, and 60 wt% albumen (Stadelman, 2000). The yolk is surrounded by albumen, which in turn is enclosed by ESM and finally a hard eggshell (Li-Chan and Kim, 2008), as illustrated in Figure 2.3.

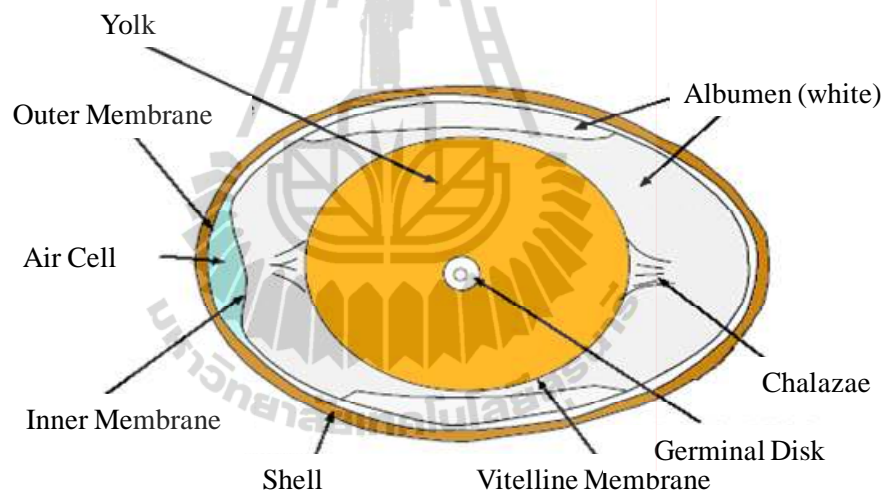


Figure 2.3 Schematic of different parts of egg structure

(<http://ag.ansc.purdue.edu/poultry/class.htm>).

2.3.2 Structure of eggshell (ES)

The eggshell is composed of ESM and calcified eggshell matrix. The ESM is made up of two protein fiber layers, inner and outer membranes, located between the white and the inner surface of the shell (Li-Chan, Powrie, and Nakai, 1995). The total thickness of two membranes was approximately 70 μm (Lammie, Bain, Solomon, and Wess, 2006). The outer membrane (shell membrane) of about 50

μm is attached firmly to the calcified shell whereas the inner membrane (egg membrane) being about $20 \mu\text{m}$ is in direct contact with the albumen (Nys and Gautron, 2007).

The calcified eggshell, composed of mammillary knob layer (lamellar layer), palisade layer (sponge layer), places on the eggshell membranes (Hincke et al., 2000). Figure 2.4 illustrates the morphology of eggshell matrix and eggshell membranes. The palisade and mammillary layers form a matrix composed of protein fibers bonded to calcium carbonate (calcite crystal) (Rivera et al., 1999; Tsai et al., 2006) in a ratio of 1 : 50 (Rivera et al., 1999).

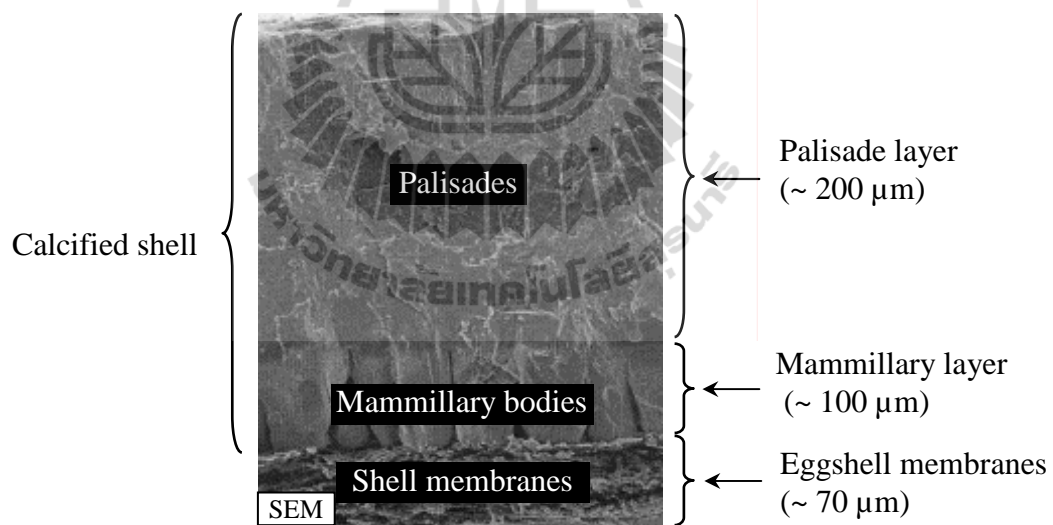


Figure 2.4 SEM micrograph of a fractured eggshell (Hincke et al., 2000).

2.3.3 Chemical composition of eggshell

2.3.3.1 Eggshell membrane (ESM)

The ESM contains 95% protein, 2% carbohydrate, and 3% lipid (Arias, Mann, Nys, Garcia-Ruiz, and Fernández, 2007). Although, the early studies reported that eggshell membranes contain keratin, it is now well verified that they are not composed of keratin (Arias et al., 2007). More recently, it was reported that type X collagen is the main constituent (Li-Chan and Kim, 2008). The ESM also consists of keratin sulfate (Li-Chan and Kim, 2008), type I and V collagens, osteopontin, siloprotein (Hincke et al., 2000; Yi, Guo, Zhang, Yu, and Li, 2004), ovalbumin, ovotransferrin and lysozyme (Arias et al., 2007). Protein composition of ESM is reported in Table 2.1. The elemental analysis shows that the constituent of ESM consists of C, N, and O as major element, Al, S, and Cl as minor element, and Ca as trace element (Heredia et al., 2005).

2.3.3.2 Eggshell matrix

Avian eggshell is sometimes referred to as a “natural composite bioceramic” (Li-Chan and Kim, 2008) or “composite biomaterial” (Hincke et al., 2000). The eggshell matrix is a complex mixture of 94 wt% CaCO₃ (calcite crystal), 1 wt% magnesium carbonate, 1 wt% calcium phosphate, and 4 wt% organic substances (Stadelman, 1995). The content of CaCO₃ can vary in a range of 94 – 98 wt% (Daengprok, Garnjanagoonchorn, and Mine, 2002; Murakami, Rodrigues, Campos, and Silva, 2007). The organic matrix composed mainly of matrix proteins, at least 70%, (Gautron and Nys, 2007) consisting chiefly of glycoproteins and proteoglycans (Hincke et al., 2000) and trace amounts of fatty acid (Daengprok et al., 2002; Li-Chan and Kim, 2008). Osteopontin and clusterin are the example of

glycoprotein (Nys, Gautron, Garcia-Ruiz, and Hincke, 2004). The proteoglycans are, for instance, keratan sulphate proteoglycan, dermatan sulphate proteoglycan (Gautron and Nys, 2007), oversulfated keratin proteoglycan, chondroitin 6-sulfate proteoglycan, and ovoglycan (Arias et al., 2007). The eggshell matrix proteins can be divided into three groups : eggshell-specific proteins, egg white proteins, and bone matrix proteins (Hincke et al., 2000). Ovocleidines and ovocalyxins are eggshell-specific proteins. Ovalbumin, ovotransferrin, and lysozyme are the egg white protein. In addition, osteopontin is bone matrix protein. The mammillary layer is composed of collagens (type I, V, and X) (Lammie et al., 2006). In addition, the other eggshell matrix proteins are listed in Table 2.1. Fatty acid composition of decalcified eggshell is presented in Table 2.2.

The elemental composition of eggshell is Ca, C, and O as major elements and Mg as minor element (Heredia et al., 2005). Trace element of eggshell includes Na, K, P, S, Cl (Heredia et al., 2005), Al, F, Fe, Cu, B, Cr, Zn, Sr, V, Pb, Cd, and Hg (Schaafsma et al., 2000).

Table 2.1 Different types of proteins localizing in eggshell membrane and eggshell matrix (adapted from Arias et al., 2007).

ESM	Mammillary layer	Palisade layer
Type I collagen	Type I collagen	C-Type lectin-like proteins
Type V collagen	Type V collagen	Hyaluronic acid
Type X collagen	Type X collagen	Ovoglycan
Ovalbumin	Ovalbumin	Ovocleidin-116
Ovotransferrin	Ovotransferrin	Ovocalyxin-25
Lysozyme	Lysozyme	Ovocalyxin-36
Osteopontin	Mammillan	
Lysyl oxidase	C-Type lectin-like proteins	
Siloprotein	Clusterin	
Ovocalyxin-36	Ovocalyxin-36	

Table 2.2 Types and compositions of fatty acid of eggshell matrix (adapted from Li- Chan and Kim, 2008).

Fatty acid	Composition (ng/ μ g)	
	Palisade layer	Mammillary layer
Decanoic acid (10 : 0)	1.1	0.4
Lauric acid (12 : 0)	0.9	0.3
Eicosapentaenoic acid (20 : 5)	0.2	0.2
Linolenic acid (18 : 3)	1.7	1.1
Myristic acid (14 : 0)	1.8	1.3
Docosahexaenoic acid (24 : 6)	2.4	1.0
Palmitoleic acid (16 : 1)	1.7	1.5
Arachidonic acid (20 : 4)	1.7	0.9
Linoleic acid (18 : 2)	2.3	1.7
Palmitic acid (16 : 0)	12.6	10.4
Oleic acid (18 : 1, c9)	3.3	2.7
Petroselinic acid (18 : 1, c6)	0.7	0.4
Elaidic acid (18 : 1, c9)	0.2	0.1
Stearic acid (18 : 0)	5.7	4.5
Arachidic acid (20 : 0)	3.3	1.3
Behenic acid (22 : 0)	6.8	3.1
Total saturated fatty acids	32.2	21.3
Total unsaturated fatty acids	14.2	9.6
Total fatty acids	46.4	30.9

2.3.4 Applications of eggshell

In recent years, there were many attempts to focus on the utilization of calcified eggshell in various applications. With eggshell containing Ca as main element, the eggshell was utilized as good source of calcium in human nutrition (Schaafsma et al., 2000; Suguro, Horiike, Masuda, Kunou, and Kokubu, 2000). Since Ca from eggshell powder was absorbed easier than that from commercial calcium carbonate in small intestine of rat (Daengprok et al., 2002). In addition, eggshell contains not only Ca but also Sr and F which may have positive effect on bone metabolism (Schaafsma et al., 2000).

According to Ca as one of the main components of synthetic hydroxyapatite (HA : $\text{Ca}_{10}(\text{PO}_4)_6(\text{OH})_2$), main component of hard tissues in bones, (Dasgupta, Singh, Adak, and Purohit, 2004), the eggshell was employed as a starting material for preparing hydroxyapatite to use in tissue engineering and bone substitute (Balázsi, Wéber, Kövér, Horváth, and Németh, 2007; Lee and Oh, 2003; Wei, Xu, and Li, 2009). This was due to its chemical similarity to bone minerals (Lee and Oh, 2003).

Due to pore structure of the calcified eggshell and high content of calcium carbonate, it was used as raw material for preparing a solid catalyst in catalytic process for biodiesel production (Wei et al., 2009). By calcination eggshell, calcium oxide (CaO) became eggshell-derived catalyst.

Pore structure, CaCO_3 , and protein acid mucopolysaccharide of eggshells were good adsorptive properties. The important functional groups of protein acid mucopolysaccharide are carboxyl, amine, and sulfate that can form ionic bond with heavy metal ion (Arunlertaree, Kaewsomboon, Kumsopa, Pokethitiyook,

and Panyawathanakit, 2007). For this reason, the eggshell was employed as adsorbent for removal of toxic heavy metals such as Cd, Cr, and Pb in industrial wastewater (Arunlertaree et al., 2007; Park, Jeong, Yang, Kim, and Lee, 2007).

In addition, eggshell was recently applied as a filler for polymer composites. For example, it was used as a new bio-filler for polypropylene composites (Toro, Quijada, Yazdani-Pedram, and Arias, 2007), epoxy resin composites (Ji, Zhu, Qi, and Zeng, 2009), LDPE composites modified with isophthalic acid (Shuhadah and Supri, 2009), SEBS and SEBS/silk composites (Kang, Pal, Park, Bang, and Kim, 2010), and LDPE composites modified with PE-g-MAH (Supri, Ismail, and Shuhadah, 2010).

2.3.5 Preparation of eggshell powder (ESP)

2.3.5.1 Mechanical approach

Thoroski (2003) explained the method of separation shell membranes from eggshell powder. The egg liquid adhering to the membrane of the eggshell is removed using a centrifuge. After the liquid removal, the eggshell is washed in a screw conveyor with either a downward spray washer or a counter current washing system to remove any residual materials left on the shell. After washing, the eggshell is again centrifuged to reduce the moisture content. Next, the eggshell is dried and tumbled simultaneously at 88°C for 2 minutes. During drying process, the membranes shrink since the protein-protein bond in the membrane is stronger than the protein-shell bond, it results in the pulling away from eggshell matrix. The dried eggshell is broken down into smaller particles by tumbling action of the drum dryer. The smaller particles of eggshell are again cleaned and dried. After the completion of

the drying step, the eggshell and eggshell membrane are separated using a gyratory sifter where the large pieces of membrane are held back, while the smaller and denser eggshell particles fall through the screen. The eggshell from the gyratory sifter is then delivered to a hammer mill to further reduce the particle size. A suitable hammer mill is a Schutte Hammer mill due to possessing a pneumatic membrane removal system along with a lower outlet having a valve.

Macneil (2006) proposed the method to prepare eggshell powder without eggshell membrane. The eggshell is first performed in a reducing device for abrading the linking structure between the eggshell and the membranes and outputting the eggshell particles of a particular size. After exiting the reducing device, the abraded membrane particles are then separated from the eggshell particles in a tank containing plain water at room temperature. Since the membrane particles is much lighter than the eggshell particles, the membrane particles tend to stay in the water a longer time without settling. The eggshell particles tend to settle onto the bottom of tank due to their relatively greater density. However, some membrane particles are buried under the eggshell particles settling of the bottom of the tank. In order to promote the dissociation of the eggshell particles and the membrane particles, the particles on the bottom of the tank are slowly stirred. The water containing the entrained membrane particles is suctioned out of the tank and screened to remove the membrane particles from water. Next, the dewatered membrane particles are collected. After that, the eggshell particles at the bottom of the tank are conveyed to a recover device and dried. Finally, the eggshell particles are collected.

2.3.5.2 Chemical approach

In addition to mechanical technique, the eggshell powder was prepared by chemical way (Sakullertphasuk, Piriyesyangkul, Jitthai, and Haruthaithanasan, 2003). The eggshell was first washed with water. The washed eggshell was boiled at 100°C for 15 min. Then the boiled eggshell was dried at temperature of 105°C for 2 h. After that, the dried eggshell was ground by disc mill for reduction in particle size. The eggshell powder was subsequently treated to remove organic substances. The eggshell powder was first treated with a solution of 2% HCl in a ratio of eggshell powder to HCl of 1 : 5 at 40°C for 15 min. The acid-treated eggshell powder was neutralized with distilled water. Next, the neutralized eggshell powder was treated with a solution of 3% NaOH in the ratio of eggshell powder to NaOH of 1 : 5 at the temperature of 40°C for 15 min. Then, alkali-treated eggshell powder was washed with distilled water until weak basic eggshell powder. Secondly, the eggshell was dried at 105°C for 2 h. Finally, the eggshell powder was sieved.

Shuhadah and Supri (2009) prepared eggshell powder by the following step. First, the eggshells were washed, dried, and ground to a powder using the blender. Secondly, the eggshell powder was sieved to be a particle size of 63 µm. After that, the eggshell powder was dried in a vacuum oven at 80°C until its weight was constant. Next, the eggshell powder was mixed with a solution of 10% NaOH and stirred for 6 min. Then, alkali-treated eggshell powder was kept at room temperature until two layers were formed. The eggshell powder after deproteinizing was washed with distilled water and dried in the oven at 80°C.

2.3.6 Properties of eggshell

Freire and Holanda (2006) studied the crystalline phase and thermal properties of eggshell. They reported that XRD pattern of eggshell powder showed the characteristic of calcite. In addition, it was reported that the calcite was rhombohedral crystal structure. Moreover, it was reported that the decomposition temperature of organic matter deposited in eggshell was about 324°C. The decomposition temperature of CaCO_3 was around 765°C.

Murakami et al. (2007) investigated thermal properties of CaCO_3 obtained from eggshell compared to industrial CaCO_3 . It was reported that the eggshell CaCO_3 decomposed at 30°C higher than the industrial CaCO_3 . This evidently demonstrated that thermal stability of CaCO_3 obtained from eggshell was higher than that of industrial CaCO_3 .

Da Costa et al (2007) studied the XRD pattern of eggshell powder without thermal treatment in comparison with that of thermal treated eggshell at 150 - 800°C for 1 h. The XRD patterns of treated eggshell up to 700°C were in agreement with the pattern of calcite. It was also observed that the XRD pattern was changed only at the treatment temperature of 800°C.

Balázsi et al. (2007) studied phase composition of eggshell after calcinations at 900°C for 3 h by XRD. They found that the XRD pattern showed Ca(OH)_2 as major component. They explained that, in fact, calcium oxide (CaO) was the product from calcinations, but as the powder sample was in contact with ambient atmosphere the product changed to calcium hydroxide (Ca(OH)_2). In addition, CaO and MgO was observed as small amount.

Naemchan, Meejoo, Onreabroy, and Limsuwan (2007) used eggshell without eggshell membrane and its particle size of less than 200 μm to prepare eggshell at 200-900°C for 1 h and identify its crystal structure by XRD. They found that the crystal structure of calcined eggshell was identified as calcite (CaCO_3) only at the treatment temperature from 200°C up to 600°C corresponded to the previous report from Engin, Demirtaş, and Eken (2006). However, the calcium carbonate phase decreased and CaO appeared as the eggshell was treated above 700°C. In addition, it was reported that the treatment of eggshell at 900°C for 1 h led to the complete phase transformation from CaCO_3 to CaO as reported from Engin et al. (2006). On the other hand, Lee and Oh (2003) reported that CaCO_3 was completely transformed into CaO at 800°C for 1 h.

Sanmuang, Ruksakulpiwat, Suppakarn, and Sutapun (2008) studied the properties of eggshell after thermal treatment at 700°C for 1-3 h and 800°C for 1-4 h. They reported based on XRD pattern that CaCO_3 was obtained when eggshell was treated at 700°C. However, the content of CaCO_3 decreased with increasing the treatment time. Ca(OH)_2 was a major component when the eggshell was treated at 800°C.

Wei et al. (2009) reported that the calcination of eggshell below 600°C for 2 h did not cause to the formation of CaO. However, the eggshell was calcined at 700°C for 2 h obtained CaCO_3 as a major component and CaO as a minor component.

2.4 Polymer filled with eggshell powder (ESP)

2.4.1 Polyethylene filled with ESP

Shuhadah and Supri (2009) studied the effect of chemical modification by isophthalic acid and ESP content at 5-25% on the mechanical properties of ESP/LDPE composites. The ESP after deproteinizing with 10% NaOH was chemically modified with 6% of isophthalic acid and ethanol. They found that the tensile strength of the composites decreased with increasing ESP content. This was due to the poor adhesion between ESP and LDPE matrix and the agglomeration of filler particles. The tensile strength of ESP/LDPE composites with chemical modification was higher than that of ESP/LDPE composites without chemical modification. This was probably due to the better interfacial adhesion between filler and matrix after chemical modification. The stronger the interfacial adhesion, the better the stress transfer from the matrix to the filler.

Young's modulus of the composites with and without chemical modification increased with increasing filler content. This was due to the filler exhibiting high stiffness compared to LDPE matrix. In addition, the Young's modulus of the composites with chemical modification was lower than that of the composites without modification. This was attributed to isophthalic acid toughening the composites and reduction in Young's modulus of the composites.

In addition, it was reported that the elongation at break of the unmodified composites and modified composites was decreased as the filler content was increased. This was because the increasing in filler content resulted in the stiffening of the composites. It was also reported that the elongation at break of the unmodified LDPE composites was higher than that of the modified LDPE composites.

Supri et al. (2010) investigated the effect of PE-g-MAH on the tensile properties, morphology and thermal properties of ESP/LDPE. The ESP/LDPE composites were prepared from different ESP content and the addition of PE-g-MAH. The tensile strength, elongation at break and thermal stability of ESP/LDPE composites with PE-g-MAH were greater than ESP/LDPE composites, and their differences became more pronounced at higher filler content. The interfacial adhesion between ESP and LDPE was improved with the addition of PE-g-MAH.

2.4.2 Polypropylene filled with ESP

Toro et al. (2007) investigated the Young's modulus of ESP/PP composites compared to that of CaCO₃/PP composites. It was reported that ESP with particle size of 8.4 μm led to higher Young's modulus of composites than CaCO₃ with particle sizes of 17.1, 2.0, and 0.7 μm. This was due to ESP/PP composites having better phase continuity than CaCO₃/PP composites.

2.4.3 Epoxy filled with ESP

Ji et al. (2009) examined the possibility of ESP used as a filler for epoxy composites. The epoxy composites were prepared from ESP at content of 1-10 wt%. They found that the strongly improvement of impact strength of epoxy composites at ESP content of 5 wt% were 16.7 kJ/m² compared with 9.7 kJ/m² of neat epoxy resin. When increasing ESP content to 10 wt%, the impact strength of the composites decreased from 16.7 kJ/m² to 12.3 kJ/m². They concluded that ESP had a potential source of filler for epoxy composites.

2.4.4 Poly (styrene-*b*-ethylene/butylenes-*b*-styrene) tri block copolymer filled with ESP

Kang et al. (2010) studied the use of ESP as a filler for poly (styrene-*b*-ethylene/butylenes-*b*-styrene) (SEBS) tri block copolymer. The content of eggshell powder was 2.5 and 5 wt% for SEBS/ESP composites. In addition, silk fibroin was introduced into SEBS/ESP composites. The SEBS/ESP/silk composites were done at ESP : silk ratio of 2.5 : 2.5 and 5 : 2.5 by wt%. Morphological and thermal properties of the SEBS/ESP and SEBS/ESP/silk composites were observed. They found that interfacial interaction between ESP and SEBS matrix was improved by incorporation of silk fibroin. This was possibly due to the high aspect ratio of silk fibroin. It was reported that the initial decomposition temperature of the composites was lower than that of ESP and silk fibroin. However, the composites had insignificant change in thermal properties.

CHAPTER III

EXPERIMENTAL

3.1 Materials

Chicken eggshell (ES) waste of Bolvans Goldline and ISA Brown (hybrid) breeds was obtained from the SUT Farm, Suranaree University of Technology. A GCC (OFIL-1) was kindly supplied by Sand and Soil Industry Co., Ltd. A commercial injection grade HDPE (EL-Lene™ H5814J) was purchased from SCG Chemicals Co., Ltd. It has a melt flow index (MFI) of 14 g/10 min (2.16 kg at 190°C), a density of 0.958 g/cm³, and a melting temperature (T_m) of 131°C. The HDPE-g-MAH (Fusabond® MB100D, DuPont™) was kindly supplied by Chemical Innovation Co., Ltd. It has a MFI of 2 g/10 min (2.16 kg at 190°C), a density of 0.960 g/cm³, a melting temperature of 136°C, and a maleic anhydride content of 0.9 wt%.

3.2 Preparation of eggshell powder (ESP)

First of all, the chicken eggshell waste was thoroughly cleaned with tap water to remove the chicken dung and the residual of albumen (egg white) and yolk adhering to the eggshell. After cleaning, the eggshell was subsequently dried in an open air for 24 h. The cleaned eggshell (Figure 3.1 (a)) was stored in plastic bags for further use in the next processing step.

The ESP was prepared by grinding the eggshell via a ball mill with 20 balls of 30 mm-diameter, 40 balls of 25 mm-diameter, and 60 balls of 15 mm-diameter. One kilogram of broken ES, illustrating in Figure 3.1 (b), was put into a cylindrical

porcelain pot and ground for 24 h. The pot has an inner diameter of 185 mm and a depth of 217 mm. The porcelain pot was turned about a horizontal axis with a rotational speed of 35 rpm. The image of ESP as shown in Figure 3.1 (c) was kept in a desiccator for the subsequent characterizations and composites preparations.



Figure 3.1 Images of ES after cleaning and drying (a), broken ES for preparing ESP and HT-ES (b), ESP (c), and HT-ES (d).

3.3 Preparation of heat-treated eggshell (HT-ES)

For preparing HT-ES, the ES was treated at four different temperatures, 650°C, 670°C, 770°C, and 800°C, in a chamber furnace (Carbolite, CWF) with a heating rate of 10°C/min under air atmosphere. First, the broken eggshell (Figure 3.1

(b)) of 50 g was placed in a silica-alumina plate. Secondly, they were treated at a predetermined temperature and time as mentioned in Table 3.1. After the treatment, the treated eggshell was kept in the furnace until the temperature was cooled down by a cooling rate of 10°C/min to 40°C. Thirdly, they were kept in a desiccator prior to characterizations and composite preparations. Finally, the HT-ES (Figure 3.1 (d)) was ground for 12 h using a ball mill under the same procedure as the eggshell was ground as explained in section 3.2.

Table 3.1 Heat treatment conditions for preparing HT-ES in a chamber furnace.

Treatment temperature (°C)	Treatment time (h)
650	16
	20
	24
670	12
	16
770	4
	6
800	3
	4
	5

3.4 Preparation of CaCO₃ powder

One kilogram of CaCO₃ was put in a cylindrical porcelain pot and ground by a ball mill with 20 balls of 30 mm-diameter, 40 balls of 25 mm-diameter, and 60 balls of 15 mm-diameter for 24 h at a rotational speed of 35 rpm. The ground CaCO₃ was kept in a desiccator before characterizations and composite preparation.

3.5 Preparation of HDPE composites

3.5.1 Mixing process

The uncompatibilized HDPE composites were prepared at 10, 20, 30, and 40 wt% filler content. Three types of filler, ESP, CaCO₃ powder, and HT-ESP were used. They were separately sieved using mesh no 325 sieve (ϕ 45 μ m) and mesh no 230 sieve (ϕ 63 μ m). The sieved ESP and HT-ESP were referred to as ESP1 and HT-ESP1. After that, the ESP1, HT-ESP1, and CaCO₃ were dried in an oven overnight at a temperature of 70°C before they were mixed with HDPE. The filled HDPE composites were prepared in an internal mixer (HAAKE PolyLab System, Rheomix3000p). The mixing process was operated at 170°C under a rotor speed of 70 rpm and a mixing time of 15 min. For preparing ESP/HDPE and CaCO₃/HDPE composites, HDPE was melted for 1 min before either the ESP or CaCO₃ was added into the mixing chamber. In cases of preparing HT-ESP/HDPE composites, the HT-ESP was first added into the mixing chamber and then HDPE was added immediately.

In order to study the effect of particle size on the mechanical properties of HDPE composites, the ESP was sieved by mesh no 500 sieve (ϕ 25 μ m) and mesh no 450 sieve (ϕ 32 μ m) referring to as ESP2. The HDPE composites were prepared at the ESP2 content of 40 wt%.

For studying the effect of HDPE-g-MAH on the compatibility improvement of HDPE composites, the HDPE composites were prepared at the ESP2 and HT-ESP1 content of 40 wt%. The ESP2 used for preparing the compatibilized HDPE composites was the one sieved with mesh no 500 and 450 sieves, as mentioned above. The HDPE-g-MAH was employed at 2 wt% of HDPE. For the mixing procedure, the HT-ESP was initially added into a mixing chamber and then the

mixture of HDPE and HDPE-g-MAH was immediately added. For preparing ESP/HDPE composite, the mixture of HDPE and HDPE-g-MAH was first added into the mixing chamber after 1 minute past the ESP was added.

All compositions of preparing HDPE composites in this work were shown in Table 3.2. After mixing, all filled HDPE were ground using a plastic grinding machine.

3.5.2 Molding process

The specimens of tensile (dumbbell-shape), flexural, heat distortion temperature (HDT), impact and hardness were prepared by an injection molding machine (Chuan Lih Fa, CLF 80T). The ground HDPE composites were dried overnight in an oven at temperature of 70°C before molded. The injection process was carried out at a melting temperature of 190°C and a mold temperature of 25°C, a screw speed of 104 rpm, an injection speed of 57 mm/s, a holding pressure of 960 kg/cm², and a cooling time of 20 s.

Table 3.2 All compositions of material for preparing HDPE composites.

Designation	Content (wt%)					HDPE-g-MAH (2 wt%)
	HDPE	ESP1	ESP2	CaCO ₃	HT-ESP1	
HDPE	100	0	0	0	0	0
10% ESP	90	10	0	0	0	0
20% ESP	80	20	0	0	0	0
30% ESP	70	30	0	0	0	0
40% ESP	60	40	0	0	0	0
40% ESP	60	0	40	0	0	0
40% ESP+HDPE-g-MAH	60	0	40	0	0	2
10% CaCO ₃	90	0	0	10	0	0
20% CaCO ₃	80	0	0	20	0	0
30% CaCO ₃	70	0	0	30	0	0
40% CaCO ₃	60	0	0	40	0	0
10% HT-ESP	90	0	0	0	10	0
20% HT-ESP	80	0	0	0	20	0
30% HT-ESP	70	0	0	0	30	0
40% HT-ESP	60	0	0	0	40	0
40% HT-ESP+HDPE-g-MAH	60	0	0	0	40	2

3.6 Material characterizations

3.6.1 Characterizations for ESP, HT-ES, and CaCO₃

3.6.1.1 Crystal form and chemical composition

The X-ray diffractometer (XRD, Bruker AXS, D5005) was employed to analyze the crystal form of ESP, HT-ES (white portion), and commercial CaCO₃. The measurement was carried out by using CuK_α radiation (at $\lambda = 0.15406$ nm), 2θ between 5 and 70° with a scan step of 0.02°, a scan speed of 0.5 s/step, an accelerating voltage of 40 kV, and a current of 40 mA.

In addition, wavelength dispersive X-ray fluorescence spectrometer (XRF, Philips, PW2400) was used to quantitatively determine the Ca composition of the ESP and HT-ES (white portion) obtained by heat treatment at 800°C for 3 h. The measurement was done by using K_α radiation under an accelerating voltage of 80-100 kV and current of 24-30 mA.

3.6.1.2 Thermal properties

The decomposition temperature and weight loss of ES, ESP, HT-ES (white portion), and commercial CaCO₃, were monitored by thermogravimetric analyzer (TGA, Mettler Toledo, TGA/DSC1). The characterization was performed at temperature between 30°C and 1,100°C with a heating rate of 20°C/min under a nitrogen atmosphere. The sample weight of the examination was approximately between 15 and 25 mg.

3.6.1.3 Particle size and size distribution

The particle size and size distribution of ESP1, ESP2, and HT-ESP1 were characterized via particle size analyzer (Malvern, Mastersizer S) with a range lens of 300RF and a beam length of 2.40 mm. Water was used as medium for characterization. In addition, the particle size and size distribution of commercial CaCO₃ obtained after sieving were determined as well.

3.6.1.4 Particle morphology

The morphology of ESP1, ESP2, HT-ESP1, and commercial CaCO₃ was investigated by scanning electron microscope (SEM, JEOL, JSM-6400) with an accelerating voltage of 20 kV. The samples were coated with gold using an ion sputtering device (JEOL, JFC-1100E) for 6 min at a current of 10 mA before examination in order to avoid charging under an electron beam and make them electrically conductive.

3.6.2 Characterization of HDPE composites

3.6.2.1 Rheological properties

According to ASTM D 1238, MFI of HDPE and all HDPE composites were determined via a melt flow indexer (Kayeness, D4004HV) at 190°C with a standard weight of 2.16 kg. The sample was preheated about 5 min before the weight was introduced onto the piston. After the sample flow through the die, it was cut at a desired period of time and then weighed.

The apparent shear viscosity of HDPE and the HDPE composites at a shear rate range of 12.16-4256.46 s⁻¹ were also measured using a capillary rheometer (Kayeness, D5052M) at a melting temperature of 190°C and a melting time of 5 min before measuring.

3.6.2.2 Mechanical properties

Tensile properties of HDPE and the HDPE composites were determined in accordance with ASTM D 638 (Type I specimens) using a universal testing machine (Instron, 5565). The specimen was tested at a crosshead speed of 10 mm/min under a load cell of 5 kN and a gauge length of 50 mm. The dimensions of test specimens were 12.7 mm in width, 3.6 mm in thickness, and 165 mm in length. At least five specimens were tested. The images of tensile specimens prepared by injection molding machine were shown in Figure 3.2.

Flexural properties of HDPE and the HDPE composites were tested according to ASTM D 790 (Procedure B) using a universal testing machine (Instron, 5565) at a crosshead speed of 17 mm/min under a load cell of 5 kN and a fixed span length of 64 mm. The dimensions of test specimens were 127 mm in length, 13 mm in width, and 4 mm in depth.

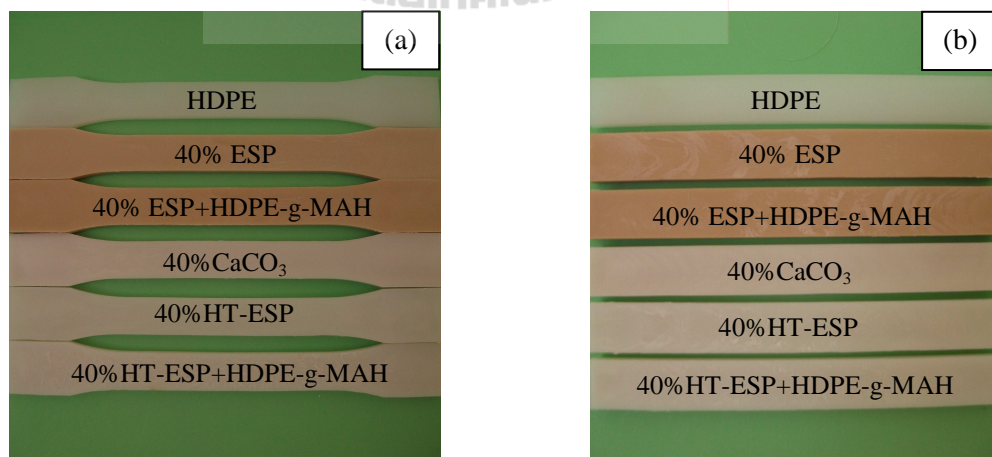


Figure 3.2 Images of test specimens for tensile test (a) and flexural test (b) of HDPE and HDPE composites.

Unnotched Izod impact strength of HDPE and the HDPE composites was evaluated on a pendulum impact tester (Atlas, BPI) following ASTM D 256. The dimensions of test specimens were 3.55 mm in width, 12.80 mm in depth, and 62.5 mm in length, as shown in Figure 3.3. At least five specimens were tested and the average impact strength was calculated.

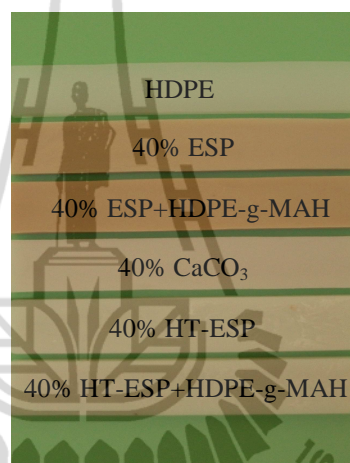


Figure 3.3 Images of test specimens for impact test of HDPE and HDPE composites.

For hardness test of HDPE and HDPE composites, the sample was indented using a durometer hardness tester following ASTM D 2240 (Shore D).

3.6.2.3 HDT

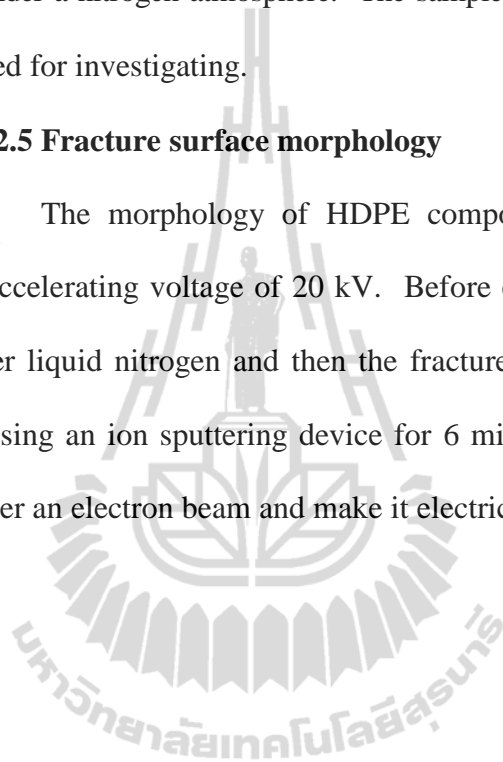
The HDT of HDPE and the HDPE composites was evaluated using heat distortion temperature instrument (HDV 1 Manual DTVL/VICAT). The measurement was operated under a heating rate of 2°C/min and a specified applied stress of 0.455 MPa in accordance with ASTM D 648 (Method B).

3.6.2.4 Thermal properties

Thermal properties of HDPE and the HDPE composites were investigated by TGA. The sample was heated from 30°C to 1,100°C with a heating rate of 20°C/min under a nitrogen atmosphere. The sample of ground composite about 15 – 25 mg was used for investigating.

3.6.2.5 Fracture surface morphology

The morphology of HDPE composites was investigated by SEM operated at accelerating voltage of 20 kV. Before examination, the composite was fractured under liquid nitrogen and then the fracture surface of specimens was coated with gold using an ion sputtering device for 6 min at a current of 10 mA to avoid charging under an electron beam and make it electrically conductive.



CHAPTER IV

RESULTS AND DISCUSSION

4.1 Characterization of ESP and HT-ES

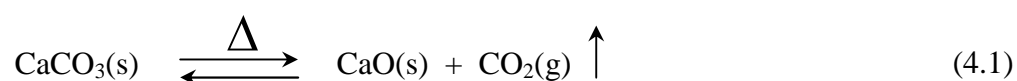
4.1.1 Crystal form of ESP and HT-ES by XRD

4.1.1.1 Crystal form of ESP

XRD patterns of ESP and commercial CaCO₃ were illustrated in Figure 4.1. The strongest peak of the CaCO₃ occurred at 2θ of 29.5°. The XRD pattern of ESP was well matched with that of the commercial CaCO₃. Its pattern is characteristic of calcite which has rhombohedral hexagonal axes structure (a = 4.9887, b = 4.9887, c = 17.0529, α = 90°, β = 90°, γ = 120°) (JCPD number 01-083-0577).

4.1.1.2 Chemical composition of HT-ES

XRD patterns of HT-ES prepared at 650°C for 16 h, 20 h, and 24 h are shown in Figure 4.2. It should be noted that when the ES was treated at 650°C for less than 16 h, the treated ES was black in color because of the incomplete decomposition of matrix protein and ESM. The XRD patterns of the HT-ES prepared at 650°C for 16 h composed of three components, CaO, Ca(OH)₂, and CaCO₃. However, the HT-ES prepared at 650°C for 20 and 24 h comprised only CaO and Ca(OH)₂. The CaO was derived from decomposition of CaCO₃ as the following equation (4.1).





However, when the treated ES was exposed to atmosphere, it adsorbed moisture. The adsorbed water reacted with the CaO giving rise to Ca(OH)₂ as shown in equation (4.2). With increasing treatment time, the CaCO₃ content significantly decreased but the CaO content increased. The CaCO₃ almost completely decomposed after 16 h treatment time.

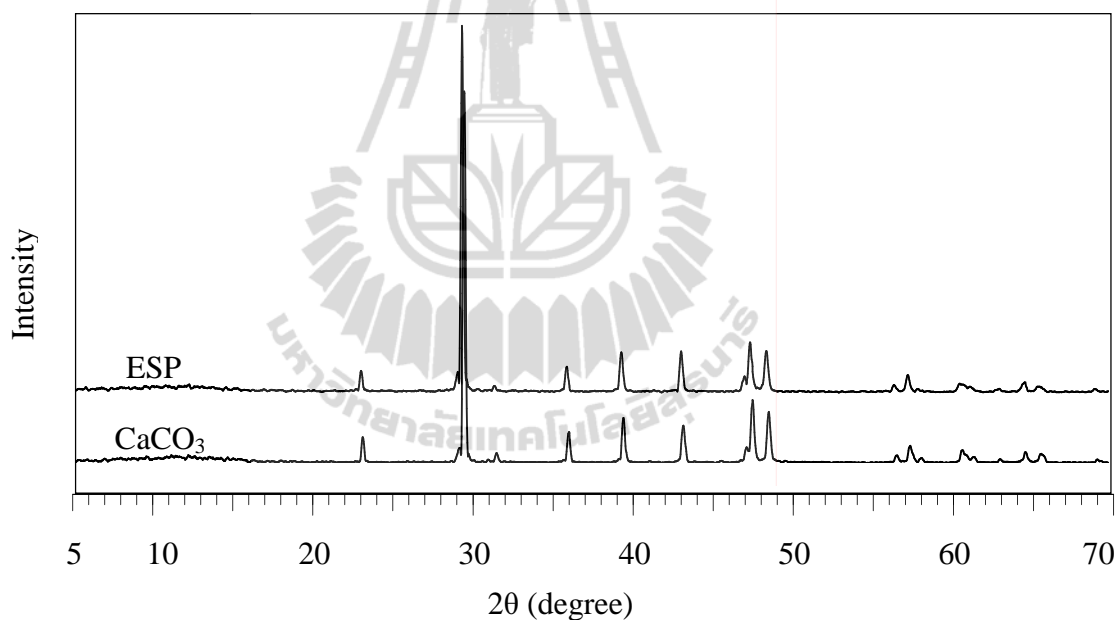


Figure 4.1 XRD patterns of ESP and commercial CaCO₃.

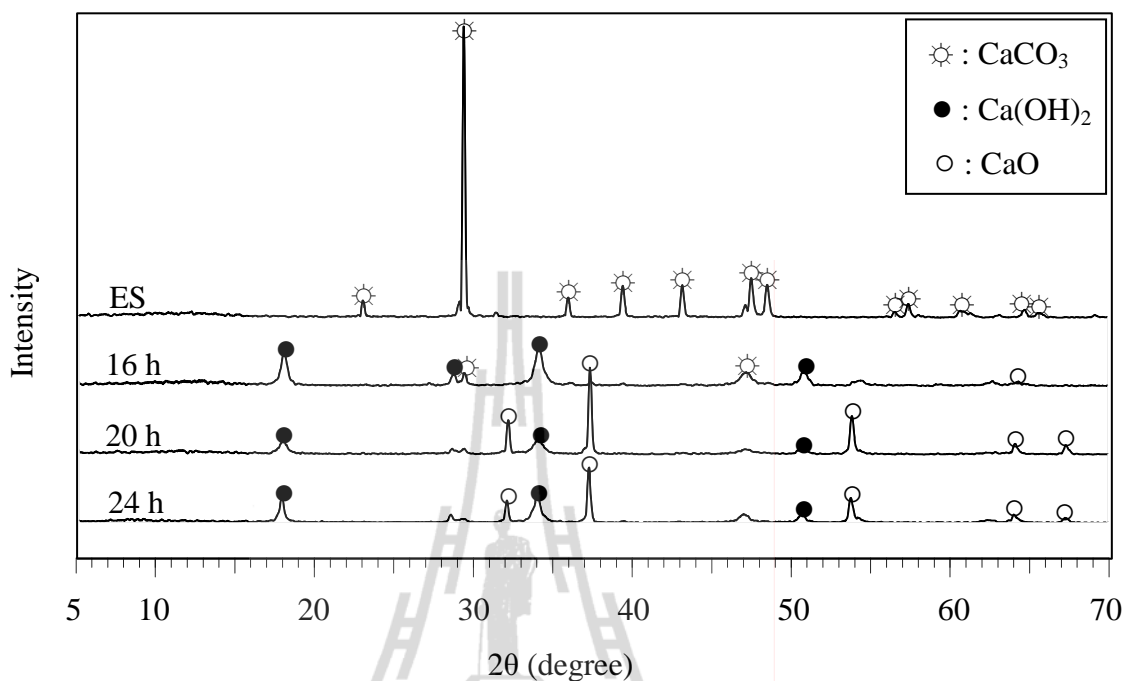


Figure 4.2 XRD patterns of HT-ES prepared at 650°C for 16, 20, and 24 h.

XRD patterns of HT-ES prepared at 670°C for 12 and 16 h are shown in Figure 4.3. When ES was heated at 670°C for less than 12 h the treated ES was black. The ES treated at 12 h composed of three components, CaO, Ca(OH)₂, and CaCO₃. It was clearly observed that the treated ES prepared at 670°C for 16 h comprised two main components, CaO and Ca(OH)₂. The calcination of CaCO₃ was almost completely at treatment time of 16 h.

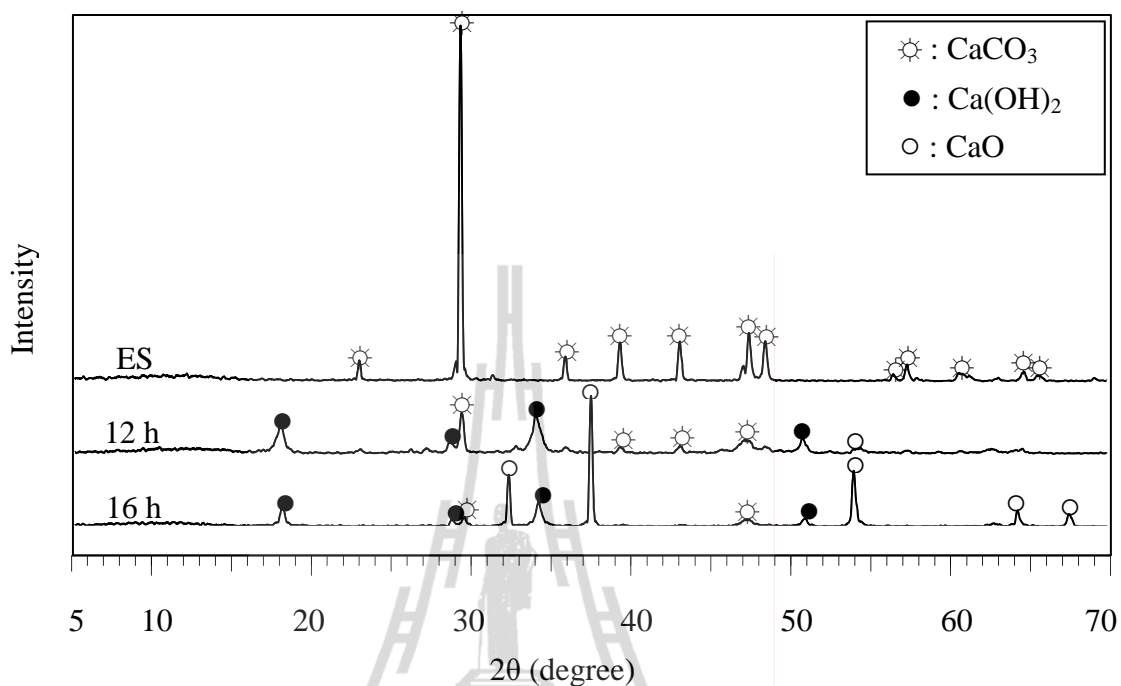


Figure 4.3 XRD patterns of HT-ES prepared at 670°C for 12 and 16 h.

XRD patterns of HT-ES prepared at 770°C for 4 and 6 h are illustrated in Figure 4.4. The ES was also treated for 3 h; however, the organic substances were not completely removed indicated by black color of the treated ES. The patterns presented that the treated ES composed of two chemicals, CaO and Ca(OH)₂. It was obviously seen that CaCO₃ was entirely decarbonated at 4 h.

When the ES was treated at 800°C for 3, 4, and 5 h, the characteristic peaks of CaCO₃ were not observed, as shown in Figure 4.5. The decarbonation of CaCO₃ was complete at treatment time of 3 h. The composition of the treated ES was CaO and Ca(OH)₂.

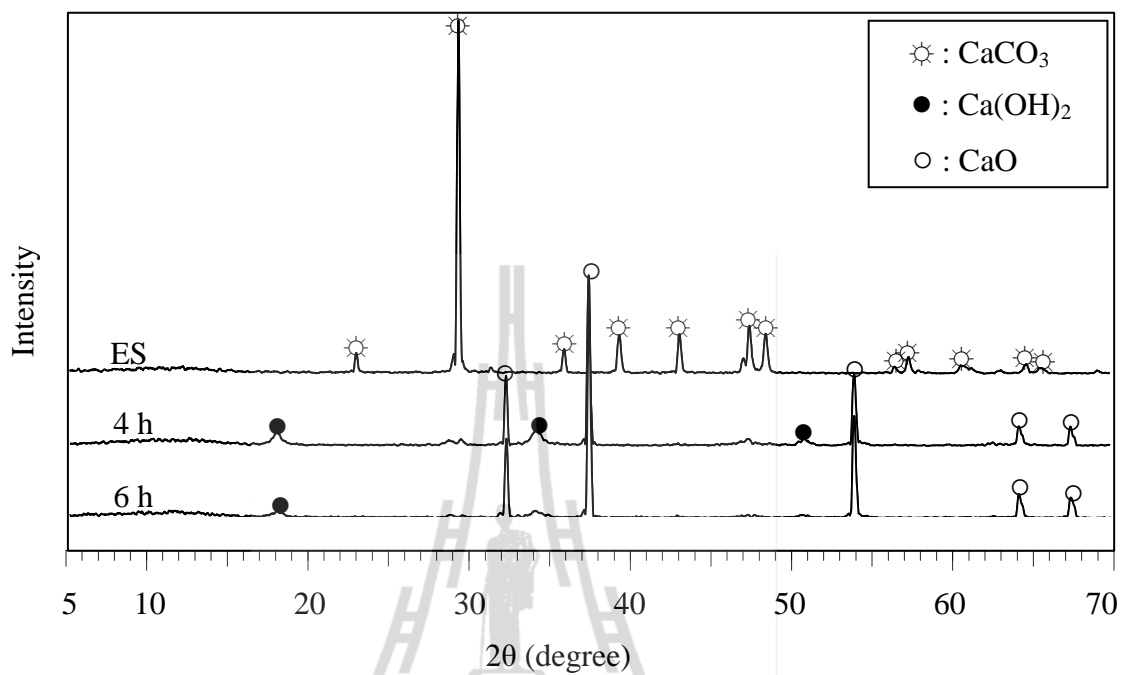


Figure 4.4 XRD patterns of HT-ES prepared at 770°C for 4 and 6 h.

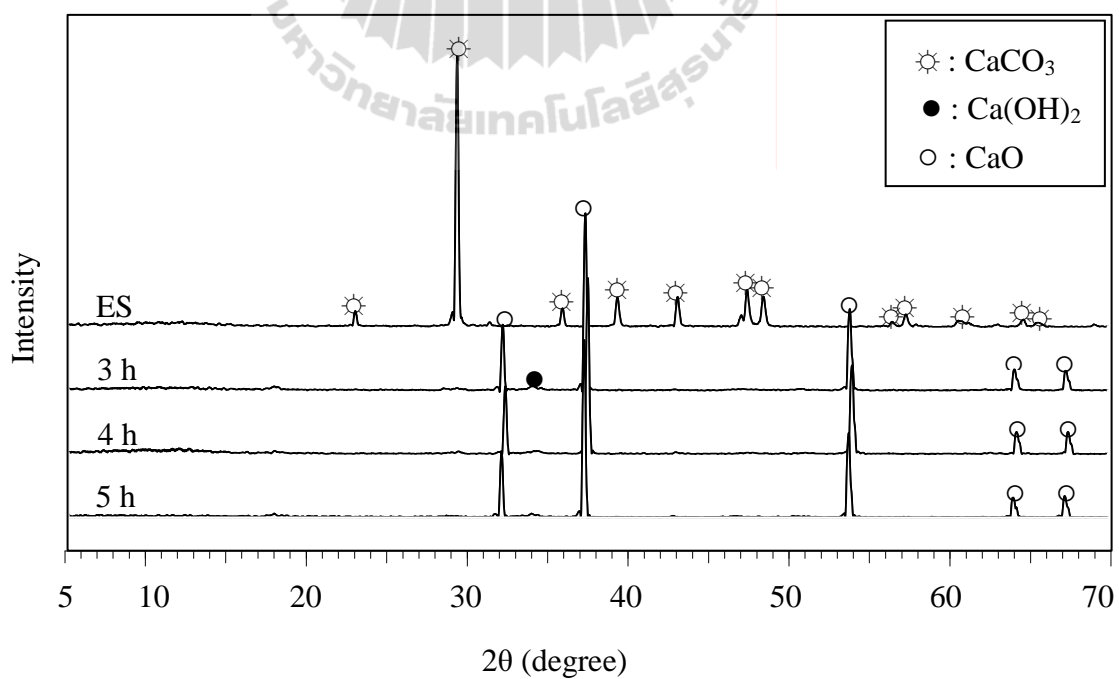


Figure 4.5 XRD patterns of HT-ES prepared at 800°C for 3, 4, and 5 h.

Note that, the removal of organic substances deposited in ES by being treated at 650°C and 670°C required the longer time than treated at 770°C and 800°C. This was because the treatment temperatures at 770°C and 800°C were close to the decomposition temperature of CaCO_3 and were much higher than the decomposition temperature of organic substances.

In summary, when the treatment time was increased, more CaO was obtained, and more organic substances were removed. The shortest duration for removing organic substances and obtaining high content of CaO was 3 h when ES was treated at 800°C.

4.1.2 Chemical composition of ESP and HT-ES by XRF

The elements of ESP and HT-ES prepared at 800°C for 3 h determined by XRF is shown in Table 4.1. Ca content in ES was 38 wt%. It was also previously reported that Ca content of chicken ES was 37.7-38.0 wt% (Masuda and Hiramatsu, 2008; Suguro et al., 2000). The Ca content of HT-ES prepared at 800°C for 3 h was 2 times higher than that of ES. This was because the organic substances were removed and the main component in HT-ES was CaO. In addition, other minor components in ESP and HT-ES were Mg, Na, S, P, K, and Cl and trace amount of Al, Si, Fe, Ni, Zn, and Sr.

Table 4.1 Elemental analysis of ESP and HT-ES at 800°C for 3 h.

Elements	Content (wt%)	
	ESP	HT-ES (800°C, 3 h)
Ca	38.04	70.01
Mg	0.31	0.62
Na	0.07	0.14
S	0.15	0.11
P	0.11	0.22
K	0.03	0.03
Cl	0.02	<0.01
Al	<0.01	<0.01
Si	<0.01	<0.01
Fe	<0.01	<0.01
Ni	<0.01	<0.01
Zn	<0.01	<0.01
Sr	<0.01	0.01

4.1.3 Thermal properties

4.1.3.1 Thermal properties of ES and ESP

TGA and DTGA curves of ES, ESP, ESM, and commercial CaCO_3 are shown in Figure 4.6. From TGA and DTGA curves, the commercial CaCO_3 decomposed at 790°C. The decomposition reaction of the CaCO_3 is as shown in equation (4.1). After the complete decomposition, CaO was left about 55 wt% and carbon dioxide (CO_2) was released about 45 wt%.

The TGA and DTGA of ESM show two decompositions at 245°C and 333°C. This was due to the different organic components containing in ESM. The decomposition temperature of ESM previously reported was between 200°C and 350°C (Dong, Su, Xu, Zhang, and Wang, 2007). The transition at 72°C was due to the removal of adsorbed water.

The TGA and DTGA curves of ES and ESP show three thermal transitions. The first transition at 50-60°C resulted from the water evaporation (Freire and Holanda, 2006). The second transition occurred at 320-326°C and the third transition at 789-800°C. The second transition was derived from the decomposition of organic substances deposited in both ESM and ES matrix. The transition at about 800°C was caused by the decomposition of CaCO₃. The decomposition of CaCO₃ deposited in ES was 10°C higher than that of commercial CaCO₃ because of the organic substances containing in ES matrix. It was previously reported that the CaCO₃ deposited in ES decomposed at about 30°C higher than commercial CaCO₃ (Murakami et al., 2007). However, the CaCO₃ decomposition temperature of ESP was close to the decomposition temperature of the commercial CaCO₃ because some organic substances were removed out from the ES by grinding and sieving process. The CaCO₃ decomposition temperature of ESP was lower than that of ES because the decomposition temperature of CaCO₃ depended on amount of matrix protein and ESM existing as impurities (Singh, N. B., and Singh, N. P., 2007).

For the TGA curve of ES, it shows about 1 wt% of adsorbed water and 4 wt% of organic substances. The ES composed of 95 wt% CaCO₃ which was in good agreement with CaCO₃ content, 94-98 wt%, in avian ES (Daengprok et al., 2002; Heredia et al., 2005; Hincke et al., 2000; Hunton, 2005; Nys and Gautron,

2007; Stadelman, 2000). In addition, the residue as stable CaO was about 52 wt%. The transition temperature and weight loss of commercial CaCO₃, ES, and ESP were summarized in Table 4.2.

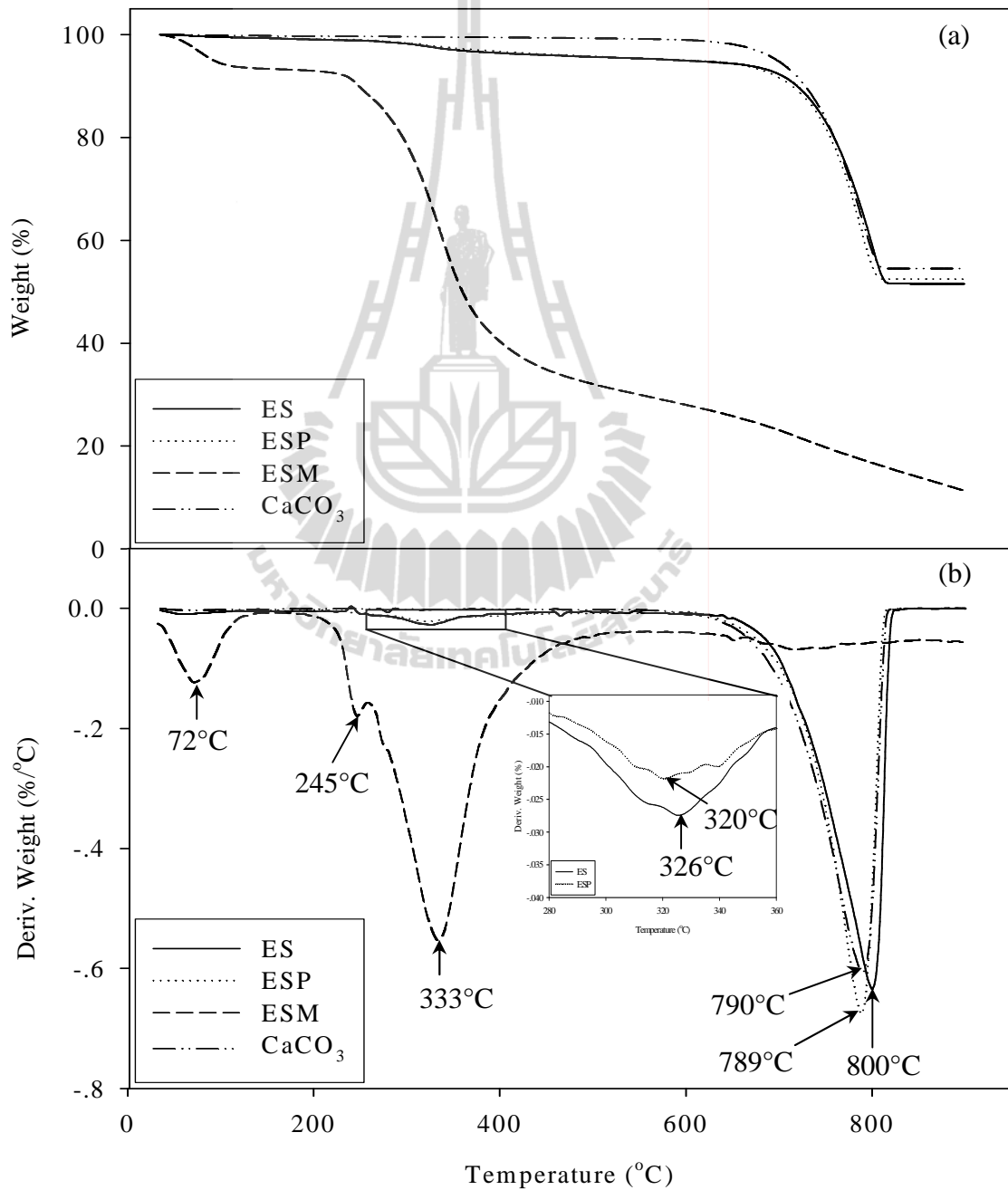
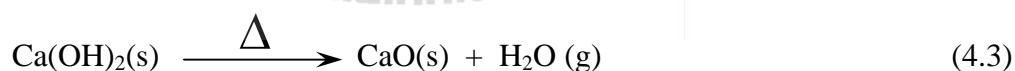


Figure 4.6 TGA (a) and DTGA (b) curves of ES, ESP, ESM, and commercial CaCO₃.

4.1.3.2 Thermal properties of HT-ES

TGA and DTGA curves of HT-ES prepared at 650°C for 16 h, 20 h, and 24 h were shown in Figure 4.7. The decomposition peak of organic substances was not observed from the curves of HT-ES. It confirmed that the organic substances were entirely removed from ES by the heat treatment at 650°C for 16-24 h. The DTGA curves of HT-ES show three transitions. The first transition, 70-80°C, was resulted from moisture removal. The weight loss according to water evaporation was 1 wt%. The second transition occurred at 444°C for 16 h, 440°C for 20 h, and 445°C for 24 h. This transition was derived from dehydration of Ca(OH)₂. It was previously reported that the dehydration of Ca(OH)₂ was taken place at 350-600°C, depending on the moisture content in testing atmosphere (Irabien, Viguri, and Ortiz, 1990). The dehydration reaction of Ca(OH)₂ was shown in equation (4.3).



The weight loss of this transition was about 18 wt%, 16 wt%, and 14 wt% for HT-ES prepared at 650°C for 16, 20, and 24 h, respectively. The third transition occurred at a temperature of 670-700°C. The weight loss of the third transition was in a range of 6-11 wt%. The possible way to explain this transition was derived from two main reasons. First, it was due to the decomposition of CaCO₃ left after the heat treatment (Singh and Singh, 2007). The second transition was caused by the decomposition of in-growth of CaCO₃ formed by the reaction between HT-ES and CO₂ during the heating under atmosphere (Marra et al., 1999). Since, the TGA experiment was

performed under a nitrogen atmosphere; therefore, the third transition must be derived from the decomposition of CaCO_3 left after the heat treatment. The complete decomposition of HT-ES, CaO was left about 70-80 wt%. The transition temperature and weight loss of the treated ES at 650°C were summarized in Table 4.2.

TGA and DTGA curves of HT-ES prepared at 670°C for 12 h and 16 h are shown in Figure 4.8. The TGA and DTGA curves show three thermal transitions. The first transition appeared at about 70-80°C caused by moisture evaporation. The weight loss by the evaporation was 1 wt%. The second transition was due to the decomposition of Ca(OH)_2 occurring around 440-445°C. The weight loss derived from decomposed Ca(OH)_2 was 10-15 wt%. The third transition was due to the decomposition of CaCO_3 appearing at 732°C for treatment time of 12 h, and 683°C for 16 h. The weight loss of this transition was in a range of 5-15 wt%. The transition temperature and weight loss of the treated ES at 670°C were summarized in Table 4.2.

Figure 4.9 shows TGA and DTGA curves of HT-ES prepared at 770°C for 4 h and 6 h. The TGA and DTGA show three thermal transitions. The first transition showed the evaporation of water around 65-82°C. The weight loss of water was 1-2 wt%. The second transition was due to the decomposition of Ca(OH)_2 at about 430-440°C. The weight loss due to Ca(OH)_2 decomposition was about 23 wt%. The final transition was attributed to the decomposition of CaCO_3 at about 600-615°C. The weight loss for this decomposition was 2-3 wt%. The transition temperature and weight loss of the treated ES were summarized in Table 4.2.

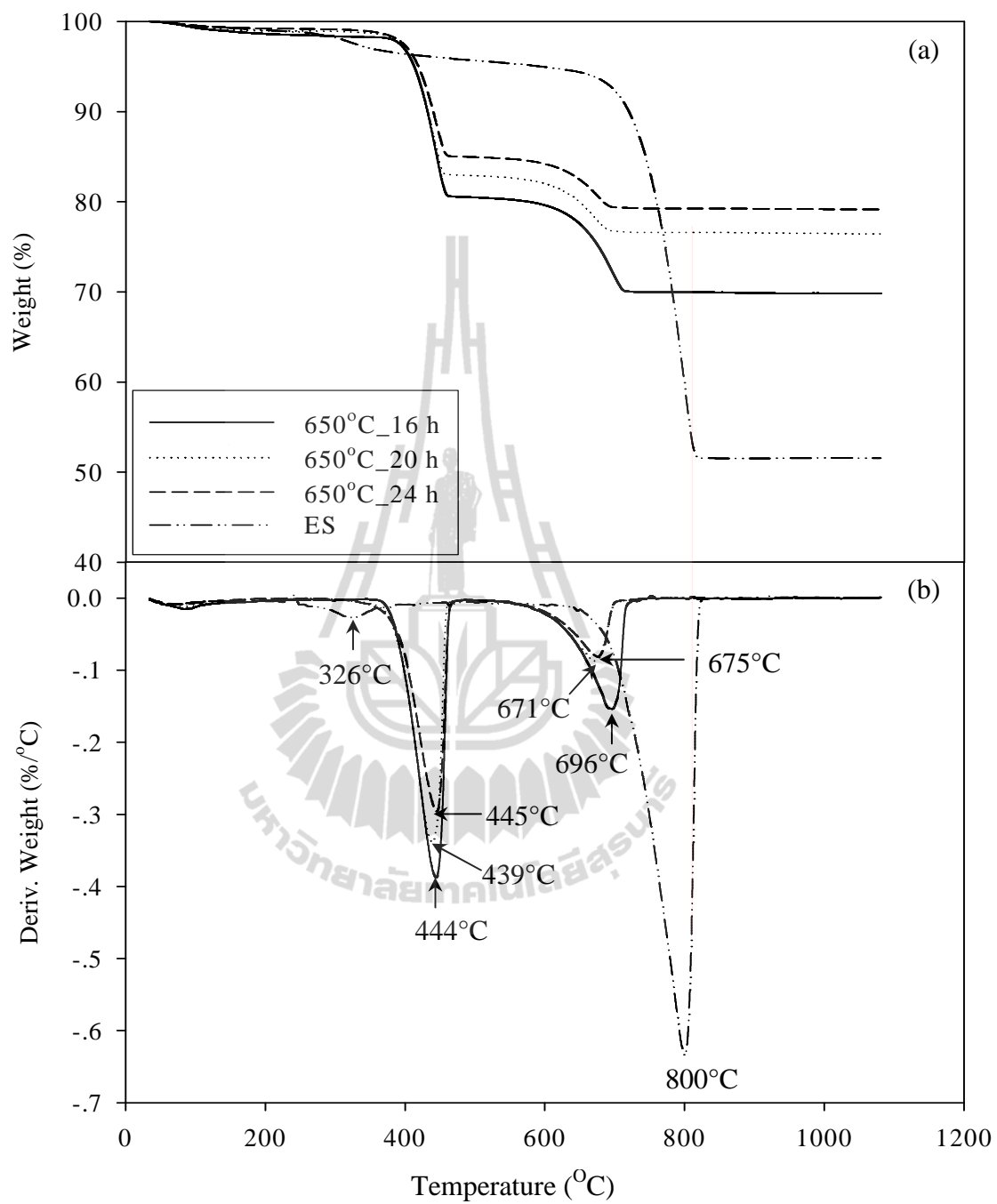


Figure 4.7 TGA (a) and DTGA (b) curves of HT-ES prepared at 650°C for 16 h, 20 h, and 24 h.

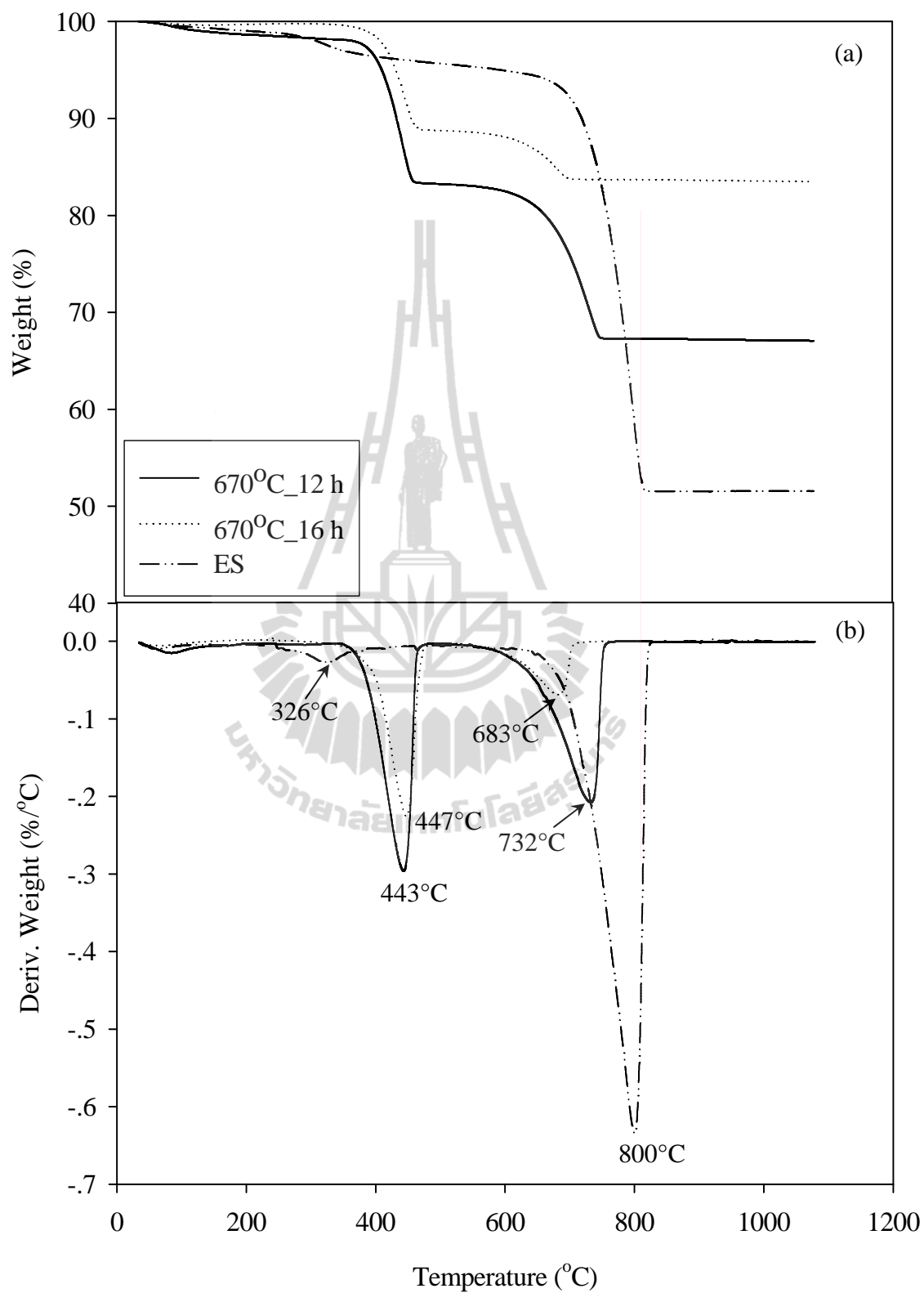


Figure 4.8 TGA (a) and DTGA (b) curves of HT-ES prepared at 670°C for 12 h and 16 h.

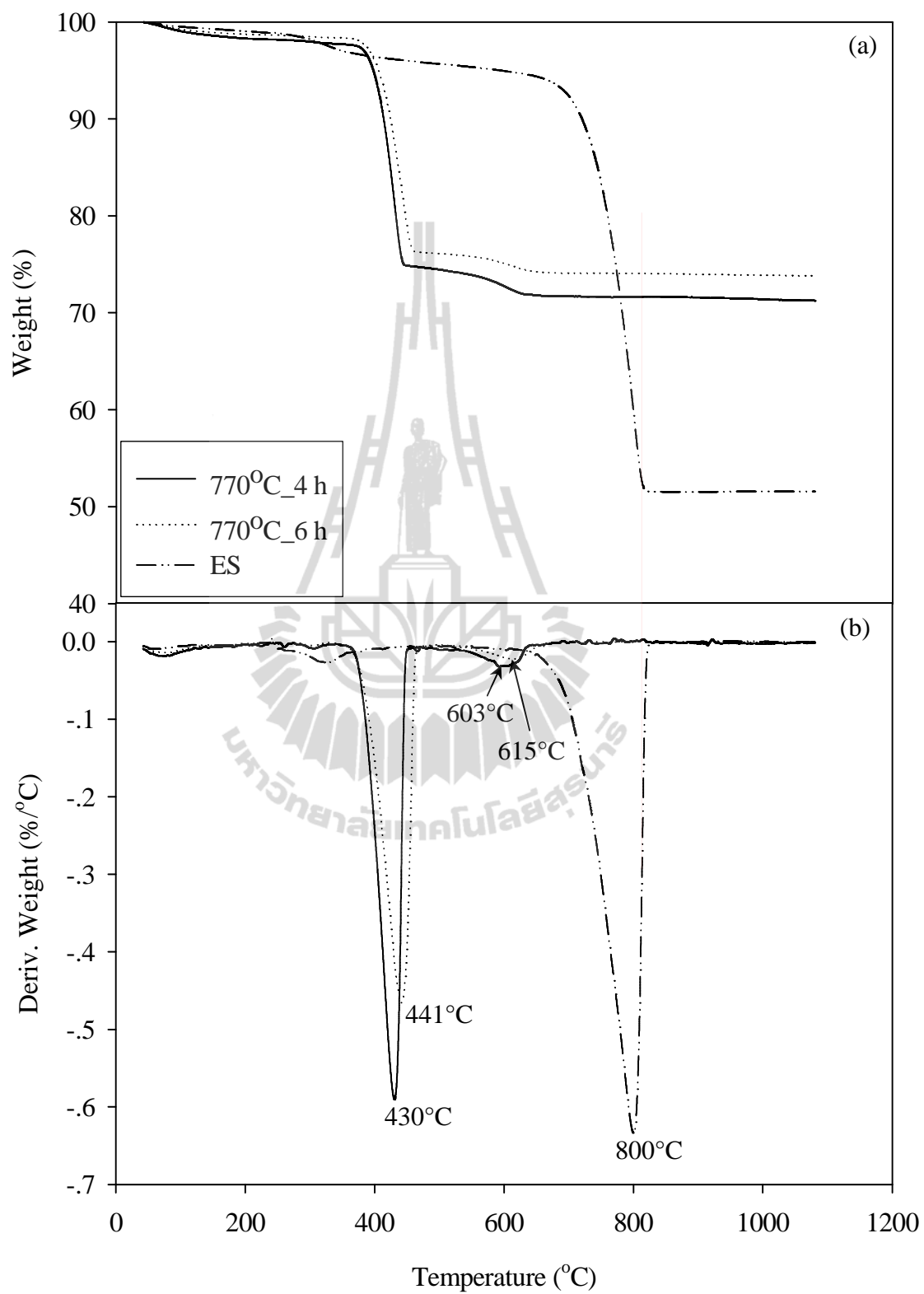


Figure 4.9 TGA (a) and DTGA (b) curves of HT-ES prepared at 770°C for 4 h and 6 h.

TGA and DTGA curves of HT-ES prepared at 800°C for 3 h, 4 h, and 5 h are shown in Figure 4.10. The TGA and DTGA curves display three thermal transitions. The first transition by the evaporation of water occurred at 70-80°C with the weight loss of about 1-2 wt%. The second transition at about 440°C was caused by decomposition of Ca(OH)_2 with the weight loss of 23 wt%. The third transition around 610-620°C was due to the decomposition of CaCO_3 .

It should be noted that the decomposition temperature of CaCO_3 of HT-ES shifted to a lower temperature compared to commercial CaCO_3 . This was because it was initiated by the decomposition of Ca(OH)_2 . In addition, the decomposition peak of CaCO_3 was all observed from DTGA curves of HT-ES but CaCO_3 of some HT-ES was not detected by XRD. This is because the sensitivity of thermogravimetric analysis is better than X-ray diffraction spectroscopy especially when the detected substance is lower than 5 wt%.

The TGA confirms that the main composition of ES and ESP was CaCO_3 and the main compositions of HT-ES are two calcium compounds as Ca(OH)_2 and CaO . The organic substances as shell membrane and matrix protein were entirely removed by the treatment at 770°C for 4 h. The shortest treatment time to remove organic substances and to obtain CaO was 3 h at the treatment temperature of 800°C. Therefore, the treatment condition at 800°C for 3 h was employed to prepare HT-ES for further use as reinforcing filler in HDPE composites.

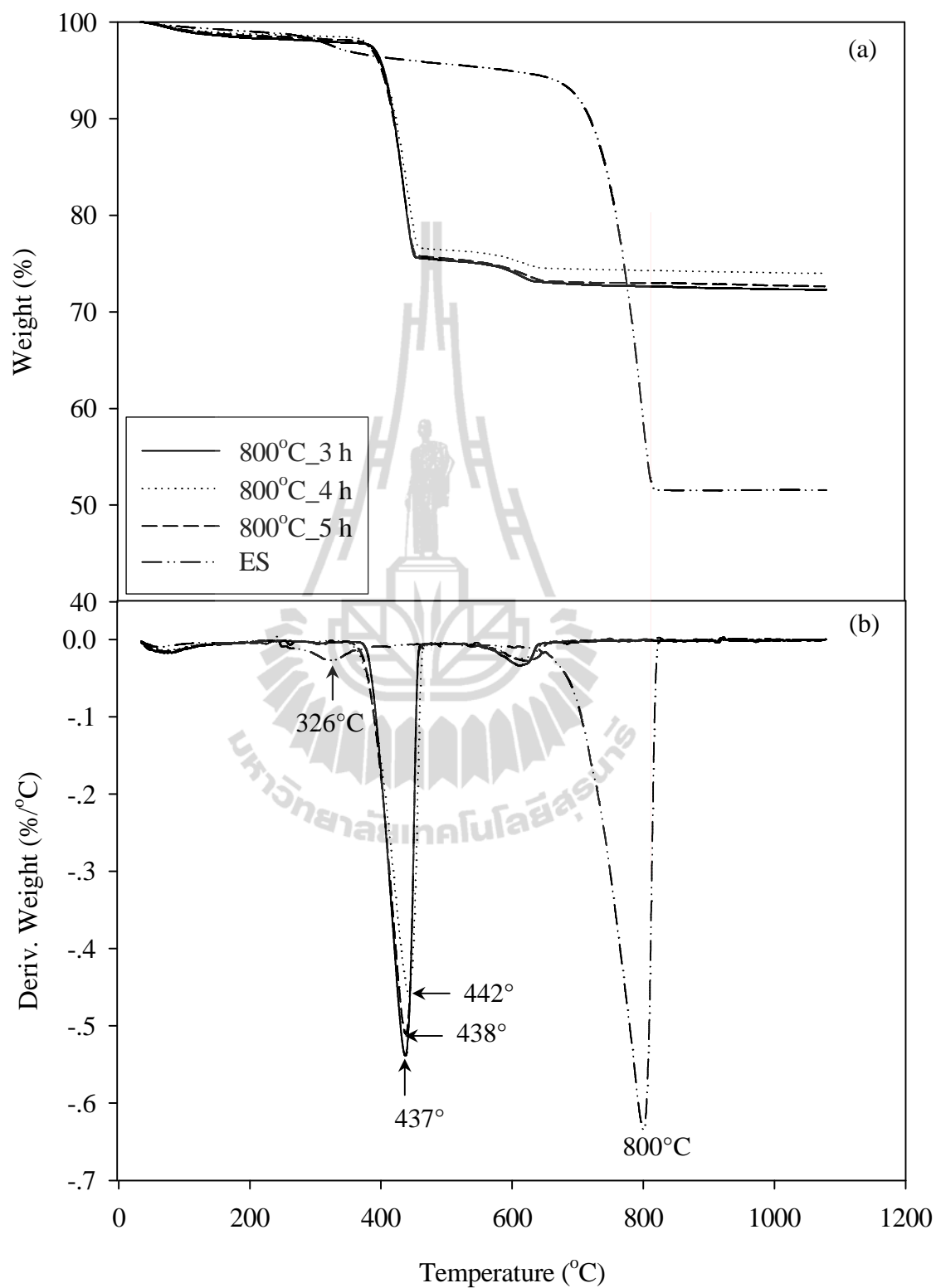


Figure 4.10 TGA (a) and DTGA (b) curves of HT-ES prepared at 800°C for 3 h, 4 h, and 5 h.

Table 4.2 Peak temperature (T_{peak}) and weight loss of ES, ESP, commercial CaCO_3 , and HT-ES at various treatment temperatures and times.

Material	Water evaporation		Organic decomposition		$\text{Ca}(\text{OH})_2$ decomposition		CaCO_3 decomposition		Final weight (%)
	T_{peak} ($^{\circ}\text{C}$)	Weight loss (%)	T_{peak} ($^{\circ}\text{C}$)	Weight loss (%)	T_{peak} ($^{\circ}\text{C}$)	Weight loss (%)	T_{peak} ($^{\circ}\text{C}$)	Weight loss (%)	
ES	55	1	326	4	-	-	800	45	52
ESP	60	1	320	4	-	-	789	45	52
Commercial CaCO_3	-	-	-	-	-	-	790	45	54
HT-ES (650 $^{\circ}\text{C}$, 16 h)	83	1	-	-	444	18	696	11	70
HT-ES (650 $^{\circ}\text{C}$, 20 h)	82	1	-	-	439	16	671	6	77
HT-ES (650 $^{\circ}\text{C}$, 24 h)	69	1	-	-	445	14	675	6	79
HT-ES (670 $^{\circ}\text{C}$, 12 h)	84	1	-	-	443	16	732	16	67
HT-ES (670 $^{\circ}\text{C}$, 16 h)	70	<1	-	-	447	11	683	5	84
HT-ES (770 $^{\circ}\text{C}$, 4 h)	65	2	-	-	430	23	603	3	72
HT-ES (770 $^{\circ}\text{C}$, 6 h)	82	1	-	-	441	23	615	2	74
HT-ES (800 $^{\circ}\text{C}$, 3 h)	74	2	-	-	437	23	611	3	72
HT-ES (800 $^{\circ}\text{C}$, 4 h)	80	1	-	-	442	22	613	3	74
HT-ES (800 $^{\circ}\text{C}$, 5 h)	69	1	-	-	438	23	621	3	73

4.1.4 Particle size and size distribution

The particle size and size distribution of ESP before and after sieving and HT-ESP prepared at 800°C for 3 h after sieving were shown in Table 4.3. The ESP before sieving had D_{50} of 12.7 μm with a particle size range of 0.9-124 μm . The ESP after sieving with test sieve of 325-230 mesh (ESP1) had D_{50} of 17.1 μm with a range of 0.7-113 μm . Comparatively, the D_{50} of commercial CaCO_3 was 20 μm with a particle size range of 0.6-121 μm . D_{50} of ESP2, ESP after sieving with test sieve of 500-450 mesh, was 14.4 μm and a particle size range of 0.9-60 μm . The size distribution of ESP2 was narrower than that of ESP1 as observed from size distribution curve of ESP1 and ESP2 in Figure 4.11.

For the HT-ESP after sieving with test sieve of 325-230 mesh (HT-ESP1), the D_{50} was 4.6 μm with a particle size range of 0.14-20.3 μm . The size distribution of HT-ESP1 was quite homogeneous and narrow. The large particles might be formed by the agglomeration of primary particles as observed from SEM micrograph in Figure 4.11 (b) and (c).

Table 4.3 The particle size and size distribution of ESP before and after sieving, HT-ESP (800°C for 3 h), and commercial CaCO₃.

Material	Sieve no.	Particle size and size distribution						
		D ₁₀	D ₅₀	D ₉₀	D _[4,3]	D _[3,2]	Range	Span
ESP	before sieving	2.2	12.7	61.5	23.6	6.1	0.9-124	4.68
ESP1	325-230 [†]	2.7	17.1	56.1	24.1	7.3	0.7-113	3.12
ESP2	500-450 [‡]	3.4	14.4	34.4	16.9	8.0	0.9-60	2.15
HT-ESP1	325-230 [†]	0.4	4.6	10.7	5.1	1.5	0.14-20.3	2.25
CaCO ₃	500-450 [‡]	2.6	20.0	64.6	27.6	7.2	0.6-121	3.10

Remarks : † = mesh size (45-63 μm)

‡ = mesh size (25-32 μm)

4.1.5 Morphology of ESP and HT-ESP

SEM micrographs of ESP1, ESP2, commercial CaCO₃, and HT-ESP1 are shown in Figure 4.11. The SEM micrograph of the commercial CaCO₃ shows the typical morphology of calcite which is in cubic shape with sharp defined edge and smooth surface. On the other hand, the edge of ESP1 and ESP2 particles were not as sharp as and as smooth as that of the commercial CaCO₃. Furthermore, the surface of ESP1 and ESP2 was covered by thin porous layer. This layer might be the matrix protein left after the milling step. In addition, more particles in round shape and narrower size distribution were obtained after sieving with sieve of 500-450 mesh no. The SEM micrograph of HT-ESP1 shows very fine particles in round shape and homogeneous size distribution. In addition, the particles of HT-ESP1 formed the agglomeration.

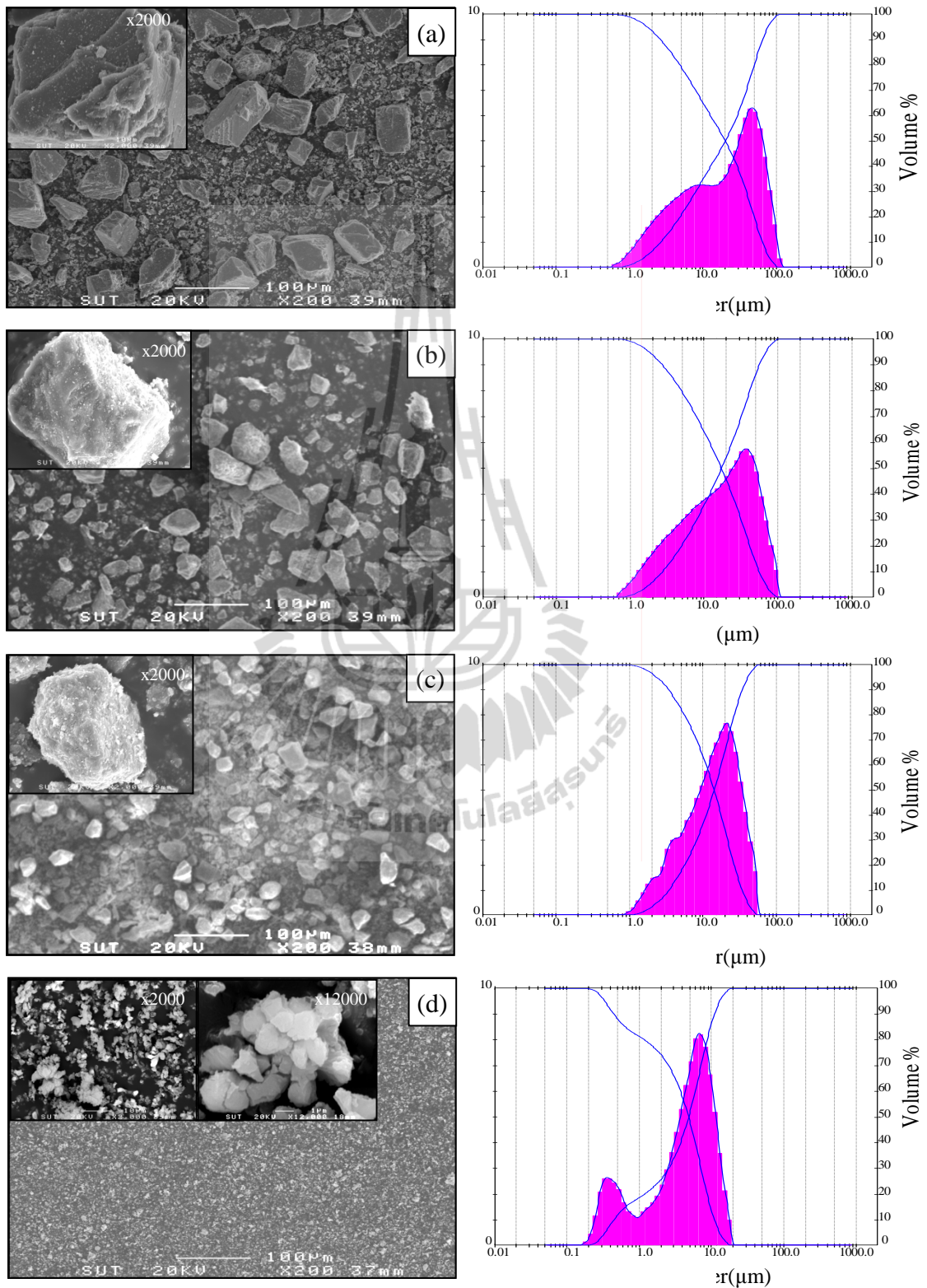


Figure 4.11 SEM micrographs (x200) and size distribution curves of commercial CaCO_3 (a), ESP1 (b), ESP2 (c), and HT-ESP1 (d).

4.2 Characterization of HDPE composites from ESP

4.2.1 Effect of ESP content on physical properties of HDPE composites

4.2.1.1 Rheological properties

The dependence of apparent shear viscosity on apparent shear rate of neat HDPE, ESP1/HDPE composites, and CaCO₃/HDPE composites is illustrated in Figure 4.12. The apparent shear viscosity of the HDPE composites was higher than that of neat HDPE and the apparent shear viscosity of HDPE composites increased with increasing ESP1 and CaCO₃ content. This was due to the more content the filler, the shorter the particle-particle distance caused by more content of the fillers. Therefore, the molten HDPE was more obstruct to flow. In addition, the apparent shear viscosity of the HDPE and the HDPE composites decreased with increasing apparent shear rate. This was attributed to more polymer chains alignment in the direction of shear at high shear rate resulting in better molecular flow ability of polymer molecules, the lower the viscosity. With the inclusion of ESP1 and CaCO₃, HDPE composites still behaved like a pseudoplastic material as neat HDPE did. In addition, the apparent shear viscosity of ESP1/HDPE and CaCO₃/HDPE composites was in the same range. It should be noted that the difference in apparent shear viscosity between neat HDPE and the HDPE composites at 10 wt% ESP1 was lower than that between neat HDPE and the HDPE composites at 10 wt% CaCO₃. This might be due to the less cube and higher surface porosity of ESP1 particles as compared with that of CaCO₃ particles gave rise to enhancement of fluid flow ability.

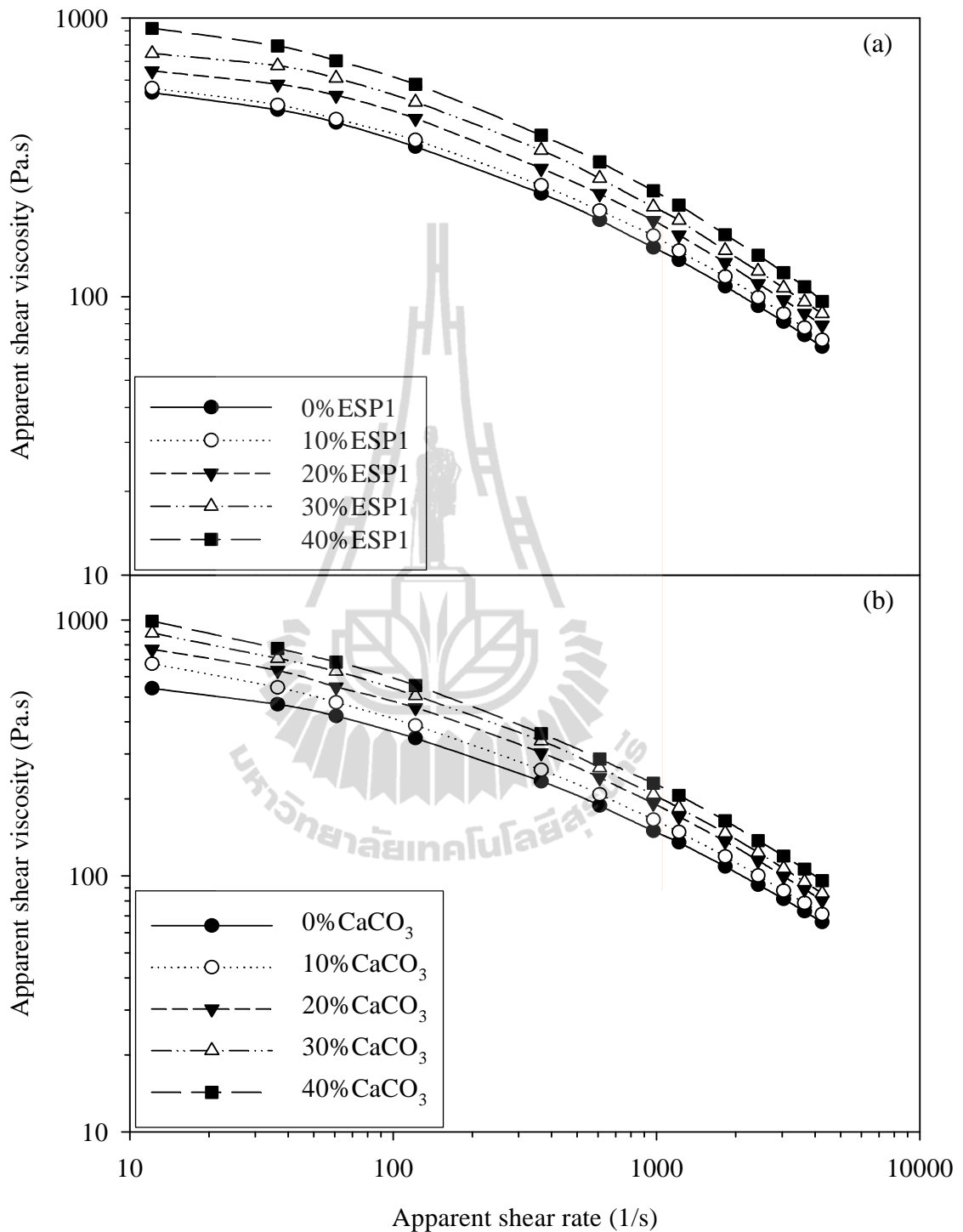


Figure 4.12 Plot of apparent shear viscosity as a function of apparent shear rate of ESP1/HDPE composites (a) and CaCO₃/HDPE composites (b) at various contents of ESP1 and CaCO₃.

MFI of neat HDPE, ESP1/HDPE composites, and CaCO₃/HDPE composites at various filler contents is shown in Table 4.4. The MFI of HDPE was higher than that of ESP1/HDPE and CaCO₃/HDPE composites. The MFI of the composites decreased with increasing content of ESP1 and CaCO₃. The decrease in MFI of chalk/HDPE composites with increasing content of chalk (96.8% of CaCO₃) had also been reported (Domka, Wąsicki, and Kozak, 2003). Comparatively, the MFI of ESP1/HDPE composites and CaCO₃/HDPE composites was insignificantly different.

Table 4.4 MFI of neat HDPE, ESP1/HDPE composites, and CaCO₃/HDPE composites.

ESP1 or CaCO ₃ content (wt%)	MFI (g/10 min)	
	ESP1/HDPE composites	CaCO ₃ /HDPE composites
0	12.4	12.4
10	12.2	11.4
20	11.0	10.3
30	9.8	9.3
40	8.3	8.4

4.2.1.2 Thermal properties

TGA and DTGA curves of HDPE and ESP1/HDPE composites are presented in Figure 4.13. From the TGA and DTGA curves, the thermal degradation of HDPE composites differed from that of neat HDPE. The neat HDPE decomposed with single transition at 493°C whereas the HDPE composites showed three transitions. The first transition at about 320-340°C was the decomposition of

organic substances embedded in both ESM and ES matrix as mentioned in 4.1.3.1. The decomposition peak of this transition could not be distinctively observed at the content of 10-20 wt% ESP1 but small decomposition peak was observed for composites prepared with 30-40 wt% ESP1. The second transition of the composites at 492-494°C was caused by the decomposition of HDPE. The third transition was the decomposition of CaCO₃, decarbonation, occurred at 727-775°C. The decomposition temperature of HDPE of the composites at various ESP1 contents was insignificantly different and almost the same as that of the neat HDPE, as shown in Table 4.5. This illustrated that the addition of ESP1 did not affect thermal stability of HDPE matrix. The decomposition temperature of CaCO₃ of the composites increased from 726°C to 775°C as ESP1 content increased from 10 wt% to 40 wt%. This was due to the strong effect of content, more particle-particle interactions, as increasing ESP1 content.

In addition, the TGA curves show the percentage of HDPE and ESP1 corresponding to the mixing ratios. The final weight after the decomposition of the composites is of CaO. The left CaO was 5, 11, 16, and 21 wt% for the composites at 10, 20, 30, and 40 wt% ESP1, respectively, as shown in Table 4.5. These were well consistent with theoretical stoichiometry.

Figure 4.14 shows TGA and DTGA thermograms of HDPE and CaCO₃/HDPE composite. The CaCO₃/HDPE composites exhibited two thermal transitions. The first transition resulted from the degradation of HDPE around 491-492°C and the second transition at 721-755°C, which was the consequence of the decarbonation of CaCO₃. The decomposition temperature of the HDPE in the composites at different CaCO₃ contents revealed that increasing CaCO₃ content did not affect the thermal stability of the composites. This was also found in

CaCO₃/LDPE nanocomposites (Wang et al., 2007). In addition, the decomposition temperature of CaCO₃ of the composites increased from 727°C to 755°C as CaCO₃ content increased from 10 wt% to 40 wt%, as reported in Table 4.5.

In addition, the TGA thermograms indicated the content of HDPE and CaCO₃ corresponding well with the mixing content. Moreover, the residue of CaO after decomposition of the composites at 10-40 wt% CaCO₃ was 5, 11, 17, and 22 wt%, respectively, in accordance with the quantitative relationship between CaCO₃ and CaO.

Thermal properties of ESP1 filled HDPE and CaCO₃ filled HDPE were not much different except that ESP1 filled HDPE composites showed the decomposition of organic substances around 320-340°C. However, this decomposition temperature was still higher than the processing temperature of the HDPE composites.

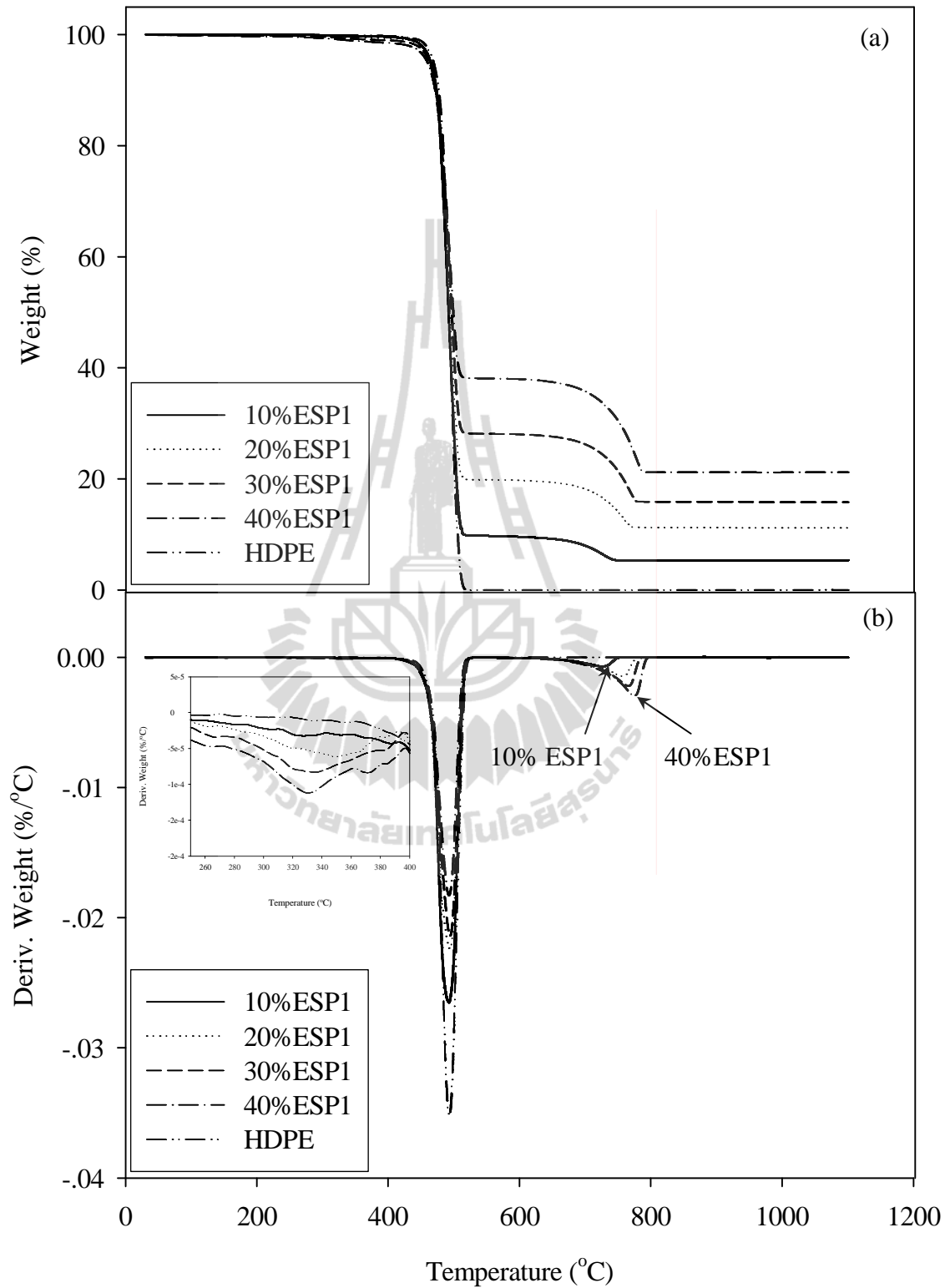


Figure 4.13 TGA (a) and DTGA (b) thermograms of HDPE and ESP1/HDPE composites with various contents of ESP1.

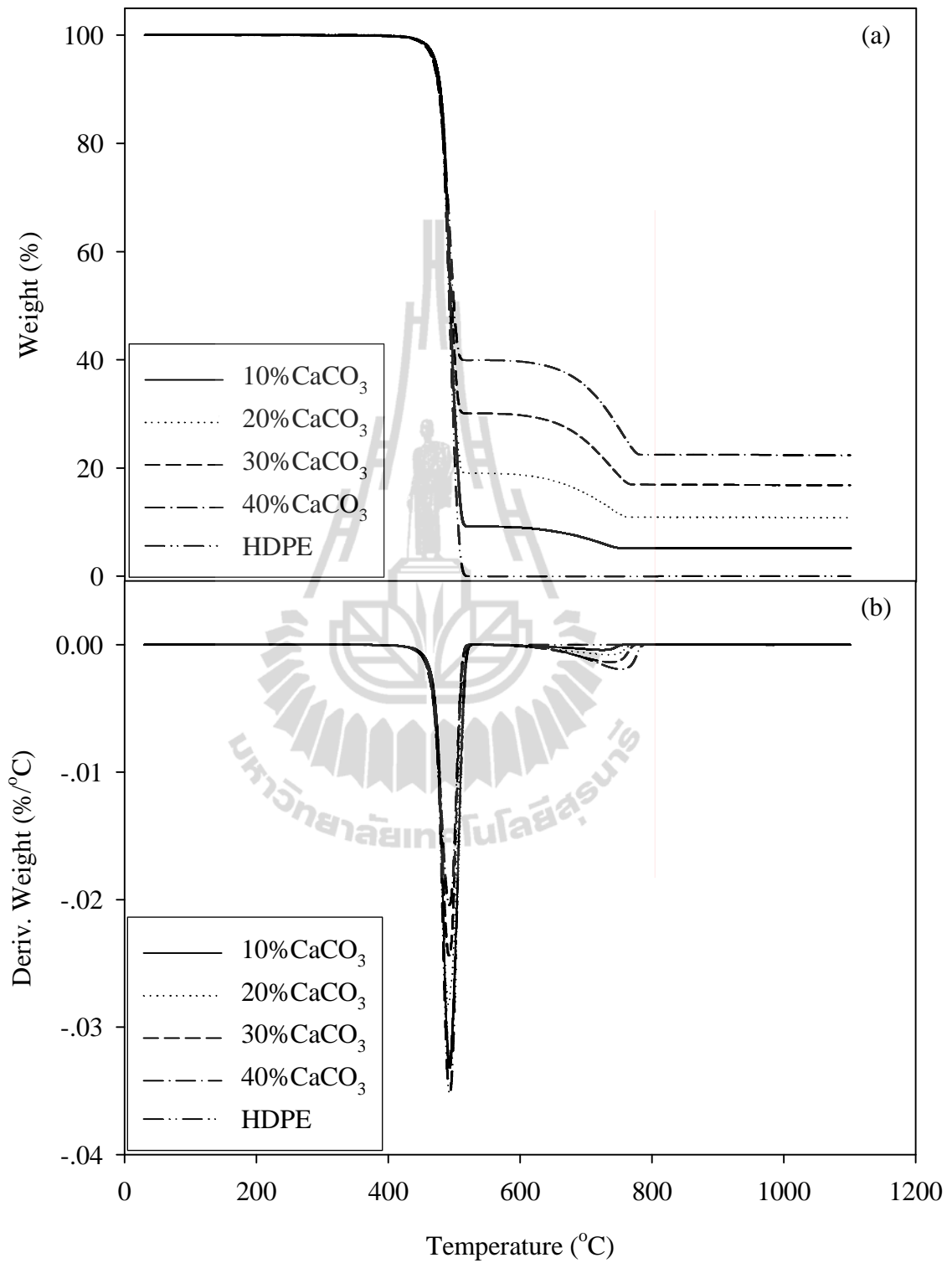


Figure 4.14 TGA (a) and DTGA (b) thermograms of HDPE and CaCO₃/HDPE composites with various contents of CaCO₃.

Table 4.5 Decomposition temperatures and weight residue of ESP1/HDPE, CaCO₃/HDPE composites and neat HDPE.

ESP1 or CaCO ₃ content (wt%)	Decomposition temperature (°C)					
	ESP1/HDPE composites			CaCO ₃ /HDPE composites		
	HDPE	ESP1	Residue (%)	HDPE	CaCO ₃	Residue (%)
0	493	-	0	493	-	0
10	492	726	5	492	727	5
20	493	757	11	491	741	11
30	494	766	16	492	738	17
40	492	775	21	492	755	22

4.2.1.3 Mechanical properties

Engineering stress-strain curves of neat HDPE, ESP1/HDPE composites, and CaCO₃/HDPE composites are presented in Figure 4.15. It should be noted that the tensile specimens of HDPE did not break within the instrument limit. Tensile curves of the HDPE and the HDPE composite at 10 wt% ESP1 and CaCO₃ exhibited cold drawing region before the test specimen was fractured. However, the HDPE composites at displacement rate of 10 mm/min, the ductile-brittle transition of ESP1/HDPE and CaCO₃/HDPE composites occurred at 20 wt% fillers content. This might be because the mobility of polymer chain was suppressed as increasing filler content. The ductile-brittle transition of CaCO₃/HDPE composites was also reported at CaCO₃ content of 15 vol% at the displacement rate of 50 mm/min (Bartczak et al., 1999) and 10 wt% at the displacement rate of 125 mm/min (Misra et al., 2004; Tanniru and Misra, 2006).

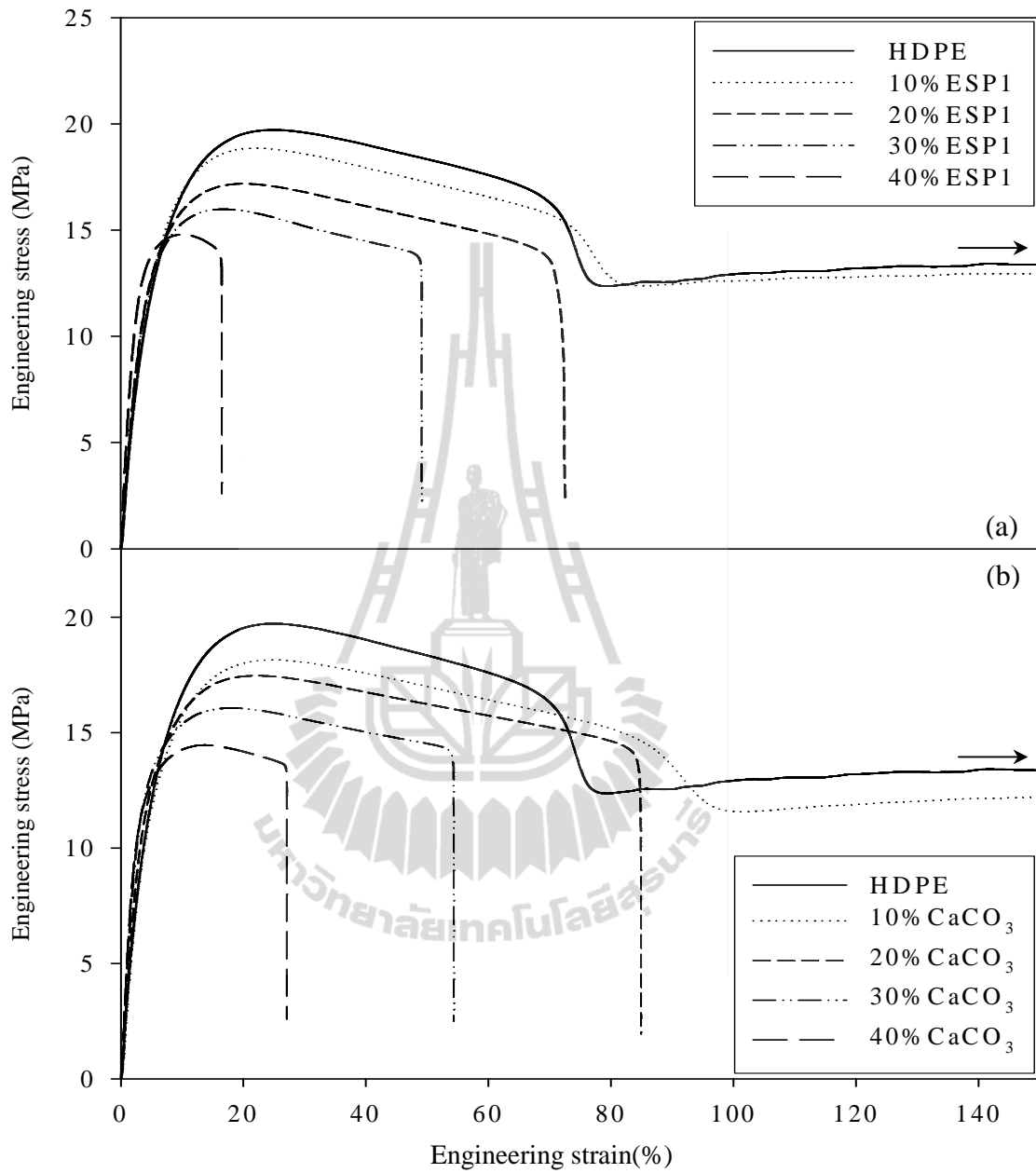


Figure 4.15 Tensile stress-strain curves of ESP1/HDPE (a) and CaCO_3 /HDPE (b) composites at various contents of ESP1 and CaCO_3 .

Figure 4.16 shows Young's modulus and elongation at break of ESP1/HDPE and CaCO_3 /HDPE composites. As expected, Young's modulus of

HDPE composites was higher than that of HDPE and increased gradually with increasing filler content. This was because the filler was much stiffer than HDPE matrix (Fu et al., 2008). In addition, the mobility and deformability of the matrix was restricted by the stiff particles of ESP1 and CaCO_3 (Misra et al., 2004). Elongation at break of the composites considerably decreased with increasing filler content.

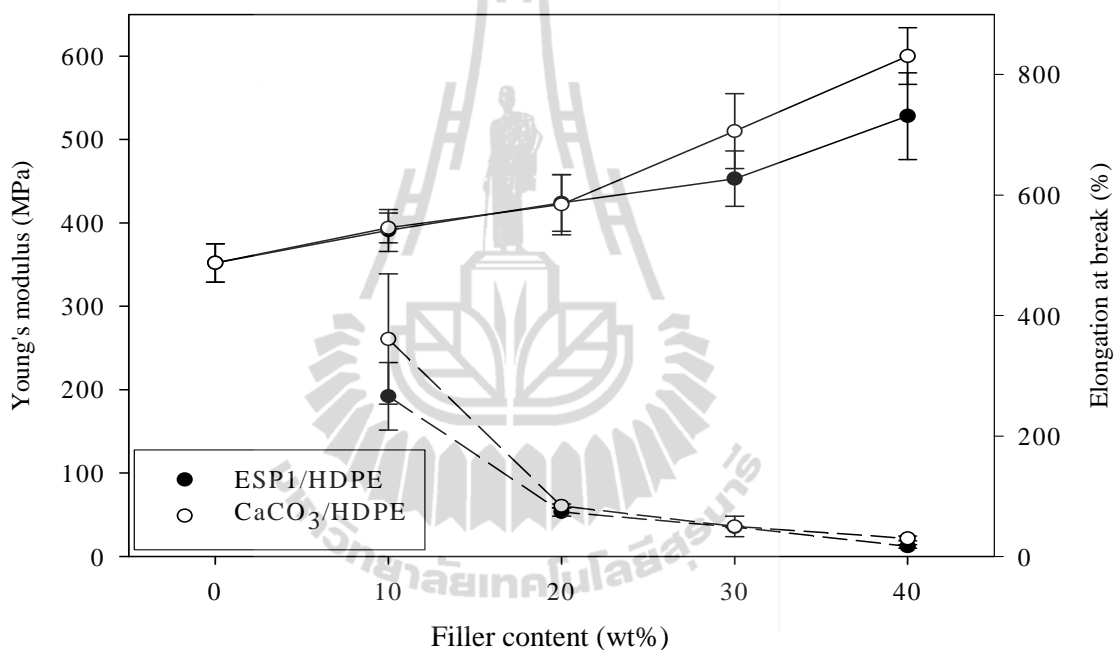


Figure 4.16 Plot of Young's modulus (—) and elongation at break (— —) of ESP1/HDPE and CaCO_3 /HDPE composites vs. filler contents.

Figure 4.17 shows yield strength of ESP1/HDPE and CaCO_3 /HDPE composites. It demonstrates that the yield strength of the composites was lower than that of the HDPE. In addition, the yield strength of ESP1/HDPE and CaCO_3 /HDPE composites was almost the same. The yield strength of the composites gradually decreased as content of ESP1 and CaCO_3 was increased. The hard particle of ESP1 and CaCO_3 also acted as a weakening point leading to the stress

concentration. The decreasing in yield strength of HDPE composites as increasing calcium carbonate content was previously reported (Bartczak et al., 1999; Suwanprateeb, Tiemprateeb, Kangwantrakool, and Hemachandra, 1998).

Figure 4.17 also shows tensile stress at break of ESP1/HDPE and CaCO₃/HDPE composites. The tensile stress at break of neat HDPE was not detected because the specimens were not fractured within the instrument limit. Tensile stress at break was slightly increased as increasing filler content from 10 wt% to 20 wt%. It was observed that the tensile stress at break of ESP1/HDPE composites and that of CaCO₃/HDPE composites were not changed even though the ESP1 and CaCO₃ were increased from 20 wt% up to 40 wt%. It indicated that the content of ESP1 and CaCO₃ had no effect on tensile stress at break of the filled HDPE. Young's modulus, elongation at break, yield strength, and tensile stress at break were listed in Table 4.6.

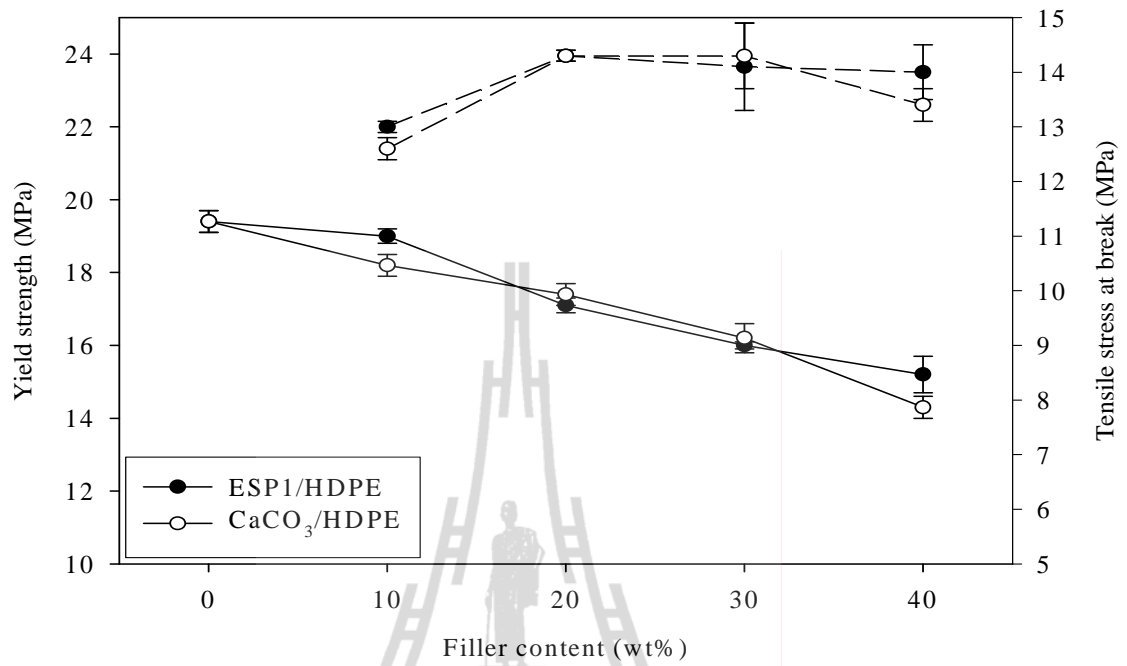


Figure 4.17 Plot of yield strength (—) and tensile stress at break (— —) of ESP1/HDPE and CaCO₃/HDPE composites vs. filler contents.

Table 4.6 Tensile properties of ESP1/HDPE and CaCO₃/HDPE composites at various contents of ESP1 and CaCO₃.

ESP1 or CaCO ₃ content (wt%)	Young's modulus (MPa)		Elongation at break (%)		Yield strength (MPa)		Tensile stress at break (MPa)	
	ESP1/HDPE	CaCO ₃ /HDPE	ESP1/HDPE	CaCO ₃ /HDPE	ESP1/HDPE	CaCO ₃ /HDPE	ESP1/HDPE	CaCO ₃ /HDPE
0	352±23	352±23	Not break	Not break	19.3±0.1	19.3±0.1	Not break	Not break
10	391±25	394±18	266±56	361±108	19.0±0.2	18.2±0.3	13.0±0.1	12.6±0.2
20	424±34	422±36	74±7	84±3	17.1±0.2	17.4±0.3	14.3±0.1	14.3±0.1
30	453±33	510±45	49±1	50±17	16.0±0.1	16.2±0.4	14.1±0.8	14.3±0.6
40	528±52	600±34	17±3	30±4	15.2±0.5	14.3±0.3	14.0±0.5	13.4±0.3

Flexural properties of ESP1/HDPE and CaCO₃/HDPE composites are shown in Table 4.7. The flexural modulus of the HDPE composites was improved by the incorporation of ESP1 and CaCO₃ and their moduli were increased with increasing the filler content. The ESP1 was more effective than CaCO₃ for improving flexural modulus of the composites. The flexural strength of ESP1/HDPE composites was similar to that of neat HDPE. As increasing ESP1 content, the flexural strength of the composites was not significantly increased. However, the addition of CaCO₃ into HDPE insignificantly improved flexural strength of the composites.

Table 4.7 Flexural modulus and strength of ESP1/HDPE and CaCO₃/HDPE composites.

ESP1 or CaCO ₃ content (wt%)	Flexural modulus (MPa)		Flexural strength (MPa)	
	ESP1/HDPE	CaCO ₃ /HDPE	ESP1/HDPE	CaCO ₃ /HDPE
0	553±21	553±21	21±0.6	21±0.6
10	628±4	583±11	22±0.3	21±0.3
20	690±29	651±24	23±0.1	21±0.2
30	852±30	792±34	24±0.1	22±0.4
40	1012±34	925±23	24±0.2	22±0.3

Unnotched Izod impact strength of neat HDPE and the HDPE composites is shown in Table 4.8. It should be noted that the impact strength of neat HDPE and the HDPE composite at 10 wt% of ESP1 and CaCO₃ was not obtained because they were not fractured within the instrument limit. The impact strength of the composites decreased with increasing the filler content. The reduction in impact strength of the composites was due to the poor interfacial adhesion between the polar surface of ESP1 and CaCO₃ and HDPE (Rukchonlatee, Prasertwong, and

Sangpakdee, 2002). The poor interfacial adhesion resulted in voids between the interface of filler and HDPE. Under the impact test, these voids acted as stress concentrator at which the impact stress was magnified and made the composites fractured at lower stress. It can be seen that the impact strength of ESP1/HDPE composites was slightly lower than that of CaCO₃/HDPE composites.

Table 4.8 Unnotched Izod impact strength of ESP1/HDPE and CaCO₃/HDPE composites.

ESP1 or CaCO ₃ content (wt%)	Impact strength (kJ/m ²)	
	ESP1/HDPE	CaCO ₃ /HDPE
0	Not break	Not break
10	Not break	Not break
20	38.0±3.2	46.3±2.3
30	22.6±1.7	25.0±2.2
40	13.4±1.6	14.9±0.9

The influence of filler content on hardness and HDT of ESP1/HDPE and CaCO₃/HDPE composite is shown in Table 4.9. The hardness of neat HDPE was slightly lower than that of the composites. The hardness of the composites slightly increased when fillers content was increased. This was because hard particle of ESP1 and CaCO₃ had higher hardness than that of HDPE. Comparatively, the hardness of ESP1/HDPE composites insignificantly differed from that of CaCO₃/HDPE composites.

It was observed that HDT of the composites was higher than that of neat HDPE as shown in Table 4.9. The HDT of the composites increased with increasing the filler content. In addition, the HDT of ESP1/HDPE composite was

slightly lower than that of CaCO₃/HDPE composite when the ESP1 content was higher than 10 wt%.

Table 4.9 Hardness and HDT of neat HDPE, ESP1/HDPE composites, and CaCO₃/HDPE composites at various filler contents.

ESP1 or CaCO ₃ content (wt%)	Hardness (shore D)		HDT (°C)	
	ESP1/HDPE	CaCO ₃ /HDPE	ESP1/HDPE	CaCO ₃ /HDPE
0	38.3±0.3	38.3±0.3	68.2±0.9	68.2±0.9
10	38.5±0.2	38.7±0.2	71.5±0.7	71.5±0.5
20	40.2±0.3	40.5±0.4	73.1±0.6	74.5±1.0
30	42.0±0.2	42.2±0.2	77.3±0.3	76.2±1.1
40	42.8±0.2	43.6±0.2	79.0±1.0	81.4±0.9

4.2.1.4 Morphological properties

Figure 4.18 shows SEM micrograph of ESP1/HDPE and CaCO₃/HDPE composites. It was clearly observed that the interfacial adhesion between ESP1 and HDPE was as poor as that between CaCO₃ and HDPE. Several holes were observed on the fracture surface. These holes were caused by debonding of filler particles from the HDPE matrix. The particles distribution in ESP1/HDPE and CaCO₃/HDPE composites was the same. In addition, the poor interfacial adhesion led to the reduction of yield strength, tensile stress at break, and impact strength of the HDPE composites.

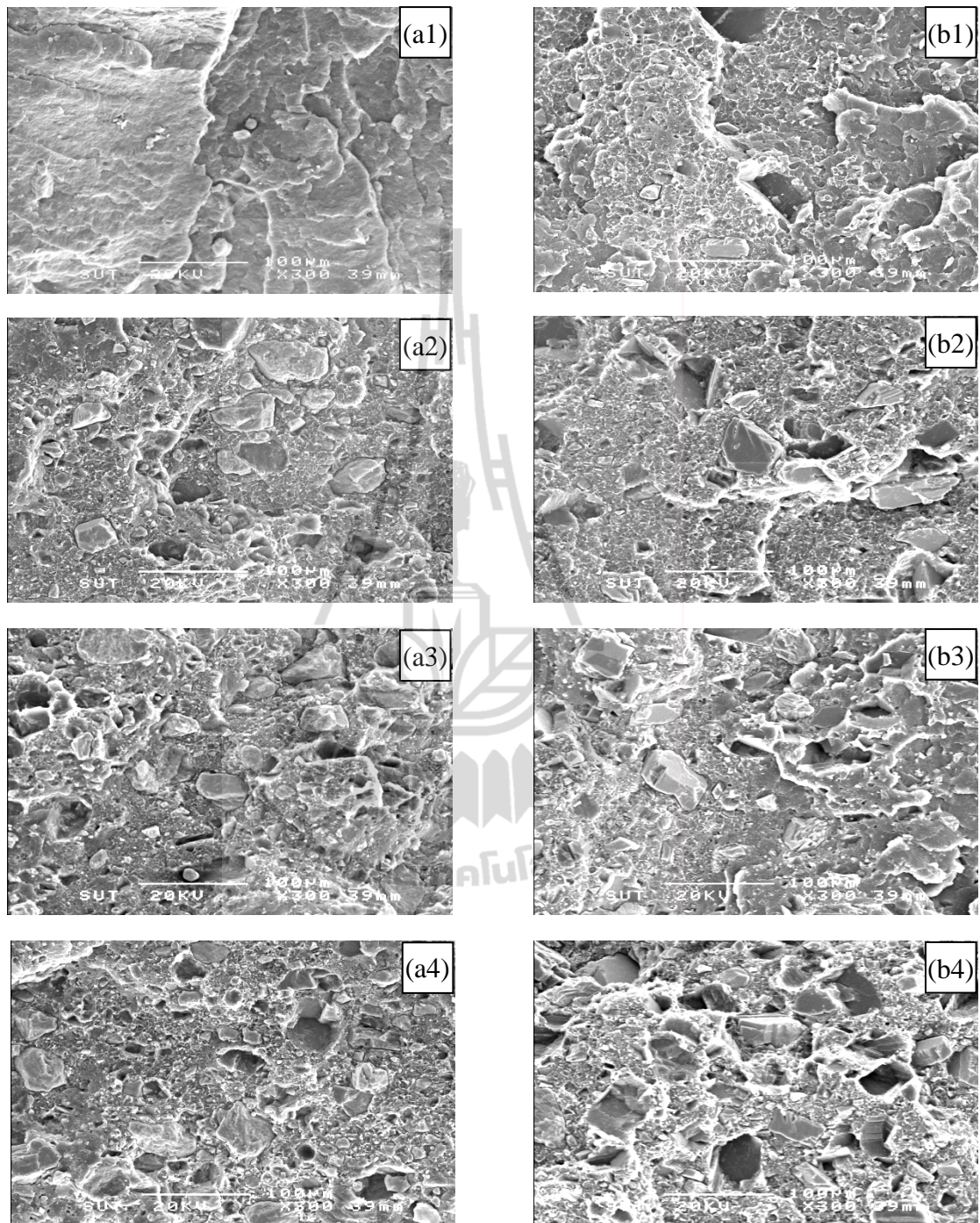


Figure 4.18 SEM micrographs (x300) of ESP1/HDPE (a) and CaCO₃/HDPE (b)

composites: 10 wt% (1), 20 wt% (2), 30 wt% (3), and 40 wt% (4)

4.2.2 Effect of particle size and compatibilization of ESP on physical properties of 40 wt% ESP/HDPE composites

As previously discussed in section 4.2.1, ESP1/HDPE composites at ESP1 content of 40 wt% showed higher tensile stress at break and Young's modulus than those at ESP1 of 10, 20, and 30 wt%. Thus, the uncompatibilized and compatibilized ESP2/HDPE composites were further prepared in order to study the effect of particle sizes and interfacial modification on physical properties of the composites. The D_{50} and range of ESP1 were 17.1 μm and 0.7-113 μm , respectively and those of ESP2 were 14.4 μm and 0.9-60 μm , respectively.

4.2.2.1 Rheological properties

The plot of the apparent shear viscosity of ESP1/HDPE, ESP2/HDPE, and compatibilized ESP2/HDPE composites as a function of shear rate is shown in Figure 4.19. Obviously, it revealed that the apparent shear viscosity of ESP1/HDPE and ESP2/HDPE composites were similar. It was not sufficient to make any significant difference in the melt viscosity. However, the apparent shear viscosity of the compatibilized ESP2 filled HDPE was slightly higher than that of uncompatibilized ESP2 filled HDPE. This was due to the reducing the amount and the size of agglomeration by adding HDPE-g-MAH (Lazzeri et al., 2005). It was previously reported that the addition of HDPE-g-MAH at 0-2 wt% of CaCO_3 slightly affected melt viscosity of the HDPE composites (Rukchonlatee et al., 2002). In addition, it was reported that the optimum content of HDPE-g-MAH was 4% by weight of CaCO_3 (Phueakbuakhao et al., 2008). The HDPE composites prepared from ESP1, ESP2, and ESP2 with compatibilizer show the shear-thinning behavior, the apparent shear viscosity decreased with increasing shear rate.

The MFI of ESP1/HDPE, ESP2/HDPE, and compatibilized ESP2/HDPE composites were 8.3, 8.2, and 7.2, respectively, as shown in Table 4.10. It was found that the reduction in particle size of ESP did not affect MFI of the ESP2/HDPE composites. The adding of HDPE-g-MAH into the HDPE composites did not lead to the significant change of the composites MFI.

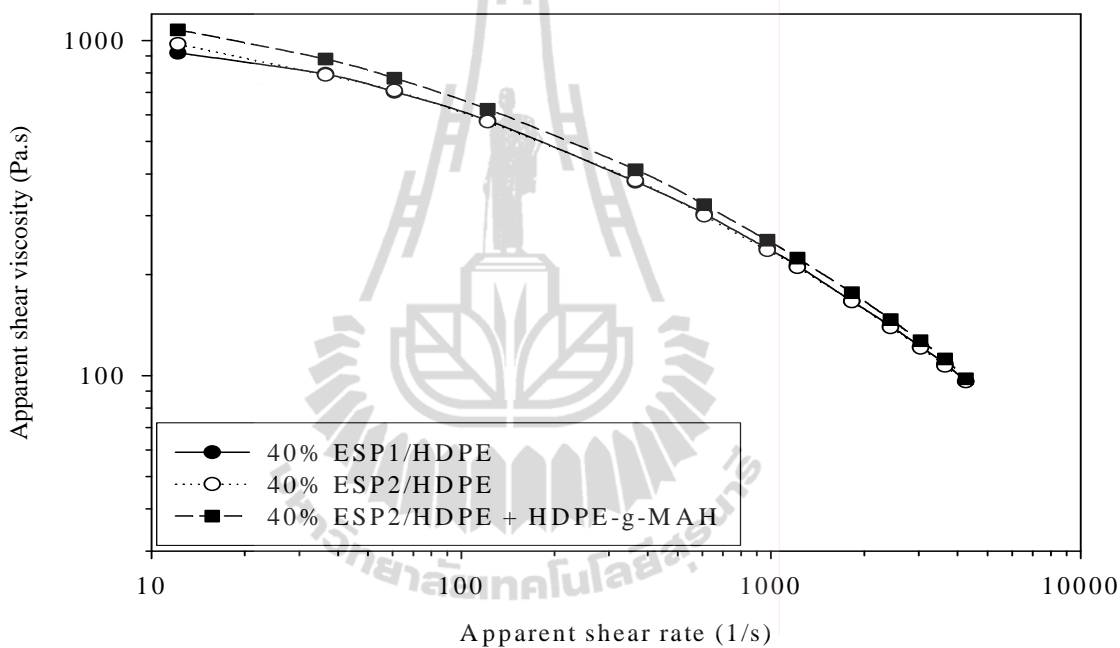


Figure 4.19 Plot of apparent shear viscosity for ESP1/HDPE, ESP2/HDPE, and compatibilized ESP2/HDPE composites at ESP content of 40 wt% versus apparent shear rate.

Table 4.10 MFI of ESP1/HDPE, ESP2/HDPE, and compatibilized ESP2/HDPE composites with ESP content of 40 wt%.

HDPE Composites	MFI (g/10 min)
40% ESP1/HDPE	8.3
40% ESP2/HDPE	8.2
40% ESP2/HDPE + 2% HDPE-g-MAH	7.2

4.2.2.2 Thermal properties

TGA and DTGA curves of ESP1/HDPE, ESP2/HDPE, and compatibilized ESP2/HDPE are shown in Figure 4.20. The composites showed three transitions: the 1st transition was the decomposition of organic substance; the 2nd transition was the decomposition of HDPE; the 3rd transition was the decomposition of CaCO₃ deposited in ESP. The decomposition temperature of HDPE filled with ESP1 and ESP2 was not much different as shown in Table 4.11. However, the decomposition temperature of CaCO₃ in ESP2/HDPE composites was lower than that in ESP1/HDPE composites. This was suggested that the activation energy of the thermal decomposition of CaCO₃ decreased by decreasing the particle size (Criado and Ortega, 1995). With addition of HDPE-g-MAH, the decomposition temperature of HDPE matrix of compatibilized ESP2/HDPE composites was similar to that of the uncompatibilized ESP2/HDPE composites. It was previously reported that after grafting with MAH, the thermal stability of grafted PP was improved (Han, Wu, Yin, and Yu, 2009). On the other hand, the decomposition temperature of CaCO₃ deposited in ESP shifted to a higher temperature by the addition of 2 wt% HDPE-g-MAH.

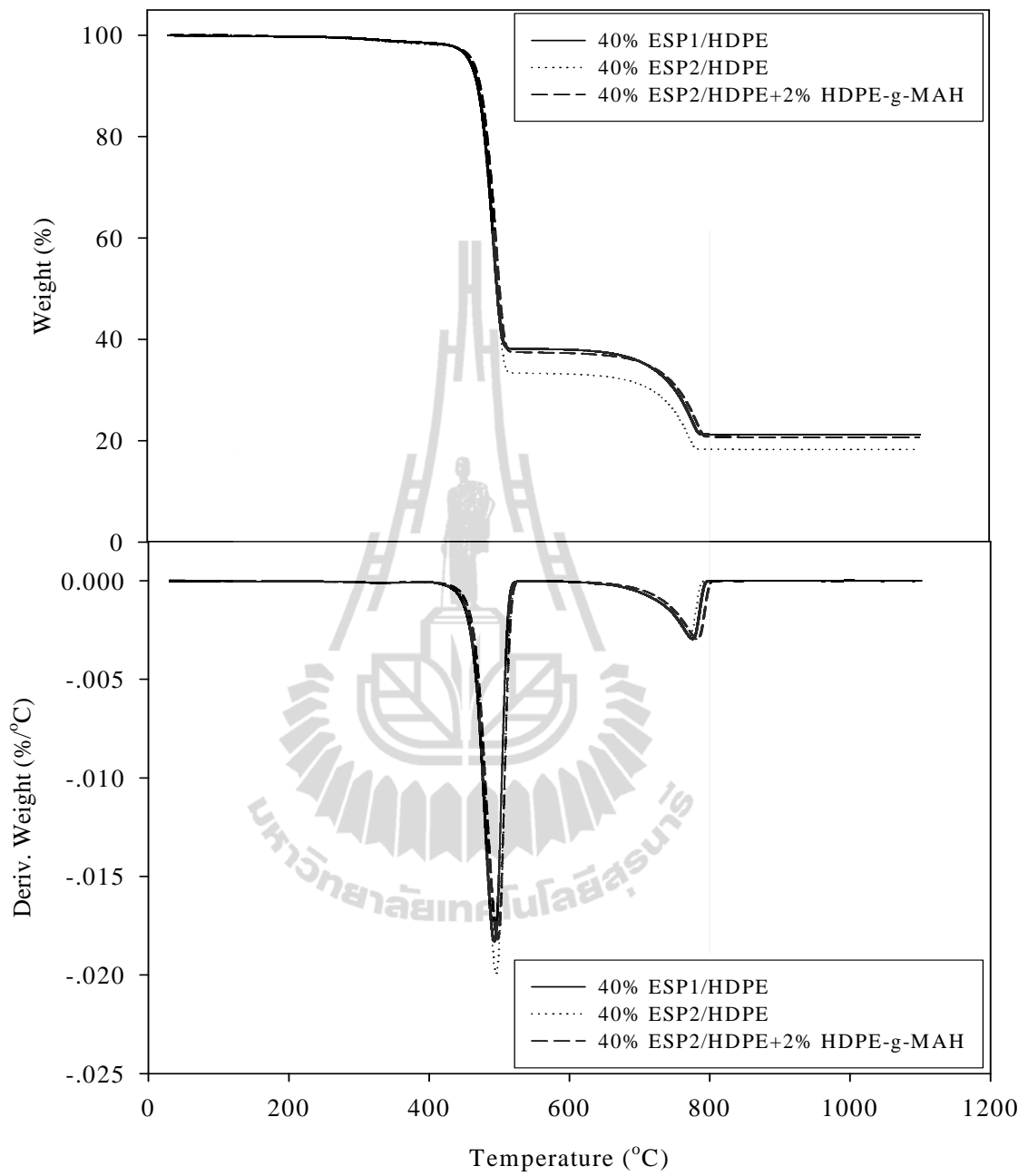


Figure 4.20 TGA (a) and DTGA (b) thermograms of ESP1/HDPE, ESP2/HDPE, and compatibilized ESP2/HDPE composites with ESP content of 40 wt%.

Table 4.11 Decomposition temperatures of ESP1/HDPE, ESP2/HDPE, and compatibilized ESP2/HDPE composites at ESP content of 40 wt%.

HDPE Composites	Decomposition temperature (°C)	
	HDPE	ESP (CaCO ₃)
40% ESP1/HDPE	492	775
40% ESP2/HDPE	495	771
40% ESP2/HDPE+2% HDPE-g-MAH	497	782

4.2.2.3 Mechanical properties

Figure 4.21 shows Young's modulus and elongation at break of ESP1/HDPE, ESP2/HDPE, and compatibilized ESP2/HDPE composites. Young's modulus of ESP2/HDPE composites was slightly improved. This was previously reported that the particle size had a little effect on composites stiffness (Fu et al., 2008). However, there was a previous study that Young's modulus of CaCO₃/PP/HDPE composites with 1.8 µm CaCO₃ was higher than that with 3.0 µm CaCO₃ (González et al., 2002). In addition, CaCO₃/PP composites with 6.0 µm had higher Young's modulus than composite that with 3.0 µm (Silva et al., 2002). Young's modulus of the composites was not influenced by 2 wt% HDPE-g-MAH addition. Young's modulus of the composites was calculated from the slope of stress-strain curve before irreversible deformation took place. Thus, the displacement at the interface did not occur (Nwabunma and Kyu, 2008; Fu et al., 2008). It was previously studied that CaCO₃ with particle sizes of 3.0 and 1.8 µm treated with Lica 12 of 0.3-0.5 wt% did not influence on Young's modulus of the PP/HDPE blend with CaCO₃ (González et al., 2002). The percentage elongation at break of ESP2/HDPE composites was higher than that of ESP1/HDPE composites. However,

the presence of 2 wt% HDPE-g-MAH in ESP2/HDPE composites slightly affected elongation at break of the compatibilized composites.

The dependence of yield strength and tensile stress at break of the composites on particle size and surface modification was depicted in Figure 4.21. The yield strength and tensile stress at break of the HDPE filled with ESP1 and ESP2 were not much different. Since, particle size and size distribution of ESP1 and ESP2 were in the same range. It was previously reported that the yield strength and tensile stress at break of CaCO₃/PP composites with size of CaCO₃, D₅₀ of 6.0 and 3.0 μm, were not different (Silva et al., 2002). However, the addition of HDPE-g-MAH into ESP2/HDPE composites enhanced the yield strength and tensile stress at break of the composites, as illustrated in Figure 4.22. This was because the interfacial adhesion between ESP and HDPE was improved via HDPE-g-MAH. The improvement in tensile strength of CaCO₃-filled recycled HDPE by addition of HDPE-MAH was also presented (Phueakbuakhao et al., 2008). Young's modulus, elongation at break, yield strength, and tensile stress at break of the composites were shown in Table 4.12.

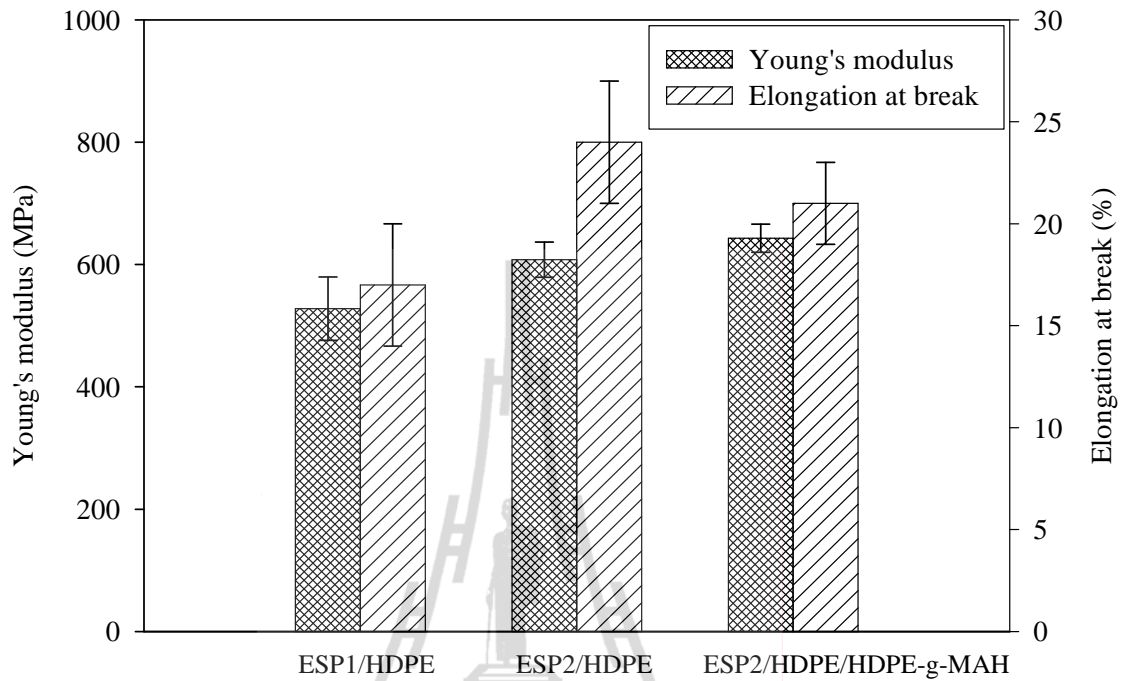


Figure 4.21 Plot of Young's modulus and elongation at break of ESP1/HDPE, ESP2/HDPE, and compatibilized ESP2/HDPE composites with ESP content of 40 wt%.

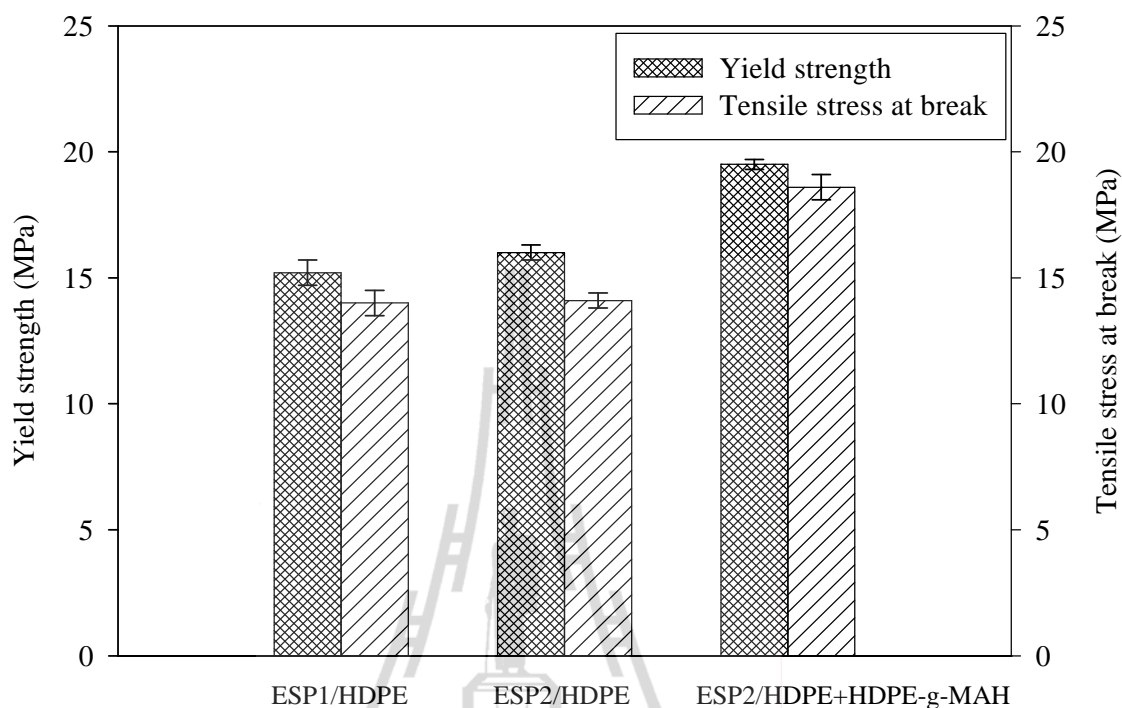


Figure 4.22 Plot of yield strength and tensile stress at break of ESP1/HDPE, ESP2/HDPE, and compatibilized ESP2/HDPE composites with ESP content of 40 wt%.

Table 4.12 Tensile properties of ESP1/HDPE, ESP2/HDPE, and compatibilized ESP2/HDPE composites with ESP content of 40 wt%.

HDPE Composites	Young's modulus (MPa)	Elongation at break (%)	Yield strength (MPa)	Tensile stress at break (MPa)
40% ESP1/HDPE	528±52	17±3	15.2±0.5	14.0±0.5
40% ESP2/HDPE	608±29	24±3	16.0±0.3	14.1±0.3
40% ESP2/HDPE+2% HDPE-g-MAH	643±23	21±2	19.5±0.2	18.6±0.5

Flexural modulus and strength of ESP1/HDPE, ESP2/HDPE, and compatibilized ESP2/HDPE composites with ESP content of 40 wt% are shown in Figure 4.23. Obviously, it was found that flexural modulus and flexural strength of the composites with ESP1 and ESP2 were not significantly different. The flexural modulus and strength of the compatibilized composites were not significantly improved. This was due to the improvement of filler-matrix interaction by HDPE-g-MAH. Flexural modulus and strength of the HDPE composites were listed in Table 4.13.

The effect of particle size and interfacial modification on unnotched Izod impact strength of HDPE composites is shown in Table 4.14. The impact strength of the composites from ESP1 and ESP2 were similar. It was obviously found that the impact strength of the composites was improved by compatibilization with HDPE-g-MAH.

The dependence of hardness and HDT of ESP/HDPE composites on particle size and surface modification is listed in Table 4.14. The particle size of ESP did not influence hardness and HDT of the composites. The compatibilization did not affect hardness of the composites; however, the compatibilization improved HDT by 6°C.

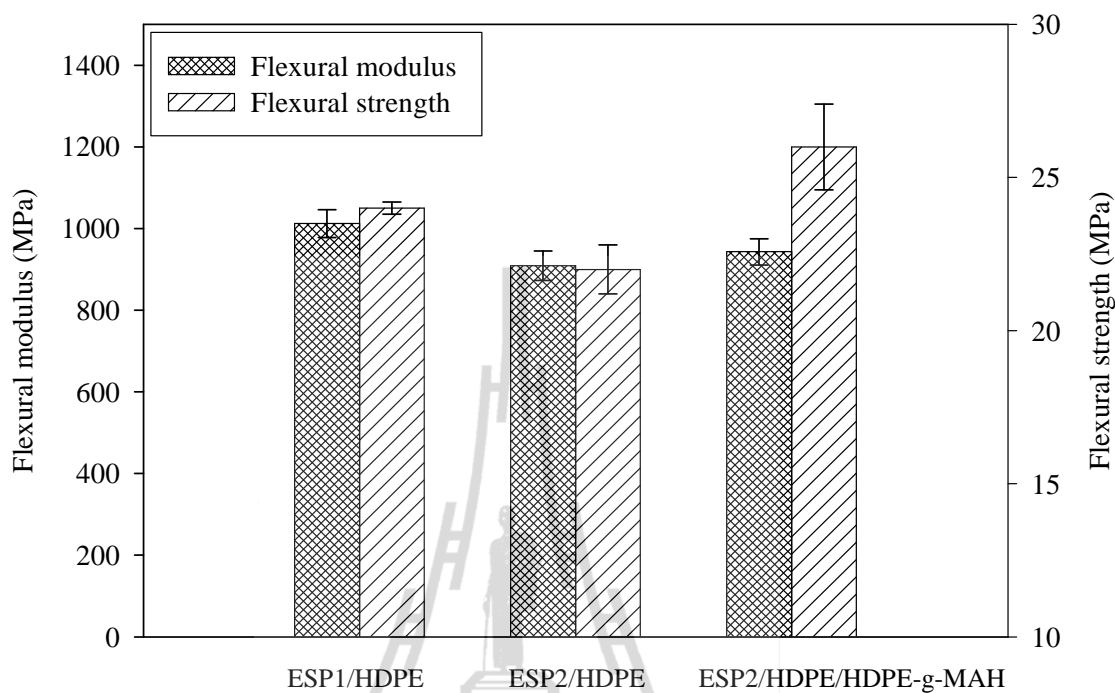


Figure 4.23 Plot of flexural modulus and strength of ESP1/HDPE, ESP2/HDPE, and compatibilized ESP2/HDPE composites with ESP content of 40 wt%.

Table 4.13 Flexural properties of ESP1/HDPE, ESP2/HDPE, and compatibilized ESP2/HDPE composites with ESP content of 40 wt%.

HDPE Composites	Flexural modulus (MPa)	Flexural strength (MPa)
40% ESP1/HDPE	1012±34	24±0.2
40% ESP2/HDPE	909±36	22±0.8
40% ESP2/HDPE+2% HDPE-g-MAH	943±32	26±1.4

Table 4.14 Impact strength, hardness, and HDT of ESP1/HDPE, ESP2/HDPE, and compatibilized ESP2/HDPE composites with ESP content of 40 wt%.

HDPE Composites	Impact strength (kJ/m²)	Hardness (Shore D)	HDT (°C)
40% ESP1/HDPE	13.4±1.6	42.8±0.2	79.0
40% ESP2/HDPE	14.0±0.7	43.0±0.3	79.2
40% ESP2/HDPE+2% HDPE-g-MAH	20.6±1.0	43.0±0.3	85.0

4.2.2.4 Morphological properties

SEM micrograph of ESP1/HDPE, ESP2/HDPE, and compatibilized ESP2/HDPE composites with 40 wt% ESP are shown in Figure 4.24. From Figure 4.24 (a1) and (b1), it was clearly observed that the particle distribution of ESP1 and ESP2 within the HDPE matrix was similar. With a larger magnification of SEM micrograph in Figure 4.24 (a2) and (b2), the observed interfacial adhesion of ESP1/HDPE and ESP2/HDPE composites were not significantly different. From Figure 4.24 (c2), it was observed the decrease of number of holes caused by detachment of particles from HDPE matrix under cryogenic fracture.

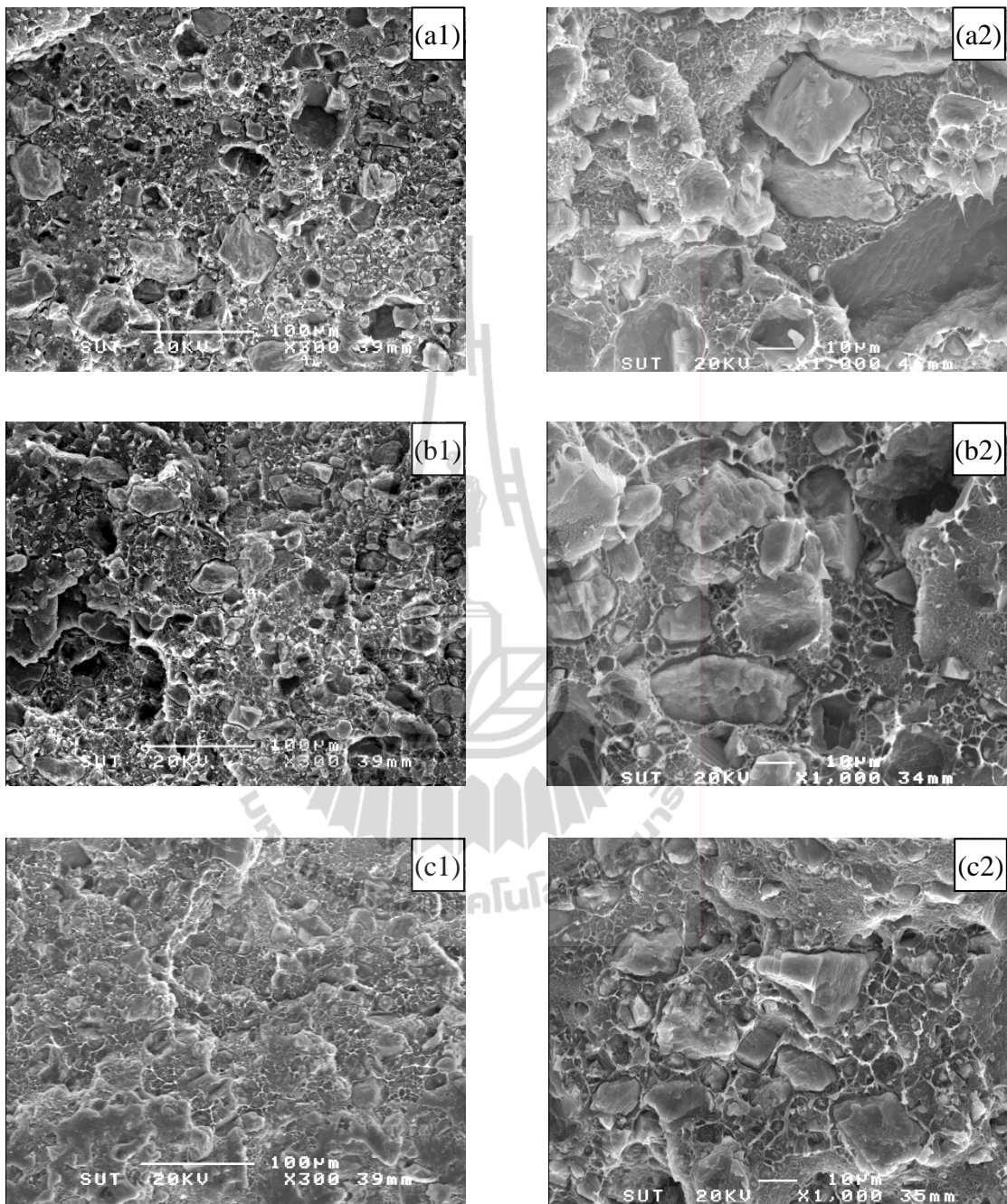


Figure 4.24 SEM micrographs at magnification of x300 (1) and x1000 (2) of ESP1/HDPE (a), ESP2/HDPE (b), and compatibilized ESP2/HDPE (c) composites with ESP content of 40 wt%.

4.3 Characterization of HDPE composites from HT-ESP

4.3.1 Effect of HT-ESP content and compatibilization on physical properties of HT-ESP/HDPE composites

4.3.1.1 Rheological properties

The plot of apparent shear viscosity as a function of apparent shear rate of HT-ESP1/HDPE and compatibilized HT-ESP1/HDPE composites are shown in Figure 4.25. The shear viscosity of the composites increased as fillers content was increased. This was because a higher content of fillers resulted in more particles closely packed together resulting in an increase of resistance to flow (viscosity) of the molten composites (<http://www.chemeurope.com/articles/e/61207/>). In addition, the apparent shear viscosity decreased with increasing apparent shear rate, shear-thinning behavior. This is because at high shear rate, the polymer chain is more deformed in the direction of shearing and then the composites easier flow as a result viscosity was decreased. Comparatively, the apparent shear viscosity of compatibilized and uncompatibilized HDPE composites at 40 wt% HT-ESP1 was not significantly different.

Table 4.15 shows MFI of HT-ESP1/HDPE and compatibilized HT-ESP1/HDPE composites. The MFI of the composites was decreased with increasing content of HT-ESP1. In addition, the MFI of compatibilized HDPE composites was the same as that of uncompatibilized composites at 40 wt% HT-ESP1.

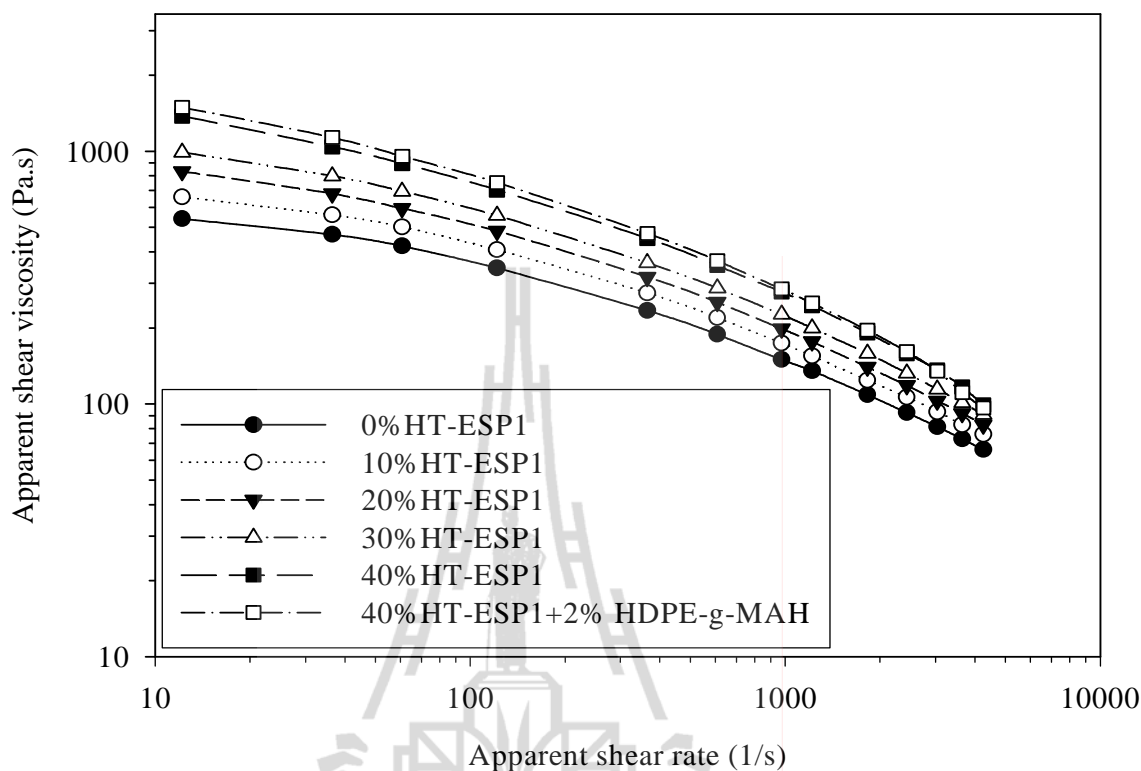


Figure 4.25 Plot of the apparent shear viscosity of HT-ESP1/HDPE and compatibilized HT-ESP1/HDPE composites against the apparent shear rate.

Table 4.15 MFI of HT-ESP1/HDPE and compatibilized HT-ESP1/HDPE composites.

Filler content (wt%)	MFI (g/10 min)
0% HT-ESP1	12.4
10% HT-ESP1	9.5
20% HT-ESP1	7.2
30% HT-ESP1	6.6
40% HT-ESP1	4.9
40% HT-ESP1+2% HDPE-g-MAH	5.0

4.3.1.2 Thermal properties

TGA and DTGA curves of HT-ESP1/HDPE composites are presented in Figure 4.26. The TGA and DTGA show two thermal transitions. The first transition at temperature of 493-498°C was the decomposition of HDPE. The second transition at 591-639°C was the decomposition of CaCO₃. The first transition of the HDPE composites began earlier than that of neat HDPE according to decomposition of Ca(OH)₂ which was close to the decomposition of HDPE. From section 4.1.3.2, the Ca(OH)₂ decomposed around 430-445°C, as shown in Table 4.2. In addition, the transition of CaCO₃ was obviously observed at HT-ESP1 content of 30-40 wt%. The DTGA curves of the HDPE composites show that the first and second transition temperatures insignificantly increased by increasing HT-ESP1 content. This might be due to the forming of more stable CaO by the decomposition of Ca(OH)₂. By the compatibilization, the first transition temperature of 40 wt% HT-ESP1/HDPE composites was not much different from that of the uncompatibilized HDPE composites. The decomposition temperature of each transition was listed in Table 4.16.

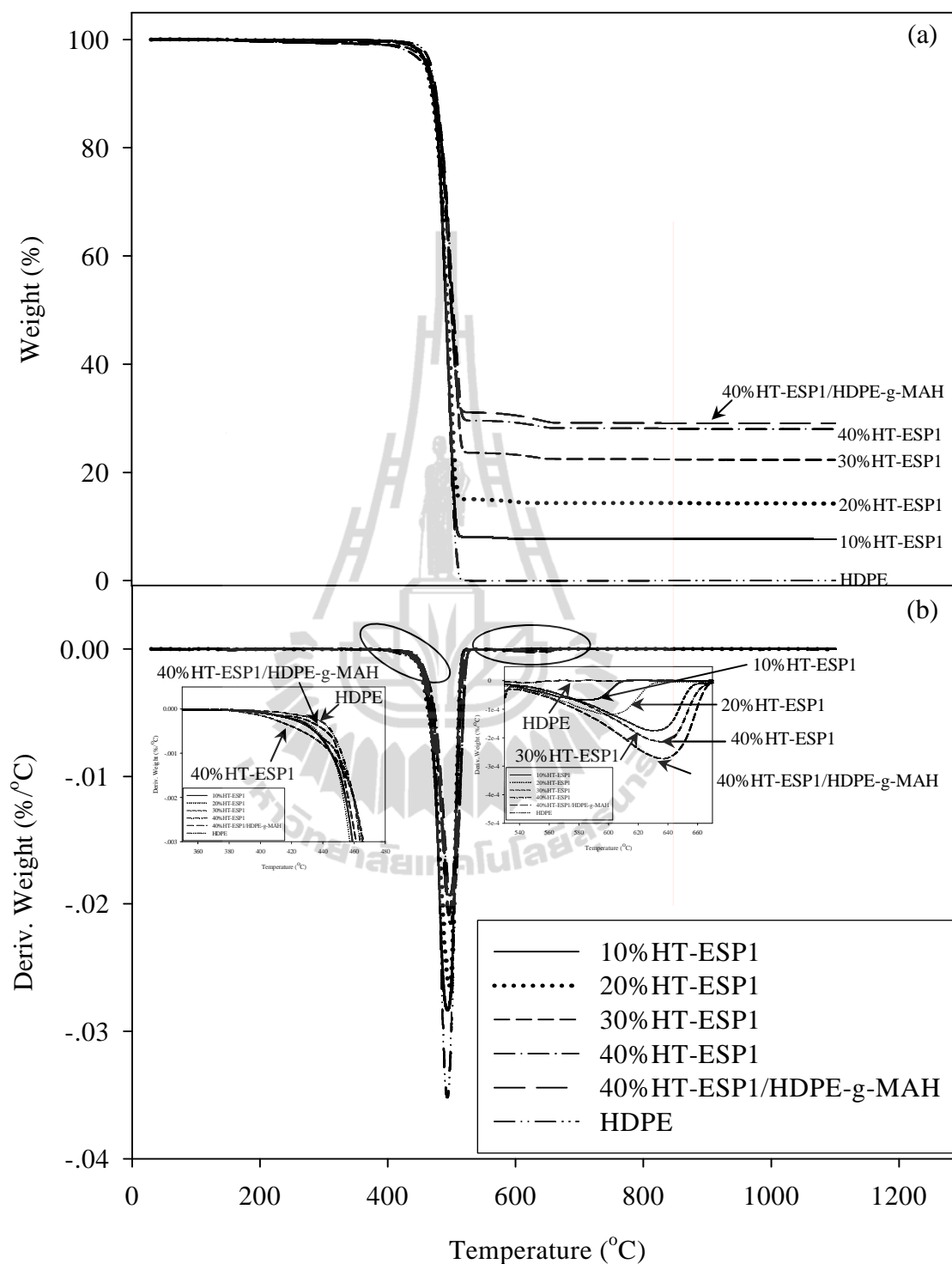


Figure 4.26 TGA (a) and DTGA (b) thermograms of HDPE, HT-ESP1/HDPE composites, and compatibilized HT-ESP1/HDPE composites.

Table 4.16 Decomposition temperature of HT-ESP1/HDPE composite and compatibilized HT-ESP1/HDPE composite.

Filler content (wt%)	Decomposition temperature (°C)		
	HDPE decomposition		CaCO ₃ decomposition
	T _{onset}	T _{peak}	T _{peak}
0% HT-ESP1	472	493	-
10% HT-ESP1	468	493	591
20% HT-ESP1	465	496	602
30% HT-ESP1	468	498	635
40% HT-ESP1	471	497	637
40% HT-ESP1+2% HDPE-g-MAH	469	495	639

4.3.1.3 Mechanical properties

Figure 4.27 shows engineering stress-strain curves of HT-ESP1/HDPE composites. Tensile curves of neat HDPE and HDPE composites at 10 and 20 wt% HT-ESP1 exhibited cold drawing region before the test specimen was ruptured. The ductile-brittle transition of the HT-ESP1/HDPE composites occurred at 30 wt% filler content. It is difficult for polymer chains to plastically flow after yielding as filler content was increased. In addition, the 40 wt% HT-ESP1/HDPE composites without and with adding the compatibilizer were fractured prior to yielding. It was explained that interfacial voids, weakening point, did not withstand crack propagation and led to brittleness of the materials (Friedrich and Karsch, 1983).

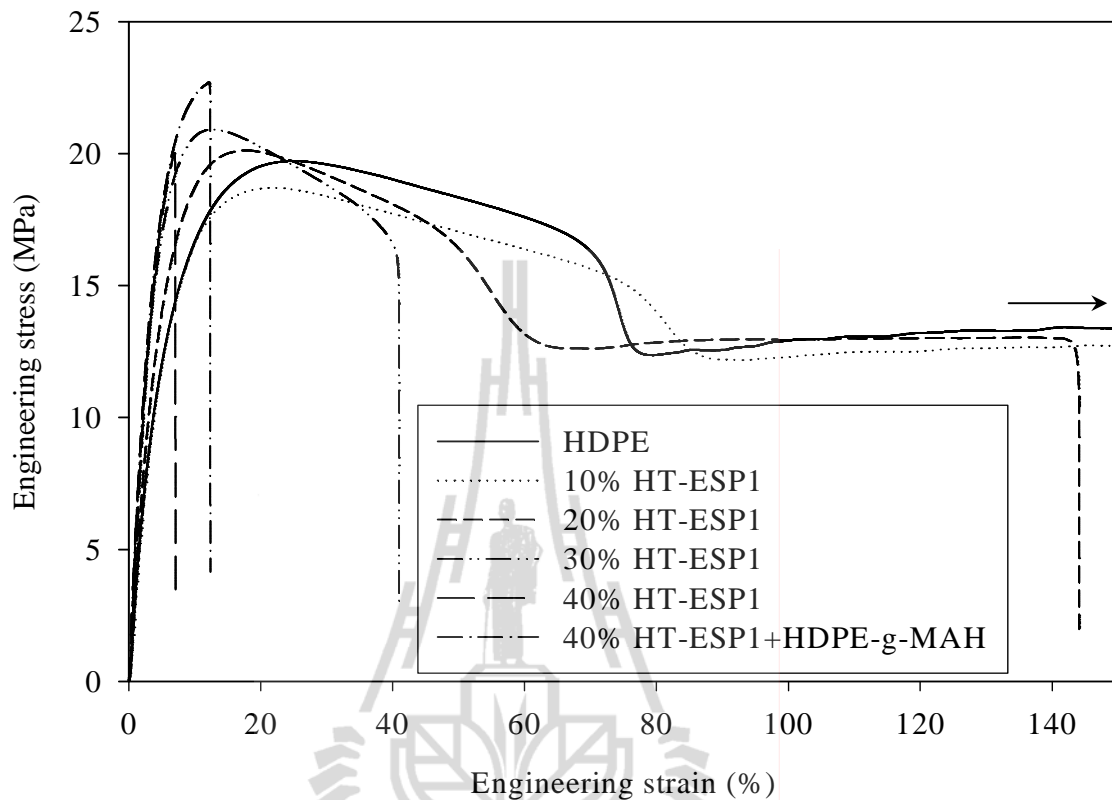


Figure 4.27 Tensile stress-strain curves of HT-ESP1/HDPE composites and compatibilized HT-ESP1/HDPE composite.

With increasing filler content, Young's modulus of the composites increased but elongation at break decreased, as shown in Figure 4.28 and 4.29, respectively. The increase of Young's modulus was caused by the incorporation of rigid particles of HT-ESP1. However, at 40 wt% HT-ESP1, the Young's modulus and elongation at break of compatibilized composites was not significantly different from that of uncompatibilized HDPE composites.

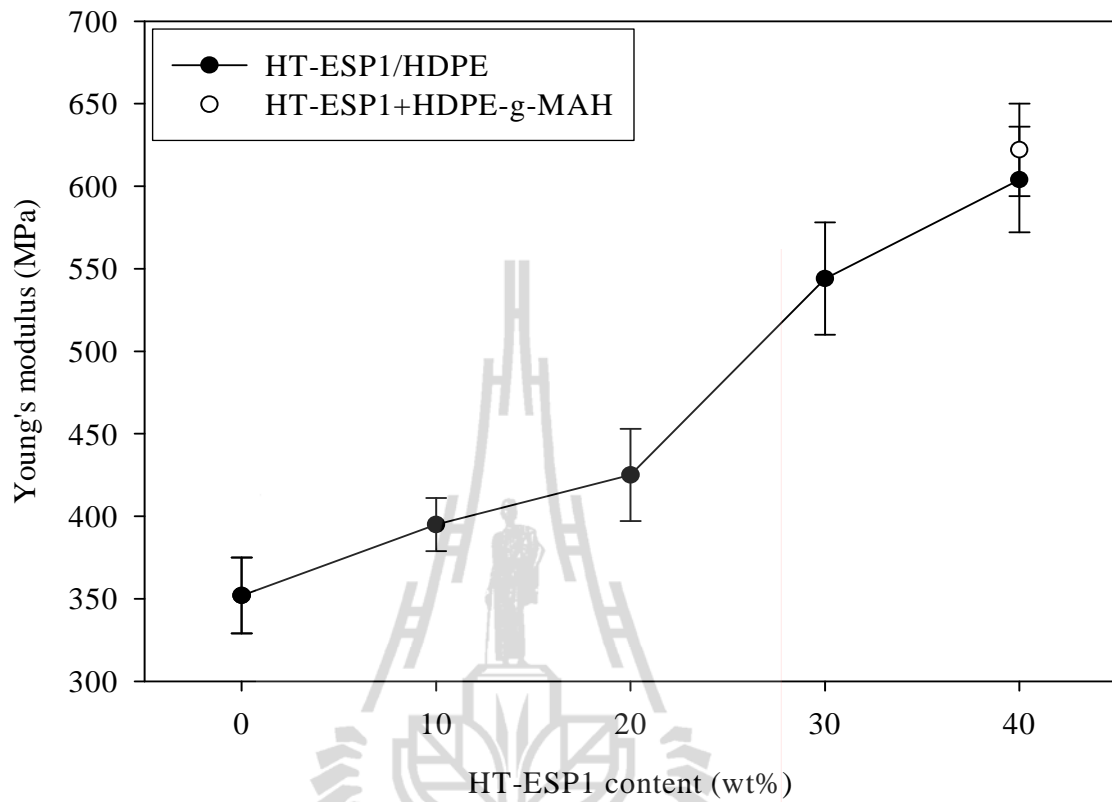


Figure 4.28 Plot of Young's modulus of HT-ESP1/HDPE composites against HT-ESP1 content.

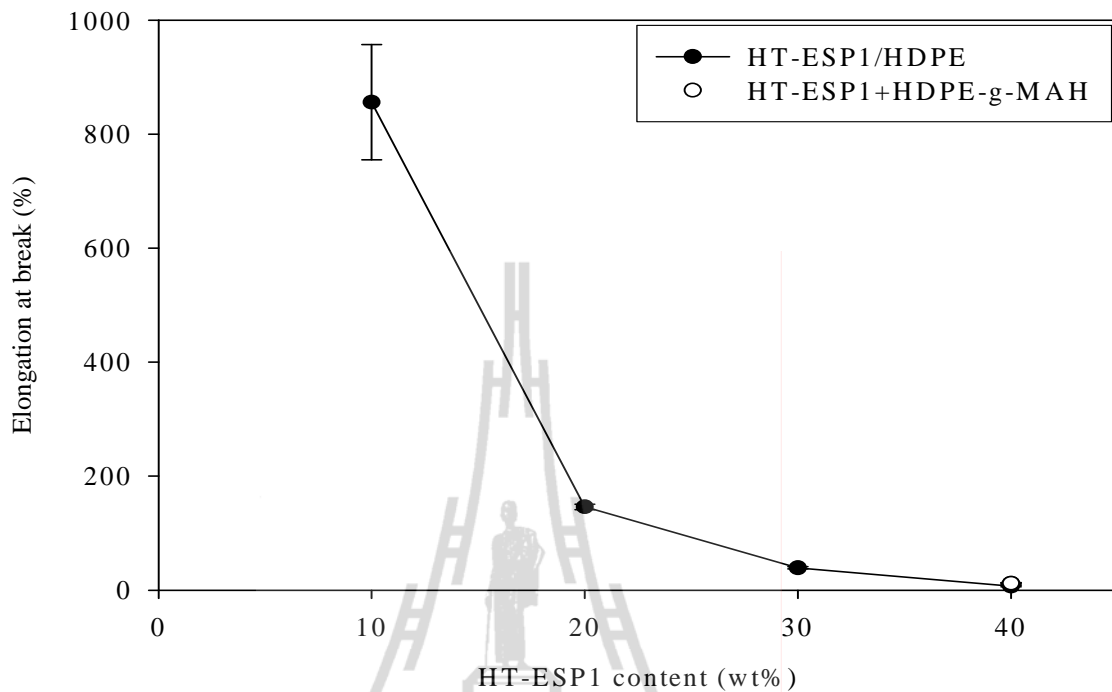


Figure 4.29 Plot of elongation at break of HT-ESP1/HDPE composites against HT-ESP1 content.

Figure 4.30 shows yield strength of the HT-ESP1/HDPE composites as a function of HT-ESP1 content. The yield strength of the HDPE composites containing 0-30 wt% HT-ESP1 was insignificantly different. This indicated that the adding of HT-ESP1 into HDPE caused no improvement of yield strength of the composites. The opposite result was reported that the yield strength of 20 and 40 wt% $\text{Ca}(\text{OH})_2$ /HDPE composites was significantly lower than that of neat HDPE (Mlecnik and La Mantai, 1997).

Figure 4.31 shows tensile stress at break of HT-ESP1/HDPE composites. The tensile stress at break of 10 and 20 wt% HT-ESP1/HDPE composites was not much different. This might be due to insignificant difference in particle distribution between 10 and 20 wt% HT-ESP1. On the other hand, the tensile

stress at break of the composites significantly increased when HT-ESP1 content was increased from 20 wt% to 40 wt%. Although the agglomerates were obviously formed at content of 20-40 wt% HT-ESP1, these agglomerates size were small. For this reason, the tensile stress at break of the composites was increased. With a content of 40 wt% HT-ESP1, the tensile stress at break of the compatibilized composites was slightly higher than that of the uncompatibilized ones. Young's modulus, elongation at break, yield strength, and tensile stress at break of uncompatibilized HDPE composites and compatibilized HDPE composites were reported in Table 4.17.

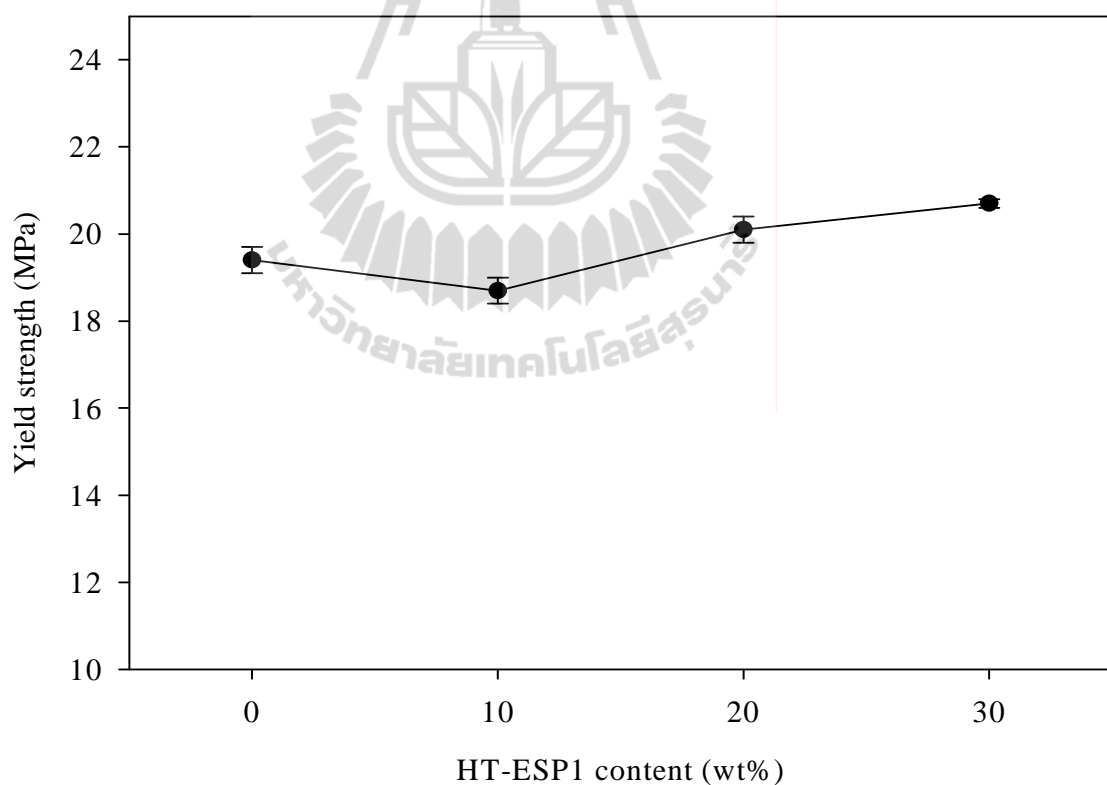


Figure 4.30 Plot of yield strength of HT-ESP1/HDPE composites against HT-ESP1 content.

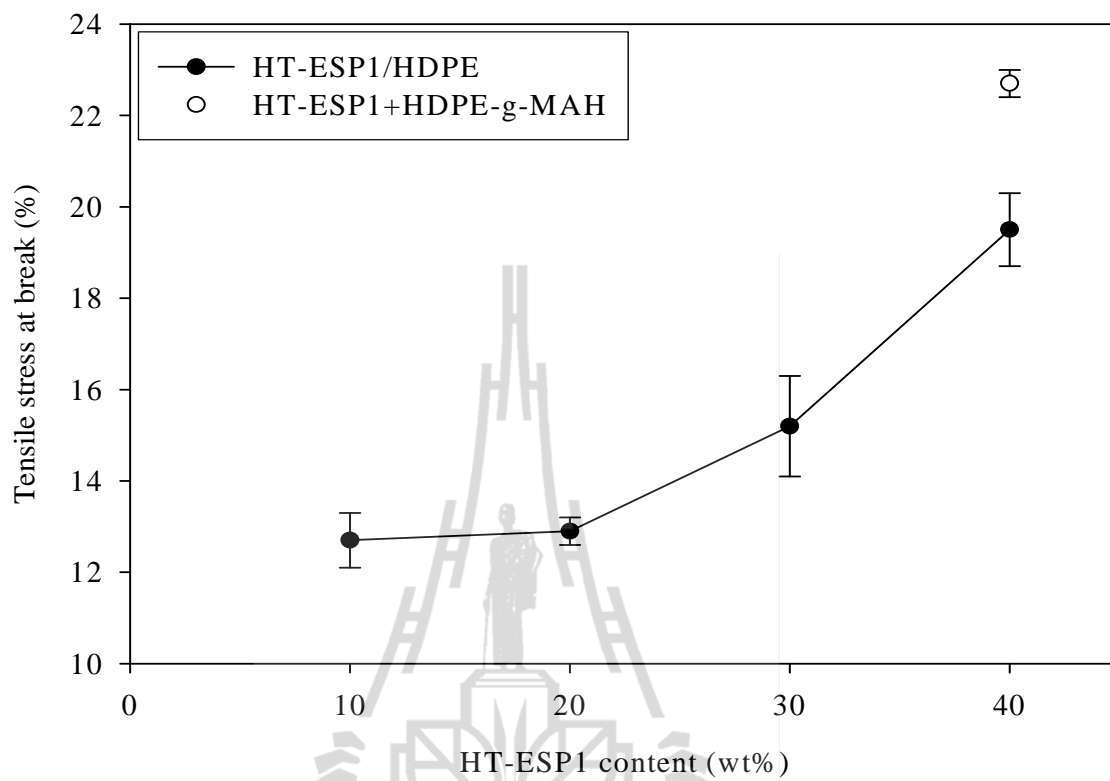


Figure 4.31 Plot of tensile stress at break of HT-ESP1/HDPE composites against HT-ESP1 content.

Table 4.17 Young's modulus, elongation at break, yield strength, and tensile stress at break of HT-ESP1/HDPE composites with and without compatibilization.

HT-ESP1 content (wt%)	Young's modulus (MPa)	Elongation at break (%)	Yield strength (MPa)	Tensile stress at break (MPa)
0% HT-ESP1	352±23	-	19.3±0.1	-
10% HT-ESP1	395±16	856±101	18.7±0.3	12.7±0.6
20% HT-ESP1	425±28	146±5	20.1±0.3	12.9±0.3
30% HT-ESP1	544±34	39±2	20.7±0.1	15.2±1.1
40% HT-ESP1	604±32	7±1	-	19.6±1.0
40% HT-ESP1+HDPE-g-MAH	622±28	12±1	-	22.7±0.3

Flexural modulus and strength of HT-ESP1/HDPE composites are shown in Figure 4.32 and 4.33, respectively. Flexural modulus of HT-ESP1/HDPE increased with increasing HT-ESP1 content. This was due to the addition of the high stiffness particle. Comparatively, at 40 wt% HT-ESP1, the flexural modulus of compatibilized composites was not significantly different from that of uncompatibilized composites. Flexural strength of HT-ESP1/HDPE composites slightly increased with increasing HT-ESP1 content. The flexural strength of compatibilized HDPE composites was insignificantly different from that of uncompatibilized composites. Flexural properties were numbered in Table 4.18.

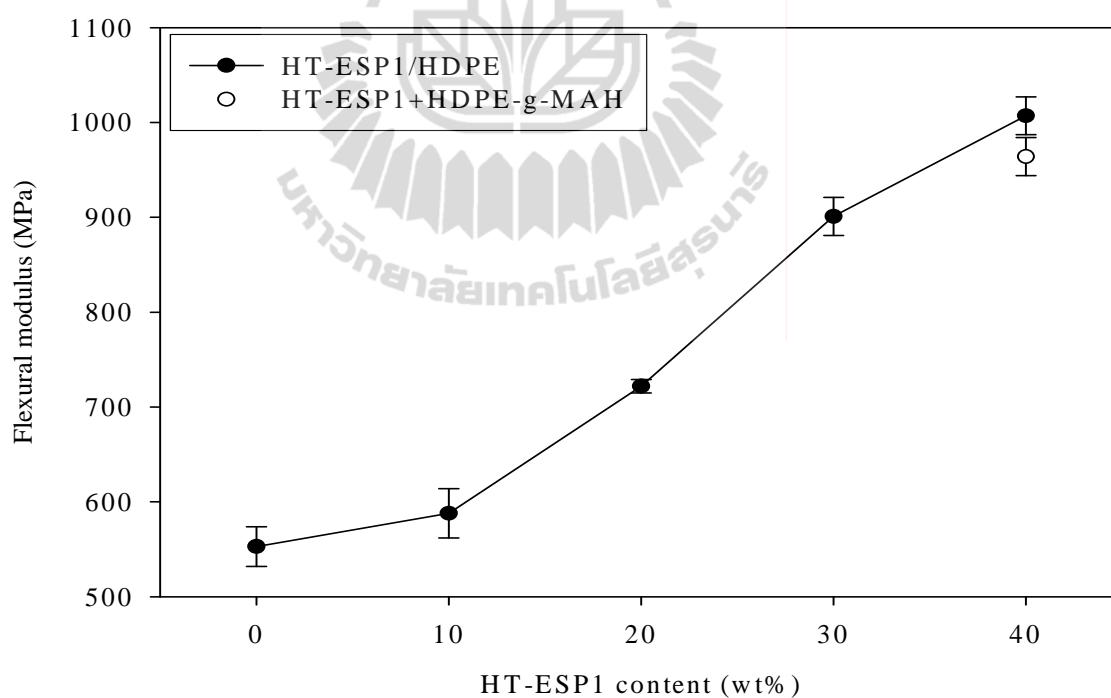


Figure 4.32 Plot of flexural modulus of HT-ESP1/HDPE composites as a function of HT-ESP1 content.

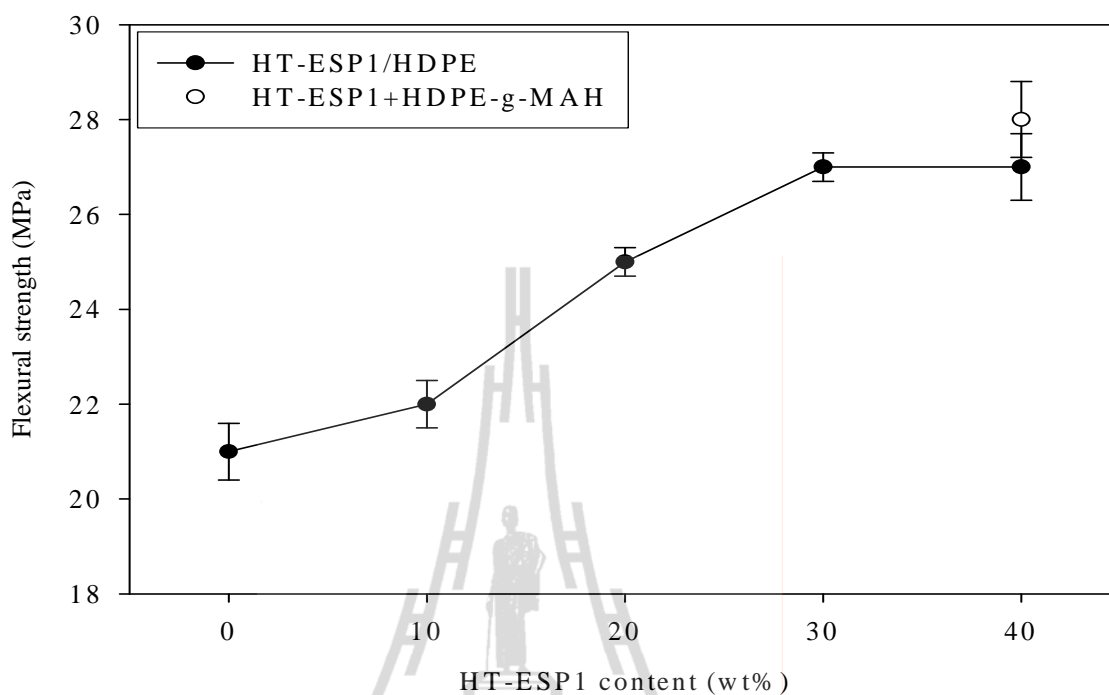


Figure 4.33 Plot of flexural strength of HT-ESP1/HDPE composites as a function of HT-ESP1 content.

Table 4.18 Flexural modulus and flexural strength of HT-ESP1/HDPE composites with and without compatibilization.

HT-ESP1 content (wt%)	Flexural modulus (MPa)	Flexural strength (MPa)
0% HT-ESP1	553±21	21±0.6
10% HT-ESP1	588±26	22±0.5
20% HT-ESP1	722±7	25±0.3
30% HT-ESP1	901±20	27±0.3
40% HT-ESP1	1007±20	27±0.7
40% HT-ESP1+HDPE-g-MAH	964±20	28±0.8

Unnotched Izod impact strength of HT-ESP1/HDPE composites is shown in Table 4.19. The impact strength of HDPE composite at 10 wt% HT-ESP1 and neat HDPE was not obtained because they were not broken under the instrument limit. The impact strength of the HT-ESP1/HDPE composites decreased with increasing HT-ESP1 content. The reduction in impact strength of the composites was probably due to insufficient interfacial adhesion between HT-ESP1 and HDPE matrix. Therefore, voids at interface acted as stress concentrators. When the specimen was impacted, these voids were expanded until they met each other. As a result, this led to the composites to be broken, finally. Hence, the ability of stress transfer between polymer matrix and filler was limited. With a content of 40 wt% HT-ESP1, the impact strength of compatibilized composites was considerably increased comparing to uncompatibilized composites. It suggested that the interfacial adhesion between HT-ESP1 and HDPE was improved by HDPE-g-MAH.

Table 4.19 Unnotched Izod impact strength of HT-ESP1/HDPE composites with and without compatibilization.

HT-ESP1 content (wt%)	Impact strength (kJ/m ²)
0% HT-ESP1	Not break
10% HT-ESP1	Not break
20% HT-ESP1	50.0±4.9
30% HT-ESP1	29.9±2.8
40% HT-ESP1	18.2±3.9
40% HT-ESP1+HDPE-g-MAH	36.8±12.3

Table 4.20 shows the influence of HT-ESP1 content and interfacial modification on hardness and HDT of HT-ESP1/HDPE composite. The hardness of the composites gradually increased as HT-ESP1 content was increased. This resulted from the rigidity of HT-ESP1 which is higher than that of HDPE. Comparatively, at the content of 40 wt% HT-ESP1, the hardness of compatibilized composites was the same as that of uncompatibilized composites. In addition, the HDT of the composites was higher than that of the neat HDPE. The HDT of the composites increased with increasing HT-ESP1 content. The HDT of the compatibilized composite was not different from that of uncompatibilized HDPE composites. Hardness and HDT of the composites was not much improved by the addition of HDPE-g-MAH.

Table 4.20 Hardness and HDT of HT-ESP1/HDPE composites with and without compatibilization.

HT-ESP1 content (wt%)	Hardness (shore D)	HDT (°C)
0% HT-ESP1	38.3±0.3	68.2
10% HT-ESP1	39.8±0.2	72.9
20% HT-ESP1	42.3±0.0	81.9
30% HT-ESP1	43.3±0.2	86.9
40% HT-ESP1	44.6±0.2	86.9
40% HT-ESP1+HDPE-g-MAH	44.0±0.3	87.2

4.3.1.4 Morphological properties

Figure 4.34 shows SEM micrograph of HT-ESP1/HDPE composites. The HT-ESP1 particles had a good distribution within the HDPE matrix at the content of 10-20 wt%. However, the distribution of HT-ESP1 in the composites was poor observed at 30 wt% HT-ESP1, as shown in Figure 4.34 (c). The large clusters of HT-ESP1 particles appeared on the fracture surface of composite at 40 wt% HT-ESP1, as shown in Figure 4.34 (d) and (e). This clearly demonstrated that the dispersion and distribution of HT-ESP1 became much worse with higher HT-ESP1 content. Thus, this was responsible for the transition of the HT-ESP1/HDPE composites from ductile to brittle behavior at 30 wt% HT-ESP1, and the decrease of the impact strength of the composites. Nevertheless, the distribution of HT-ESP1 at content of 40 wt% was improved by compatibilization with HDPE-g-MAH as observed in Figure 4.34 (f). This indicated that the interfacial adhesion between HT-ESP1 and HDPE was improved by HDPE-g-MAH. Therefore, the impact strength of the composites was considerably improved by the compatibilization.

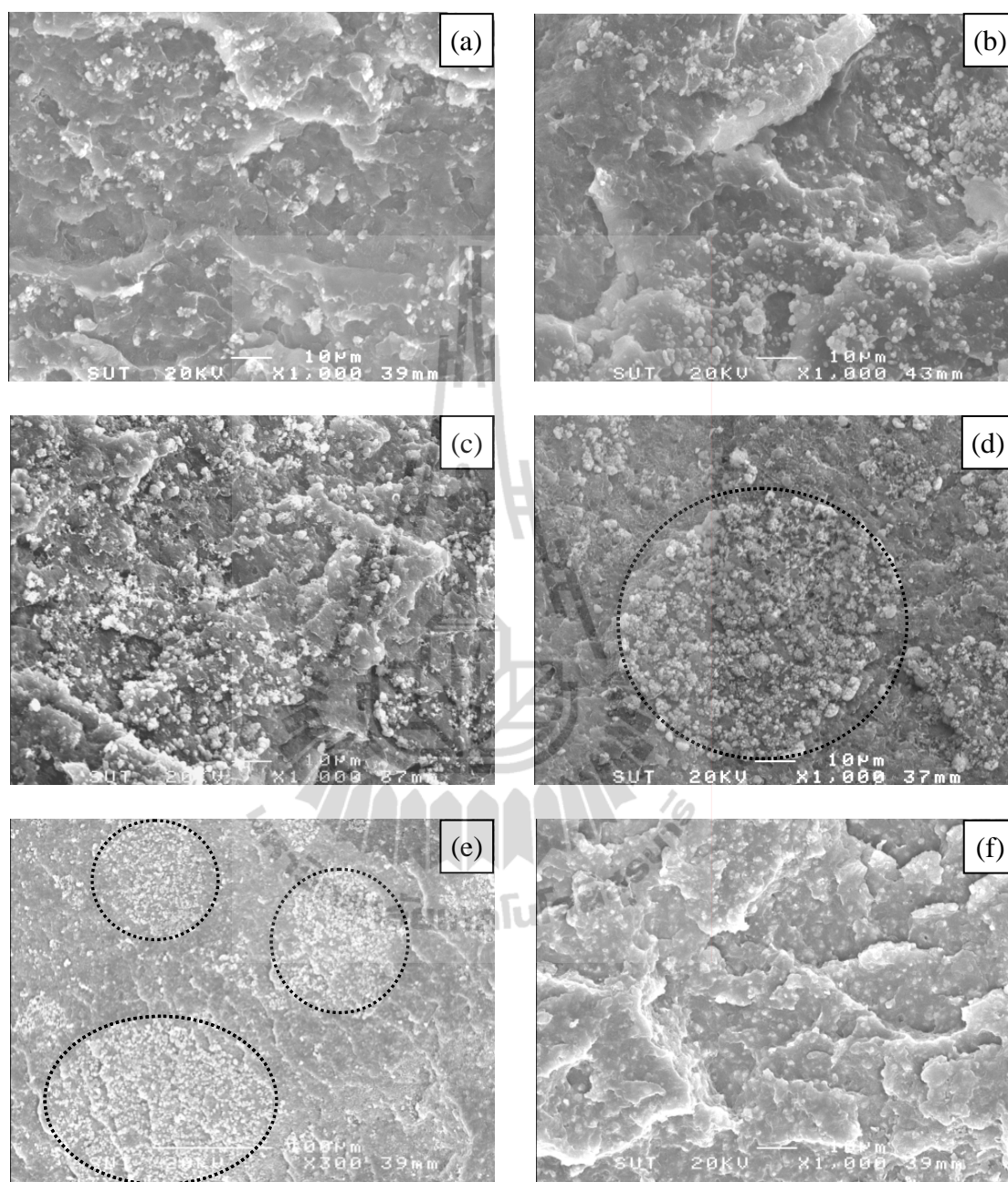


Figure 4.34 SEM micrographs (x1000) of HT-ESP1/HDPE composites: 10 wt% HT-ESP1 (a), 20 wt% HT-ESP1 (b), 30 wt% HT-ESP1 (c), 40 wt% HT-ESP1 (d), 40 wt% HT-ESP1 (x300) (e), and 40 wt% HT-ESP1+HDPE-g-MAH (f).

CHAPTER V

CONCLUSIONS

It was confirmed that chicken eggshell consisted of 95 wt% CaCO_3 in calcite crystal form and 2 wt% organic substances. Eggshell, after grinding, had a particle size (D_{50}) of 12.7 μm with a particle size range of 0.9-124 μm .

The eggshell matrix protein, eggshell membrane, and organic substances were removed by the heat treatment. The removal efficiency of those depended on treatment temperature and time. When the treatment temperatures were 650°C and 670°C, it took more than 24 h and 16 h, respectively, for removing all organic substances. At higher treatment temperatures, 770°C and 800°C, it took 4 h and 3 h, respectively to entirely remove the organic substances. However, with increasing temperature and time of treatment, CaCO_3 was transformed to CaO . In addition, after the obtained CaO was exposed to atmosphere, it was turned into Ca(OH)_2 . The heat-treated eggshell prepared at 800°C for 3 h was employed for preparing HDPE composites. Therefore, the main component of HT-ESP for preparing the composites was Ca(OH)_2 .

For ESP/HDPE composites, the shear viscosity of the composites was increased with increasing ESP content. The addition of ESP at various contents did not affect the decomposition temperature of HDPE. Yield strength, elongation at break, and impact strength of the composites were decreased by increasing ESP content. However, Young's modulus, flexural modulus, and HDT of composites were increased by increasing ESP content. Tensile stress at break and flexural strength of

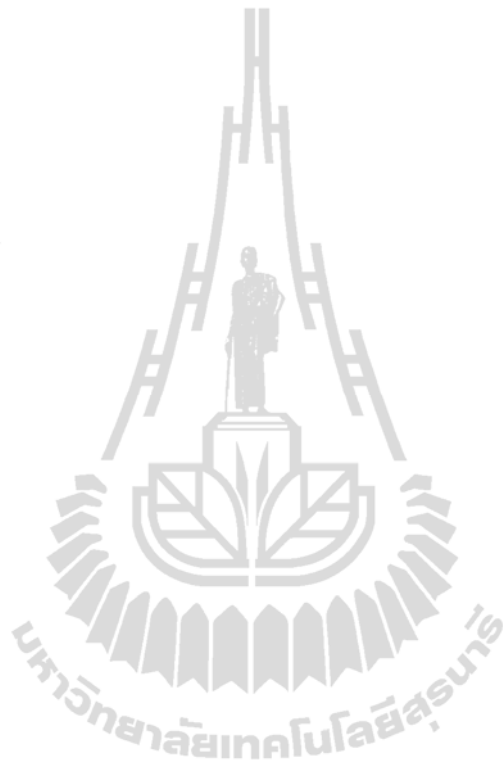
the composites were not significantly increased by increasing ESP content. The hardness of the composites slightly increased with increasing ESP content. The rheological, thermal, and mechanical properties of the HDPE composites prepared with ESP were comparable to those of the composites prepared with CaCO_3 .

When the particle size (D_{50}) of ESP was reduced from 17.1 μm to 14.4 μm , the apparent shear viscosity, thermal stability, and mechanical properties of the HDPE composites prepared with 40 wt% ESP were not significantly different. The 40 wt% ESP/HDPE composites compatibilized with 2 wt% HDPE-g-MAH did not show significant improvement in rheological, thermal, and some mechanical properties such as Young's modulus and flexural modulus. However, it was found some improvements in yield strength, tensile stress at break, flexural strength, impact strength, and HDT of the composites.

For HT-ESP/HDPE composites, the apparent shear viscosity of the composites increased with increasing HT-ESP content. The decomposition temperature of HDPE was insignificantly increased by increasing HT-ESP content. Young's modulus, tensile stress at break, flexural modulus, flexural strength, and heat distortion temperature of the composites were increased with increasing HT-ESP content. The hardness of the composites was slightly increased with increasing HT-ESP content. However, elongation at break and impact strength of the composites were decreased with increasing HT-ESP content. Yield strength of the composites was insignificantly changed with increasing HT-ESP content. The failure behavior of the composite was changed from ductile to brittle at 30 wt% HT-ESP.

The 40 wt% HT-ESP/HDPE composites compatibilized with 2 wt% HDPE-g-MAH had the same rheological, thermal, tensile, flexural, hardness, and HDT to those

of the uncompatibilized HT-ESP/HDPE composites. However, impact strength of the composites was improved by the compatibilization. In addition, the composites at 40 wt% HT-ESP with and without compatibilization were ruptured before yielding under the tensile test.



REFERENCES

- Albano, C., and Perera, R. (2008). Composites of polyolefins and some polyolefin/polyamide blends as matrices and calcium carbonate, wood flour, sisal fiber, hydroxyapatite, and montmorillonite as fillers. In D. Nwabunma and T. Kyu (eds.). **Polyolefin composites** (pp. 87-128). United States of America : John Wiley and Sons.
- Arias, J. L., Mann, K., Nys, Y., Garcia-Ruiz, J. M., and Fernández, M. S. (2007). Eggshell growth and matrix macromolecules. In E. Bäuerlein (ed.). **Handbook of biomineralization** (pp. 309-327). Weinheim : Wiley-VCH.
- Arunlertaree, C., Kaewsomboon, W., Kumsopa, A., Pokethitiyook, P., and Panyawathanakit, P. (2007). Removal of lead from battery manufacturing wastewater. **Songklanakarin J. Sci. Technol.** 29 (3) : 857-868.
- Avian Classroom. Online from <http://ag.ansc.purdue.edu/poultry/class.htm>
- Balázsi, C., Wéber, F., Kövér, Z., Horváth, E., and Németh, C. (2007). Preparation of calcium-phosphate bioceramics from natural resources. **J. Eur. Ceram. Soc.** 27 : 1,601-1,606.
- Bartczak, Z., Argon, A. S., Cohen, R. E., and Weinberg, M. (1999). Toughness mechanism in semi-crystalline polymer blends: II. High-density polyethylene toughened with calcium carbonate filler particles. **Polymer.** 40 : 2,347-2,356.
- Benham, E., and McDaniel, M. (2003). Ethylene polymer, HDPE. **Encyclopedia of polymer science and technology.** 2 : 382-412.

- Carr, F. P., and Frederick, D. K. (2004). Calcium carbonate. **Encyclopedia of chemical technology** (5th ed.). 4 : 551-556.
- Da Costa, Z. M., Pontuschka, W. M., Ludwig, V., Giehl, J. M., Da Costa, C. R., and Duarte, E. L. (2007). A study based on ESR, XRD, and SEM of signal induced by gamma irradiation in eggshell. **Radiat. Meas.** 42 : 1,233-1,236.
- Daengprok, W., Garnjanagoonchorn, and Mine, Y. (2002). Fermented pork sausage fortified with commercial or hen eggshell calcium lactate. **Meat. Sci.** 62 : 199-204.
- Dangtungee, R., Yun, J., and Supaphol, P. (2005). Melt rheology and extrudate swell of calcium carbonate nanoparticle-filled isotactic polypropylene. **Polym. Test.** 24 : 2-11.
- Dasgupta, P., Singh, A., Adak, S., and Purohit, K. M. (2004). Synthesis and characterization of hydroxyapatite produced from eggshell. In **International Symposium of research students on Materials Science and Engineering** (pp. 1-6). Chennai, India.
- Desai, S. M., and Singh, R. P. (2004). Surface modification of polyethylene. **Adv. Polym. Sci.** 169 : 231-293.
- Deshmane, C., Yuan, Q., and Misra, R.D.K. (2007). On the fracture characteristics of impact tested high density polyethylene–calcium carbonate nanocomposites. **Mater. Sci. Eng. A.** 452-453 : 592-601.
- Domka, L., Wąsicki, A., and Kozak, M. (2003). The microstructure and mechanical properties of new HDPE-chalk composites. **Physicochem. Probl. Miner. Process.** 37: 141-147.

- Dong, Q., Su, H., Xu, J., Zhang, D., and Wang, R. (2007). Synthesis of biomorphic ZnO interwoven microfibers using eggshell membrane as the biotemplate. **Mater. Lett.** 61 : 2,714-2,717.
- Drnovská, H., Lapčík J. L., Buršíková, V., Zemek, J., and Barros-Timmons, A. M. (2003). Surface properties of polyethylene after low-temperature plasma treatment. **Colloid polym, Sci.** 281 : 1,025-1,033.
- Engin, B., Demirtaş, H., and Eken, M. (2006). Temperature effects on egg shells investigated by XRD, IR, and ESR techniques. **Radiat. Phys. Chem.** 75 : 268-277.
- Freire, M. N., and Holanda, J. N. F. (2006). Characterization of avian eggshell waste aiming its use in a ceramic wall tie paste. **Cerâmica.** 52 : 240-244.
- Fu, S-Y., Feng, X-Q., Lauke, B., and Mai, Y-W. (2008). Effect of particle size, particle/matrix interface adhesion and particle loading on mechanical properties of particulate-polymer composites. **Composites Part B.** 39 : 933-961.
- Gautron, J., and Nys, Y. (2007). Eggshell matrix protein. In R. Huopalahti, R. López-Fandiño, M. Anton, and R. Schade (eds.). **Bioactive egg compounds** (pp. 103-108). New York: Springer-Verlag Berlin Heideberg.
- González, J., Albano, C., Ichazo, M., and Díaz, B. (2002). Effects of coupling agents on mechanical and morphological behavior of the PP/HDPE blend with two different CaCO₃. **Eur. Polym. J.** 38 : 2,465–2,475.
- González, J., Albano, C., Ichazo, M., Hernández, and Sciamanna, R. (2001). Analysis of thermogravimetric data of blends of polyolefins with calcium carbonate treated with Lica 12. **Polym. Degrad. Stab.** 73 : 211-224.

- Gupta, B., Hilborn, J., Hollenstein, CH., Plummer, C. J. G., Houriet, R., and Xanthopoulos, N. (2000). Surface modification of polyester films by RF plasma. **J. Appl. Polym. Sci.** 78 : 1,083-1,091.
- Heredia, A., Rodríguez-Hernández, A. G., Lozano, L. F., Peña-rico, M. A., Velázquez, R., Basiuk, V. A., and Bucio, L. (2005). Microstructure and thermal change of texture of calcite crystals in ostrich eggshell *Struthio camelus*. **Mater. Sci. Eng. C.** 25 : 1-9.
- Hincke, M. T., Gautron, J., Panheleux, M., Garcia-Ruiz, J., McKee, M. D., and Nys, Y. (2000). Identification and localization of lysozyme as a component of eggshell membranes and eggshell matrix. **Matrix Biol.** 19 : 443-453.
- Hohenberger, W. (2001). Fillers and reinforcements/coupling agents. In H. Zweifel (ed.). **Plastics additives handbook** (pp. 901-948). Munich: Hanser.
- Houssa, C. E. (2003). Minerals in plastics. **Bulletin de la Société Royale des Sciences de Liège.** 72 : 71-80.
- Hunton, P. (2005). Research on eggshell structure and quality: An historical overview. **Brazil. J. Poult. Sci.** 7 (2) : 67-71.
- Irabien, A., Viguri, J. R., and Ortiz, I. (1990). Thermal dehydration of calcium hydroxide : 1. Kinetic Model and Parameters. **Ind. Eng. Chem. Res.** 29 : 1,599-1,606.
- Ji, G., Zhu, H., Qi, C., and Zeng, M. (2009). Mechanism of interactions of eggshell microparticles with epoxy resins. **Polym. Eng. Sci.** 49 :1,383-1,388.
- Kang, D. J., Pal, K., Park, S. J., Bang, D. S., and Kim, J. K. (2010). Effect of eggshell and silk fibroin on styrene-ethylene/butylenes-styrene as bio-filler. **Mater. Des.** 31 : 2,216-2,219.

Kenrich petrochemical, Inc Online from <http://4kenrich.com>

Kitamura, M., Konno, H., Yasui, A., and Masuoka, H. (2002). Controlling factors and mechanism of reactive crystallization of calcium carbonate polymorphs from calcium hydroxide suspensions. **J. Cryst. Growth.** 236 : 323-332.

Lammie, D., Bain, M. M., Solomon, S. E., and Wess, T. J. (2006). Scanning microfocus small angle X-ray scattering study of the avian eggshell. **J. Bio Eng.** 3 : 011-018.

Lazzeri, A., Zebarjad, S. M., Pracella, M., Cavalier, K., and Rosa, R. (2005). Filler toughening of plastics. Part I-The effect of surface interactions on physic-mechanical properties and rheological behavior of ultrafine CaCO₃/HDPE nanocomposites. **Polymer.** 46 : 827-844.

Lee, S. J., and Oh, S. H. (2003). Fabrication of calcium phosphate bioceramics by using eggshell and phosphoric acid. **Mater. Lett.** 57 : 4,570-4,574.

Li-Chan, E., and Kim, H. O. (2008). Structure and chemical composition of eggs. In Y. Mine (ed.). **Egg bioscience and biotechnology** (pp. 1-95). Wiley-Interscience.

Li-Chan, E. C. Y., Powrie, W. D., and Nakai, S. (1995). The chemistry of eggs and egg products. In W. J. stadelman and O. J. Cotterill (eds.). **Egg science and technology** (pp. 105-175). New York : Food product press.

Liu, Z. H., Kwok, K. W., Li, R. K. Y., and Choy, C. L. (2002). Effects of coupling agent and morphology on the impact strength of high density polyethylene/CaCO₃ composites. **Polymer.** 43 : 2,501-2,506.

Macneil, J. H. (2006). Method and apparatus for separating a protein membrane and shell material in waste egg shells. **United States Patent 7007806.** (Unpublished manuscript).

- Masuda, Y., and Hiramatsu, H. (2008). Bioavailability and physiological function of eggshells and eggshell membranes. In Y. Mine (ed.). **Egg bioscience and biotechnology** (pp. 129-140). Wiley-Interscience.
- McCrum, N. G., Buckley, C. P., and Bucknall, C. B. (1997). **Principles of polymer engineering**. (2nd ed.). Oxford: Oxford University Press.
- Mihajlović, S., Sekulić, Ž., Daković, A., Vučinić, D., Jovanović, V., and Stojanović, J. (2009). Surface properties of natural calcite filler treated with stearic acid. **Ceram. Silik.** 53(40) : 268-275.
- Minerals technologies Online from <http://www.specialtyminerals.com/our-minerals/what-is-pcc/>
- Ministry of Agriculture and Cooperatives, Center for Agricultural Information. (2010). Online from <http://www.moac.go.th>
- Ministry of Industry, Department of Primary Industries and mines (DPIM). (2004). Online from <http://www.industry.go.th>
- Misra, R. D. K., Nerikar, P., Bertrand, K., and Murphy, D. (2004). Some aspects of surface deformation and fracture of 5 – 20% calcium carbonate-reinforced polyethylene composites. **Mater. Sci. Eng. A** 384 : 284-298.
- Mlecnik, E., and La Mantai, F. P. (1997). Influence of calcium-based fillers and vegetable oil on the processability and yield behavior of polyolefins. **J. Appl. Polym. Sci.** 65 : 2,761–2,772.
- Montes-Hernandez, G., Renard, F., Geoffroy, N., Charlet, L., and Pironon, J. (2007). Calcite precipitation from CO₂-H₂O-Ca(OH)₂ slurry under high pressure of CO₂. **J. Cryst. Growth.** 308 : 228-236.

- Murakami, F. S., Rodrigues, P. O., Campos, C. M. T., and Silva, M. A. S. (2007). Physicochemical study of CaCO₃ from egg shells. **Ciênc. Tecnol. Aliment., Campinas**. 27 (3) : 658-662.
- Naemchan, K., Meejoo, S., Onreabroy, W., and Limsuwan, P. (2007). Temperature effect on duct egg shell investigated by XRD and ESR techniques. In **33rd Congress on Science and Technology of Thailand** (pp. 1-3). Nakhon Si Thammarat.
- Navarro, F., Dávalos, F., Denes, F., Cruz, L. E., Young, R. A., and Ramos, J. (2003). Highly hydrophobic sisal chemithermomechanical pulp (CTMP) paper by fluorotrimethylsilane plasma treatment. **Cellulose**. 10 : 411-424.
- Nys, Y., and Gautron, J. (2007). Structure and formation of eggshell. In R. Huopalahti, R. López-Fandiño, M. Anton, and R. Schade (eds.). **Bioactive egg compounds** (pp. 99-102). New York: Springer-Verlag Berlin Heideberg.
- Nys, Y., Gautron, J., Garcia-Ruiz, J. M., and Hincke, M. T. (2004). Avian eggshell mineralization: Biochemical and functional characterization of matrix proteins. **C. R. Palevol**. 3 : 549-562.
- Öztürk, S. (2006). **Modification of calcium carbonate surfaces in natural gas plasma for their use in polypropylene composite systems**. M.S. thesis, Middle East Technical University, Turkey.
- Park, H. J., Jeong, S. W., Yang, J. K., Kim, B. G., and Lee, S. M. (2007). Removal of heavy metals using waste eggshell. **J. Environ. Sci**. 19 (12) : 1,436-1,441.
- Park, S. H., and Kim, S. D. (1994). Plasma surface treatment of HDPE powder in a fluidized bed reactor. **Polym. Bull**. 33 : 249-256.

Peacock, A. J. (2000). **Handbook of polyethylene: Structure, properties, and application.** United States of America: Marcel Dekker.

Petroleum Institute of Thailand. (2009). Online from <http://www.ptit.org>

Phueakbuakhao, N., Prissanaroon-Ouajai, W., and Kreua-Ongarjnkool, N. (2008). Effect of coupling agents on mechanical properties and morphology of CaCO₃-filled recycled high density polyethylene. **J. Met. Mater. Miner.** 18(2) : 131-135.

Rivera, E. M., Araiza, M., Brostow, W., Castaño, V. M., Díaz-Estrada, J. R., Hernández, R., and Rodríguez, J. R. (1999). Synthesis of hydroxyapatite from eggshells. **Mater. Lett.** 41 : 128-134.

Rosen, S. L. (1993). **Fundamental principles of polymeric materials.** (2nd ed.). New York: John Wiley and Sons.

Rukchonlatee, S., Prasertwong, T., and Sangpakdee, T. (2002). Effect of compatibilizer types on properties of CaCO₃-filled high density polyethylene. **Suranaree J. Sci. Technol.** 9 : 253-260.

Sakullertphasuk, K., Piriyesyangkul, K., Jitthai, T., and Haruthaithanasan, V. (2003). **Utilization of egg shell in cosmetic.** Faculty of Agro-Industry. Kasetsart University. (Unpublished manuscript).

Sanmuang, S., Ruksakulpiwat, Y., Suppakarn, N., and Sutapun, W. (2008). Chicken eggshell as a filler for polymer composites: Preparation and characterizations. **Adv. Mater, Res.** 47-50 : 490-493.

Saravari, O. (2003). **Polymer additives I.** Bangkok: Chulalongkorn University Press.

- Schaafsma, A., Pakan, I., Hofstede, G. J. H., Muskiet, F. A. J., Van Der Veer, E., and De Vries, P. J. F. (2000). Mineral, amino acid, and hormonal composition of chicken eggshell powder and the evaluation of its use in human nutrition. **Poult. Sci.** 79 : 1,833-1,838.
- Shi, X., Rosa, R., and Lazzeri, A. (2010). On the coating of precipitated calcium carbonate with stearic acid in aqueous medium. **Langmuir.** 26(11) : 8,474–8,482.
- Shuhadah, S. and Supri, A. G. (2009). LDPE-isophthalic acid-modified egg shell powder composites (LDPE/ESP). **J. Phys. Sci.** 20(1) : 87-98.
- Shui, M., Yue, L., and Xu, Z. (2004). The mechanical and NIR studies on ultrafine calcium carbonate treated by four surface modifiers. **Spectrochim. Acta, Part A.** 60 : 441-447.
- Silva, A. L. N., Rocha, M. C. G., Moraes, M. A. R., Valente, C. A. R., and Coutinho, F. M. B. (2002). Mechanical and rheological properties of composites based on polyolefin and mineral additives. **Polym. Test.** 21 : 57-60.
- Singh, N. B., and Singh, N. P. (2007). Formation of CaO from thermal decomposition of calcium carbonate in the presence of carboxylic acids. **J. Therm. Anal. Calorim.** 89 : 159-162.
- Stadelman, W. J. (2000). Eggs and egg products. **Wiley encyclopedia of food science and technology** 1 : 593-599.
- Stadelman, W. J. (1995). Quality identification of shell eggs. In W. J. Stadelman and O. J. Cotterill (eds.). **Egg science and technology** (pp. 39-66). New York: Food product press.

- Suguro, N., Horiike, S., Masuda, Y., Kunou, M., and Kokubu, T. (2000). Bioavailability and commercial use of eggshell calcium, membrane proteins, and yolk lecithin products. In J. S. Sim, S. Nakai, and W. Guenter (eds.). **Egg nutrition and biotechnology** (pp. 219-232). Wallingford : CABI.
- Supri, A. G., Ismail, H., and Shuhadah, S. (2010). Effect of polyethylene-grafted maleic anhydride (PE-g-MAH) on properties of low density polyethylene/eggshell powder (LDPE/ESP) composites. **Polym.-Plast. Technology. Eng.** 49 (4) : 347-353.
- Surampadi, N. L., Pesacreta, T.C., and Misra, R.D.K. (2007). The determining role of scratch indenter radius on surface deformation of high density polyethylene and calcium carbonate-reinforced composite. **Mater. Sci. Eng. A.** 456 : 218-229.
- Suwanprateeb, J., Tiemprateeb, S., Kangwantrakool, S., and Hemachandra, K. (1998). The role of filler volume fraction in the strain-rate dependence of calcium carbonate-reinforced polyethylene. **J. Appl. Polym. Sci.** 70 : 1,717-1,724.
- Tai, C.Y., and Chen, C. K. (2008). Particle morphology, habit, and size control of CaCO_3 using reverse microemulsion technique. **Chem. Eng. Sci.** 63 : 3,632-3,642.
- Tanniru, M., and Misra, R. D. K. (2006). Reduced susceptibility to stress whitening during tensile deformation of calcium carbonate-reinforced high density polyethylene composites. **Mater. Sci. Eng. A.** 424 : 53-70.
- Tanniru, M., Misra, R. D. K., Bertrand, K., and Murphy, D. (2005). The determining role of calcium carbonate on surface deformation during scratching of calcium carbonate-reinforced polyethylene composites. **Mater. Sci. Eng. A.** 404 : 208-220.
- Thoroski, J. H. (2003). Eggshell processing methods and apparatus. **United States Patent 6649203**. (Unpublished manuscript).

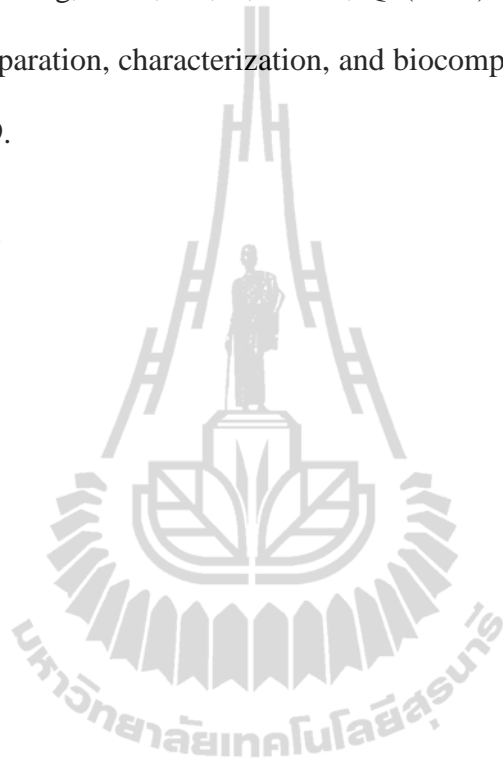
- Toro, P., Quijada, R., Yazdani-Pedram, M., and Arias, J. L. (2007). Eggshell, a new bio-filler for polypropylene composites. **Mater. Let.** 61 : 4,347-4,350.
- Tsai, W. T., Yang, J. M., Lai, C. W., Cheng, Y. H., Lin, C. C, and Yeh, C. W. (2006). Characterization and adsorption properties of eggshells and eggshell membrane. **Bioresour. Technol.** 97 : 488-493.
- Tsai, W. T., Yang, J. M., Hsu, H. C., Lin, C. M., Lin, K. Y., and Chiu, C. H. (2008). Development and characterization of mesoporosity in eggshell ground by planetary ball milling. **Micropor. Mesopor. Mater.** 111 : 379-386.
- Vlachopoulos, J., and Strutt, D. (2003). The role of rheology in polymer extrusion. In **New Technology for Extrusion Conference** (pp. 21-25). Milan, Italy.
- Wang, Q., Chen, H., and Liu, Y. (2002). LDPE-g-MAH prepared through solid-phase mechanochemistry and its compatibilizing effects on HDPE/CaCO₃. **Polym.-Plast. Technol. Eng.** 41(2) : 215-228.
- Wang, W-Y., Zeng, X-F., Wang, G-Q., and Chen, J-F. (2007). Preparation and characterization of calcium carbonate/low-density-polyethylene nanocomposites. **J. Appl. Polym. Sci.** 106 : 1,932-1,938.
- Wei, Z., Xu, C., and Li, B. (2009). Application of waste eggshell as low-cost solid catalyst for biodiesel production. **Bioresour. Technol.** 100 : 2,883-2,885.
- Wikipedia Online from http://en.wikipedia.org/wiki/Calcium_carbonate
- Wikipedia Online from [http://en.wikipedia.org/wiki/Plasma_\(physics\)](http://en.wikipedia.org/wiki/Plasma_(physics))
- Wypych, G. (2000). **Handbook of fillers** (2nd ed.). Toronto: ChemTech.
- Xanthos, M. (2005). Polymers and polymer composites. In M. Xanthos (ed.). **Functional fillers for plastics** (pp. 4-16). Weinheim : Wiley-VCH.

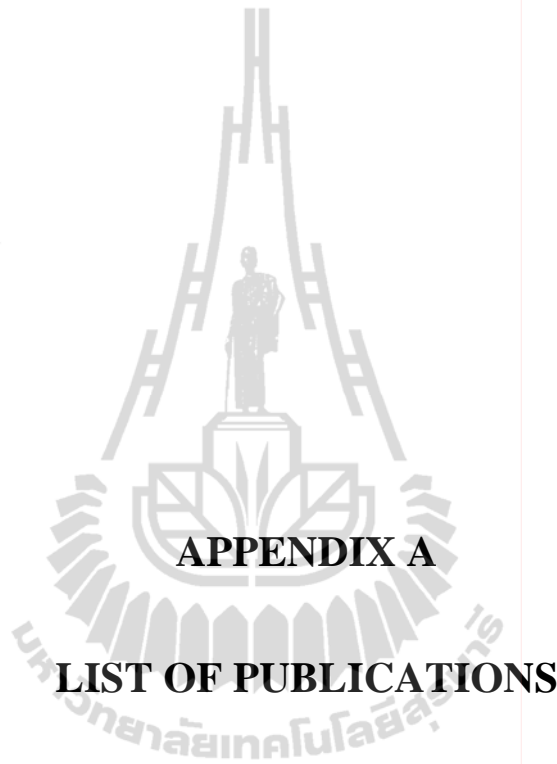
Yang, Y. L., Bai, S. L., G'Sell, C., and Hiver, J. M. (2006). Mechanism properties and volume dilatation of HDPE/CaCO₃ blends with and without impact modifier.

Polym. Eng Sci. : 1,512-1,522.

Yi, F., Guo, Z.X., Zhang, L. X., Yu, J., and Li, Q. (2004). Soluble eggshell membrane protein: preparation, characterization, and biocompatibility. **Biomaterials.** 25 :

4,591-4,599.





List of publications

- Pakdeechote, P., Ruksakulpiwat, Y., Suppakarn, N., and Sutapun, W. (2009). Preparation and characterization of heat-treated eggshell for HDPE composites: A preliminary study. In **Proceeding of PACCON2009 (Pure and Applied Chemistry International Conference)** (pp 325-327). Pitsanulok, Thailand.
- Pakdeechote, P., Ruksakulpiwat, Y., Suppakarn, N., and Sutapun, W. (2009). Mechanical properties of HDPE filled with eggshell powder. In **Proceeding of the 11th Pacific Polymer Conference 2009** (p 154). Cairns, Australia.
- Pakdeechote, P., Ruksakulpiwat, Y., Suppakarn, N., and Sutapun, W. (2010). Rheological, mechanical and morphological properties of eggshell powder (ESP) filled high density polyethylene (HDPE). In **Proceeding of the Sixth Thailand Materials Science and Technology Conference** (pp168-170). Bangkok, Thailand.

PREPARATION AND CHARACTERIZATION OF HEAT-TREATED EGGSHELL FOR HDPE COMPOSITES: A PRELIMINARY STUDY

P. Pakdeechote¹, Y. Ruksakulpiwat^{1,2}, N. Suppakarn^{1,2}, and W. Sutapun^{1,2*}

¹ School of Polymer Engineering, Institute of Engineering, Suranaree University of Technology, Nakhon Ratchasima 30000, Thailand

² Center of Excellence for Petroleum, Petrochemicals, and Advanced Materials, Chulalongkorn University, Bangkok 10330, Thailand

*E-mail: wimonlak@sut.ac.th, Tel: +66-44-224435

Abstract: The objective of this work is to extract calcium carbonate (CaCO_3) from chicken eggshell by means of heat treatment. The heat treatment of raw eggshell was carried out at 800°C for 1-6 hrs. The Heat-treated eggshell was then analyzed via X-ray diffraction spectrometer (XRD), X-ray fluorescence spectrometer (XRF), thermogravimetric analyzer, and particle size analyzer. It was revealed that the organic matter was completely removed at 3 hrs of the treatment. The XRD patterns showed that increasing the treatment times led to a decrease of calcium carbonate content. At the treatment times of 5 and 6 hrs, the treated eggshell was basically constituted by calcium oxide (CaO). The results from the XRF showed that the main composition, 66 wt%, of the treated eggshell was calcium and the minor parts were SiO_2 , Mg, P, K, Al and S. In addition, TGA curves indicated that the raw eggshell mainly consisted of calcium carbonate, approximately 95 wt%. A particle size of the treated eggshell was in a range of 8.66-11.42 μm .

Introduction

Chicken eggshell (ES) is classified as a natural biomaterial [1]. ES comprises calcium carbonate (CaCO_3 , 94%), magnesium carbonate (1%), calcium phosphate (1%) and organic materials (4%), mainly proteins, [2]. The eggshell is consisted of three distinct layers from the inside to the outside; shell membrane, mammillary layer and palisade layer [3]. Calcium carbonate is among protein matrix in the mammillary and palisade layers [4]. In recent years, many attempts have focused on the use of eggshell for various applications. For example, it has been used as a resource for calcium in nutrient production [5], absorbent for heavy metals in electroplating wastewater [6], and an alternative pharmaceutical excipient [7]. Calcium carbonate is one of the inorganic fillers that have been used in HDPE composites [8, 9]. According to its compositions and availability, ES must be a potential and renewable resources for calcium carbonate to be used in plastic industry. It was reported by Toro et al. that ES from White Leghorn hen eggs was mixed with polypropylene (PP) with various ES contents. The Young's modulus of the PP composites was improved with increasing ES contents [10]. In this research, ES was heat treated at 800°C for 1-6 hrs in order to remove the organic substances and then calcium carbonate was finally obtained.

Materials and Methods

Materials: Chicken eggshell waste of Bolvans Goldline and ISA Brown hybrid breeds were collected from the SUT Farm, Suranaree University of Technology.

Preparation of heat-treated eggshell: Firstly, the chicken eggshell waste was thoroughly cleaned with tap water to remove the chicken dung and the residual of albumen (egg white) and yolk adhering to the eggshell. After that, the cleaned eggshell was then dried in an open air for 24 hr. The eggshell from such stage was referred to *raw eggshell*. For heat treatment, the raw eggshell was heated up from room temperature to 800°C in a muffle furnace with a heating rate of $10^\circ\text{C}/\text{min}$. The eggshell was treated at 800°C for 1, 2, 3, 4, 5 and 6 hrs. After the treatment, the treated eggshell was remained in the furnace until temperature was down to 30°C . It was then kept in a desiccator prior to characterizations.

Characterizations: Compositions of heat-treated eggshell were examined by X-ray diffractometer (Bruker D5005) at 2θ between $5 - 70^\circ$ with a voltage of 40 kV and a current of 40 mA. X-ray fluorescence spectrometer (Oxford ED-2000) was employed to determine amount of calcium, and other elements and compounds of the treated eggshell. Thermal properties of the heat-treated eggshell were investigated by thermogravimetric analyzer (TA Instrument, SDT 2960) with a heating rate of $20^\circ\text{C}/\text{min}$ under a nitrogen atmosphere. Their particle size and size distribution were determined via particle size analyzer (Malvern Mastersizer S) with range lens of 300RF and a beam length of 2.40 mm.

Results and Discussion

XRD patterns of the heat-treated eggshell are shown in Figure 1. It revealed that calcium carbonate was obtained at the treatment time of 1 hr. Nevertheless, some portions of the treated eggshell obtained from the treatment time up to 2 hrs appeared black. This indicated that organic substances were not completely removed. The calcium carbonate contents significantly decreased with increasing the treatment times. When the raw eggshell was treated for 5 and 6 hrs, calcium oxide (CaO) was the main component. In

addition, the calcium oxide content increased with the treatment times. As a result, calcium oxide coexisted with calcium carbonate after the treatment for 1-6 hrs. However, the calcium carbonate was in small amount for the treatment times of 2-6 hrs. This was due to calcium carbonate was changed to calcium oxide by heated at 800°C in a presence of air [11]. Besides calcium carbonate and calcium oxide, calcium hydroxide ($\text{Ca}(\text{OH})_2$) was obtained as well. Calcium hydroxide might come from the reaction of calcium oxide and moisture when the heat-treated eggshell was exposed to the atmosphere [12].

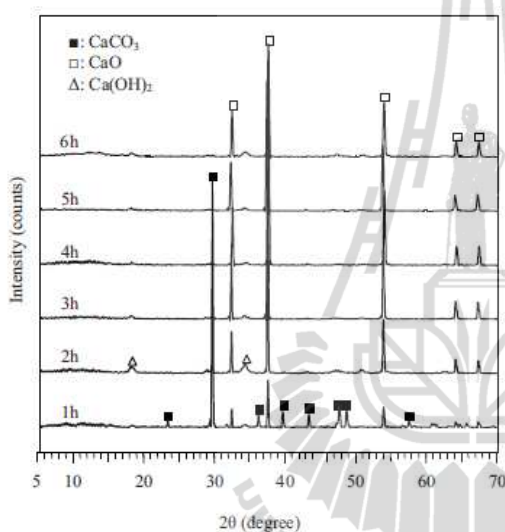


Figure 1. XRD patterns of eggshell after heat treatment at 800°C for 1-6 hrs

The compositions of heat-treated eggshell (3-6 hrs of the treatment) are shown in Table 1. Calcium was the main component of the heat-treated eggshell. Its content was about 66 wt%. In addition, other components were SiO_2 , about 0.3-1%, and Mg, S, K, Al and P in trace amounts.

Table 1: Chemical compositions of the eggshell after heat treatment at 800°C for 3-6 hrs obtained from XRF spectrometry

Composition	Amount (wt%)			
	3h	4h	5h	6h
Ca	65.83	66.14	65.57	65.60
SiO_2	1.02	0.63	0.34	0.64
Mg	0.57	0.52	1.15	0.96
S	0.17	0.22	0.20	0.18
K	0.12	0.14	0.16	0.16
Al	0.05	0.04	0.05	0.05
P	949*	981*	942*	0.11

* unit of ppm

The TGA and DTGA curves of calcium carbonate, raw eggshell and heat-treated eggshell (3-6

hrs of the treatment) are illustrated in Figure 2(a) and 2(b), respectively. From Figure 2 (a), the raw eggshell initially decomposed around 55°C due to the removal of water. In addition, the TGA curves of heat-treated eggshell showed the decomposition peak due to the evaporation of water about 55°C as well. The second decomposition temperature of the raw eggshell appeared at 326°C; this was related to the decomposition of organic matter of the ES [13]. The third decomposition temperature started at 720°C was caused by the change of calcium carbonate to calcium oxide [11]. The TGA curve of raw eggshell showed weight loss of about 5 wt% before decomposition of calcium carbonate. It means that the eggshell contained approximately 95 wt% calcium carbonate. It was reported by Stadelman that the *avian* eggshell generally contained calcium carbonate about 94 wt% [2].

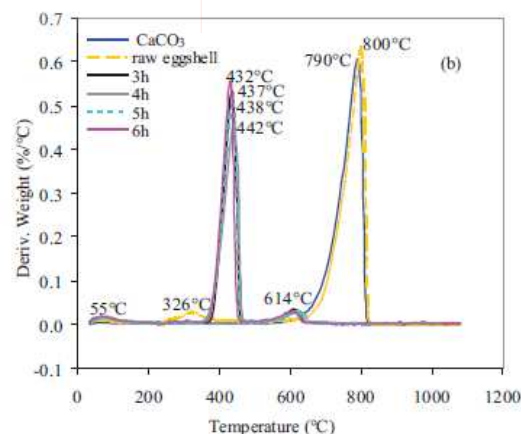
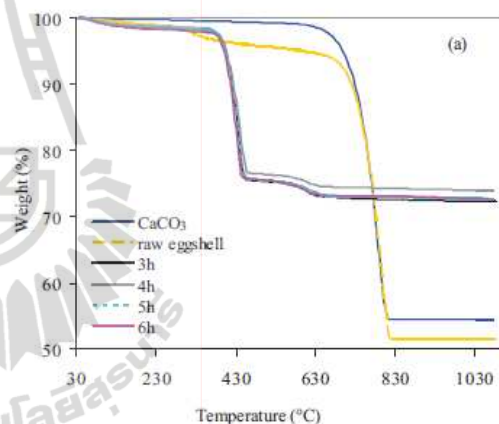


Figure 2. TGA (a) and DTGA (b) curves of raw eggshell, calcium carbonate and eggshell after the heat treatment at 800°C for 3-6 hrs

After the eggshell was treated at 800°C, decomposition peak of organic substances was disappeared. It means that organic substances were

completely removed by heat treatment at 800°C for 3 and up to 6 hrs. These results were in a good agreement with an appearance of the treated eggshell that was totally white after the treatment for 3-6 hrs. In addition, the decomposition observed in a range of 375-460°C was due to dehydration of calcium hydroxide. It was reported that upon heated between 440 and 580°C, calcium hydroxide would be dissociated and gave rise to calcium oxide and water [14]. The final thermal decomposition of the heat-treated eggshell beginning around 460°C was derived from the decomposition of calcium carbonate left in the treated eggshell [15].

The particle size and size distribution of heat-treated eggshell from the treatment for 3-6 hrs are shown in Table 2. The diameter range of those treated eggshell were in a range of 0.055-364.6 µm. Their mean particle size, $d(v, 0.5)$, were 8.66-11.42 µm. The results showed that the treatment times had no significant effect on the particle size and size distribution of the treated eggshell.

Table 2: Particle diameter of eggshell after the heat treatment at 800°C for 3-6 hrs

Time	Diameter range (µm)	Particle size distribution (by volume)			
		$d(v,0.1)$ (µm)	$d(v,0.5)$ (µm)	$d(v,0.9)$ (µm)	span
3h	0.055-364.6	0.40	8.66	37.74	4.32
4h	0.055-364.6	0.40	11.42	40.33	3.51
5h	0.055-364.6	0.38	8.72	40.08	4.58
6h	0.055-353.3	0.37	10.04	38.25	3.79

Conclusions

The raw eggshell comprises calcium carbonate around 95 wt%. Calcium carbonate was obtained when the ES was treated at 800°C for 1-2 hr. Calcium carbonate content decreased with increasing treatment times. After the raw eggshell was treated for 5-6 hrs, calcium oxide was the main component of the heat-treated eggshell. The heat-treated eggshell composed mainly calcium about 66 wt%. The others were SiO₂, Mg, P, K, Al and S. The mean particle size of the heat-treated eggshell was approximately 8.66-11.42 µm.

Acknowledgement

The authors would like to thank Suranaree University of Technology for financial support and the SUT Farm for supplying raw eggshell.

References

[1] T.-M. Wu, J.P. Rodriguez, D.J. Fink, D.A. Carrino, J.Blackwell, A.I. Caplanmony, K.A. Khalil and A.H. Heuer, *Matrix. Biol.* **14** (1994), pp. 507-513.

[2] W.J. Stadelman In: W.J. Stadelman and O.J.Cotterill, Editors, *Egg Science and Technology*, Food Product Press, New York (1995), pp. 39-66.

[3] M.T. Hincke, J. Gautron, M. Panheleux, J.GarciaRuiz, M.D. McKee and Y. Nys, *Matrix. Biol.* **19** (2000), pp. 443-453.

[4] E.C.Y. Li-Chan, W.D. Powrie and S. Nakai In: W.J. Stadelman and O.J.Cotterill, Editors, *Egg Science and Technology*, Food Product Press, New York (1995), pp. 105-175.

[5] A. Schaafsma, I. Pakan, G.J.H. Hofstede, F.A.J. Muskiet, E. Van Der Veer and P.J.F. De Vries, *Poult Sci.* **79** (2000), pp. 1833-1838.

[6] H. J. Park, S. W. Jeong, J. K. Yang, *J. Envi. Sci.* **19** (2007), pp. 1436-1441.

[7] F. S. Murakami and P. S. Silva, *Ciênc. Tecnol. Aliment. Campinas.* **3** (2007), pp. 658-662.

[8] A. Lazzeri, S.M. Zebarjad, M. Pracella, K. Cavalier and R. Rosa, *Polymer.* **46** (2005), pp. 827-844.

[9] M. Tanniru, R.D.K. Misra, K. Berbrand and D. Murphy, *Mater. Sci. Eng. A* **404** (2005), pp. 208-220.

[10] P. Toro, R. Quijada, M. Yazdani-Pedram and J.L. Arias, *Mater. Let.* **614** (2007), pp. 4347-4350.

[11] H. El-Didamony, K.A. Khalil and M.S. El-Attar, *Cem. Concr. Res.* **30** (2000), pp. 7-11.

[12] N.B. Singh and N.P. Singh, *J. Therm. Anal. Cal.* **89** (2007), pp. 159-162.

[13] M.N. Freire and J.N. Holanda, *Ceramica.* **52** (2006), pp. 240-244.

[14] T. Sinsiri, C. Jaturapitakkul and P. Chindaprasirt, *Influence of fly ash fineness on calcium hydroxide in blended cement paste*, Technology and Innovation for Sustainable Development Conf., Khon Kaen, Thailand, 2006, pp. 543-546.

[15] A.E.F.S. Almeida and E.P. Sichert, *Mater.Res.* **9** (2006), pp. 321-326.



Mechanical Properties of HDPE Filled with Eggshell Powder

*P. Pakdeechote, Y. Ruksakulpiwat, N. Suppakarn, and W. Sutapun**

School of Polymer Engineering, Institute of Engineering, Suranaree University of Technology, Nakhon Ratchasima 30000, Thailand

Center of Excellence for Petroleum, Petrochemicals, and Advanced Materials, Chulalongkorn University, Bangkok 10330, Thailand

wimonlak@sut.ac.th

Introduction

Chicken eggshell is classified as a natural biomaterial.¹ It is a waste material from food and hatchery industry. Nowadays, the eggshell waste is discarded by buried in a landfill. Actually, the discarded eggshell comprises a valuable calcium carbonate (CaCO_3) as high as 94 wt%.² From eggshell, calcium carbonate can be obtained by chemical or physical treatment.³ Calcium carbonate is popularly used as a filler for high density polyethylene (HDPE). It will be greatly beneficial if the eggshell can be employed, without any treatment, as filler for HDPE. In recent years, there was a study about incorporation of eggshell powder (ESP) into polypropylene (PP) composites.⁴ The result showed improvement of Young's modulus of PP composites with increasing ESP content. In this work, the utilization of eggshell powder as an alternative filler for HDPE was attempted. The mechanical properties of the filled HDPE were then compared to those of HDPE filled with traditional filler, calcium carbonate.

Materials and Methods

Chicken eggshell waste were collected from the SUT Farm, Suranaree University of Technology. Firstly, the chicken eggshell was washed with tap water, dried in an open air for 24 hr, and finally ground by a ball mill. The particle size of ESP was 0.055-364.6 with an average size of 17.26 μm . Calcium carbonate was obtained from Asia Pacific Specialty Chemicals Co.Ltd. Its particle size was 0.055-364.6 with an average diameter of 5.35 μm . High density polyethylene (EL-Lene H5814J) was purchased from SCG Chemicals Co.Ltd.

The ESP and CaCO_3 were dried in an oven at 140°C for 6 hr before mixing with HDPE in an internal mixer (Hakke Rheomix 600p). The contents of fillers were between 10 and 60 wt%. The mixing process was performed at 170°C under a rotor speed of 70 rpm and a mixing time of 15 min. After mixing, the filled HDPE were ground. The test specimens were subsequently prepared by an injection machine (Chuan Lih Fa, CLF 80T). The injection process was carried out with a melting temperature of 200°C, a screw speed of 104 rpm, an injection speed of 57 mm/s, a holding pressure of 960 kg/cm^2 and mold temperature of 25°C. Tensile, flexural and impact properties, and hardness of the filled HDPE were investigated

Results and Discussion

From Figure 1(a), it shows that the tensile strength of ESP- and CaCO_3 -filled HDPE was higher than that of HDPE. Noted that HDPE specimens were drawn at higher cross-head speed than the filled HDPE specimens were done (50 mm/min for HDPE and 10 mm/min for the filled HDPE). However, tensile strength of the filled HDPE was insignificantly changed with increasing the filler contents. Young's modulus of filled HDPE was significantly improved when ESP and CaCO_3 content were up to 30-60 wt%. The presence of ESP and CaCO_3 in HDPE matrix enhanced flexural strength and modulus of the filled HDPE as shown in Figure 1(b). On the other hand, impact strength of ESP-filled and CaCO_3 -filled HDPE decreased with increasing the filler content, as shown in Table 1. Nevertheless, the impact



strength of ESP-filled HDPE was higher than that of CaCO_3 -filled HDPE. In addition, the incorporation of ESP and CaCO_3 in HDPE matrix resulted in improvement of the hardness of HDPE, as shown in Table 1. Figure 1(a) -1(b) and Table 1 also show that addition of ESP affected tensile properties, flexural properties and hardness of the filled HDPE in the similar manner to a case when CaCO_3 was added. This implied that the interfacial property between ESP and HDPE matrix was not greatly different from that between CaCO_3 and HDPE.

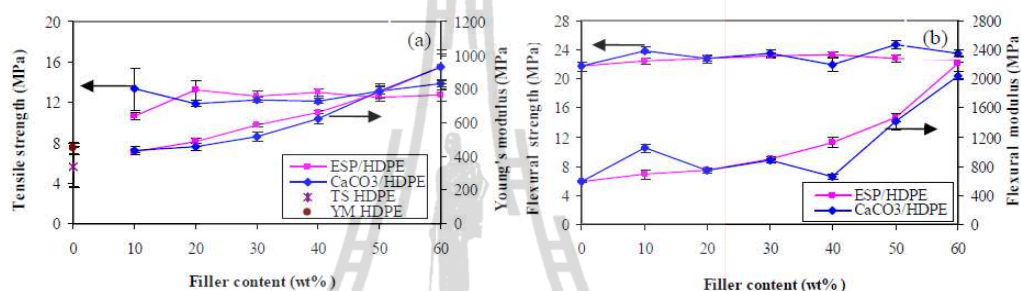


Figure 1: Plot of tensile strength and Young's modulus (a) and flexural strength and modulus (b) of ESP-filled HDPE and CaCO_3 -filled HDPE vs. filler contents.

Table 1: Impact strength and hardness of filled-HDPE.

Filler content (wt%)	Impact strength (J/m^2)		Hardness (shore D)	
	ESP/HDPE	CaCO_3 /HDPE	ESP/HDPE	CaCO_3 /HDPE
0	4162	4088	30	30
10	3655	3086	32	32
20	3597	3145	34	32
30	3720	3142	34	33
40	3854	2576	36	34
50	3165	2184	37	37
60	1603	1920	40	40

Conclusions

In a view of mechanical properties, eggshell powder has potential to be used as an filler for high density polyethylene. However, the effect of particle size and size distribution, and also an addition of a compatibilizer on mechanical and thermal properties of the ESP-filled HDPE have to be further studied. Their fracture surface has to be examined in order to reveal the distribution of the ESP in HDPE matrix.

Acknowledgement

The authors would like to thank Suranaree University of Technology for financial support and the SUT Farm for supplying chicken eggshell.

References

- Wu, T.-M.; Rodriguez, J.P.; Fink, D.J.; Carrino, D.A.; Blackwell, J.; Caplanmony, A.I.; Khalil, K.A.; Heuer, A.H. *Matrix. Biol.* **1994**, *14*, 507-513.
- Stadelman, W.J. In: Stadelman, W.J.; Cotterill, O.J., Editors, *Egg Science and Technology: Food Product Press: New York*, **1995**, 39-66.
- Sanmuang, S.; Ruksakulpiwat, Y.; Suppakarn, N.; Sutapun, W. *Adv. Mater. Res.* **2008**, *47-50*, 490-493.
- Toro, P.; Quijada, R.; Yazdani-Pedram, M.; Arias, J.L. *Mater. Let.* **2007**, *614*, 4347-4350.

Rheological, Mechanical and Morphological Properties of Eggshell Powder (ESP) Filled High Density Polyethylene (HDPE)

Panuwat Pakdeechote¹, Nitinat Suppakarn^{1,2}, Yupaporn Ruksakulpiwat^{1,2}, and Wimonlak Sutapun^{1,2*}

¹School of Polymer Engineering, Institute of Engineering, Suranaree University of Technology, Nakhon Ratchasima 30000

²Center of Excellence for Petroleum, Petrochemicals, and Advanced Materials, Chulalongkorn University, Bangkok 10330

*Corresponding author: Tel. (044) 224435, Fax. (044) 224605, Email: wimonlak@sut.ac.th

Abstract

The aim of this work was to investigate rheological, mechanical and morphological properties of eggshell powder (ESP) filled high density polyethylene (HDPE) in comparison to those of CaCO₃ filled HDPE. ESP and CaCO₃ were added at various contents, 10, 20, 30 and 40 wt%. It was found that the apparent shear viscosity of HDPE increased with increasing content of ESP and CaCO₃. The incorporation of ESP and CaCO₃ into HDPE matrix resulted in an improvement of tensile strength in the similar manner. However, a decreasing in impact strength of ESP filled HDPE was nearly the same to that of CaCO₃ filled HDPE. Also, two particle size ranges of ESP resulted in the same tensile and impact strength of filled HDPE. Thus, ESP could possibly be used as a filler for HDPE.

Keyword: Chicken Eggshell, Eggshell powder (ESP), ESP filled HDPE

1. Introduction

High density polyethylene (HDPE), semi-crystalline, is one of the most important commodity polymers widely used in packaging and transport applications such as food containers, pallets and tight-head pails owing to its superior stiffness and low permeability [1]. Calcium carbonate (CaCO₃) is one of the most

commonly used inorganic fillers in HDPE; many researchers have studied the mechanical properties of HDPE filled with CaCO₃ [2]. In fact, chicken eggshell has been reported that its major component as much as 94% is CaCO₃ [3]. However, eggshell is disposed in a landfill instead of making use of it. Therefore, the use of eggshell as a filler for HDPE may provide a great benefit in environmental concerns due to its renewable resource, reduction in energy consumed for waste disposal and reducing global warming effect.

Thus, the goal of this work was to study the use of eggshell powder as a filler for HDPE. The rheological, mechanical and morphological properties of ESP filled HDPE were investigated.

2. Experimental

2.1 Materials

Chicken eggshell waste was collected from the SUT Farm, Suranaree University of Technology. Firstly, the chicken eggshell was washed with tap water, dried in open air for 24 hr, ground by a ball mill and finally sieved into particle ranges of 0.70-112.8 μm (d(v, 0.5) of 16.23 μm) and 0.85-56.9 μm (d(v, 0.5) of 14.41 μm).

Calcium carbonate was kindly supplied from Sand and Soil Industry Co.Ltd. It was ground with ball mill

and sieved prior to mixing with HDPE. Its particle size was in a range of 0.64-124.4 μm with $d(v, 0.5)$ of 19.91 μm .

High density polyethylene (EL-Lene™ H5814J, Thai Polyethylene Co. Ltd) was purchased from SCG Chemicals Co.Ltd. Its melt flow index was 14 g/10 min (2.16 kg at 190°C).

2.2 Preparation of ESP and CaCO₃ filled HDPE

The ESP and CaCO₃ were dried in an oven over night at 70°C before mixing with HDPE. The mixing contents of ESP (0.70-112.8 μm) and CaCO₃ (0.64-124.4 μm) were 10, 20, 30 and 40 wt%. Besides, ESP with the particles range of 0.85-56.9 μm was mixed at 40 wt% content. The mixing process was performed in an internal mixer (Rheomix 600p, Hakke PolyLab System) at 170°C under a rotor speed of 70 rpm and a mixing time of 15 min. After mixing, the filled HDPE was ground using a plastic grinding machine. The test specimens were subsequently prepared by an injection machine (Chuan Lih Fa, CLF 80T). The injection process was carried out at a melting temperature of 190°C, a screw speed of 104 rpm, an injection speed of 57 mm/s, a holding pressure of 960 kg/cm² and a mold temperature of 25°C. Tensile and impact properties of the filled HDPE were further investigated.

2.3 Characterization of ESP and CaCO₃ filled HDPE

Rheological properties of filled HDPE were investigated using a capillary rheometer (Kayeness, D5052M) at a melting temperature of 190°C. The tensile properties were measured using a universal testing machine (Instron, 5565). The tensile test was performed at a crosshead speed of 10 mm/min with a fixed gauge length of 50 mm. Unnotched izod impact properties were evaluated on pendulum impact tester (Atlas, BPI). Morphologies of tensile specimens, fractured in liquid nitrogen, were investigated using scanning electron microscope (JEOL, JSM-6400). The fractured surface was coated with a thin layer of gold to make it electrically conductive.

3. Results and Discussion

The rheological behaviour of the ESP filled HDPE and CaCO₃ filled HDPE are shown in Figure 1(a) and Figure 1(b), respectively. The apparent shear viscosity of filled HDPE increased with increasing content of ESP and CaCO₃. This was attributed to the addition of rigid particles of CaCO₃.

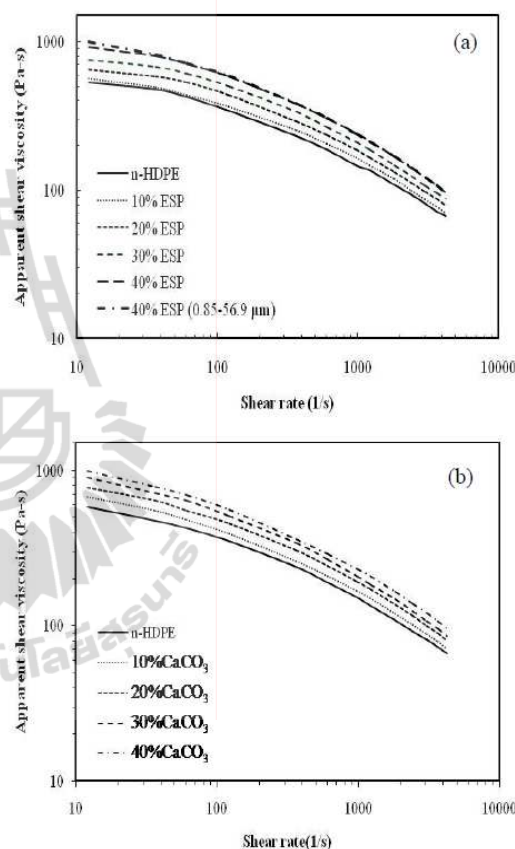


Figure 1. Plot of apparent shear viscosity vs. shear rate: ESP filled HDPE (a) and CaCO₃ filled HDPE (b)

Tensile strength and impact strength of HDPE filled with ESP and CaCO₃ is shown in Table 1. Tensile strength of HDPE was not obtained because it did not break within the instrument limit. Tensile strength of the filled HDPE slightly increased with increasing filler content. There was no significant difference in tensile strength of ESP and CaCO₃ filled

HDPE. Impact strength of the filled HDPE decreased with increasing filler content. Noted that HDPE filled with ESP with particles of 0.85-56.9 μm had the same tensile and impact strengths as that filled with ESP having particle range of 0.70-112.8 μm . The reduction of impact strength of the filled HDPE was due to the poor interfacial interaction between the polar filler surface and HDPE [2]. This corresponded well with SEM micrographs of ESP and CaCO_3 filled HDPE as shown in Figure 2. In addition, the impact strengths of ESP filled HDPE and CaCO_3 filled HDPE were almost the same.

Table 1 Tensile strength (TS) and impact strength (IS) of neat HDPE (n-HDPE) and filled HDPE

Content (wt%)	ESP filled HDPE		CaCO_3 filled HDPE	
	TS (MPa)	IS (kJ/m^2)	TS (MPa)	IS (kJ/m^2)
n-HDPE	-	>125	-	>125
10	12.9 \pm 0.1	>124	12.6 \pm 0.3	>124
20	12.9 \pm 0.1	38 \pm 3	14.3 \pm 0.2	46 \pm 2
30	14.1 \pm 0.8	23 \pm 2	14.3 \pm 0.6	25 \pm 2
40	14.0 \pm 0.6	13 \pm 2	13.4 \pm 0.3	15 \pm 1
40 (0.85-56.9 μm)	14.1 \pm 0.3	14 \pm 1	-	-

The fractured surface of ESP and CaCO_3 filled HDPE examined by SEM are shown in Figure 2. SEM micrographs obviously demonstrated the poor interfacial adhesion between ESP and HDPE as well as between CaCO_3 and HDPE.

4. Conclusions

Tensile strength of ESP and CaCO_3 filled HDPE slightly increased with increasing filler content. On the other hand, the addition of ESP and CaCO_3 resulted in a decrease of impact strength of the filled HDPE. There was no significant difference in tensile and impact strength of ESP and CaCO_3 filled HDPE. For this study, there was no effect of particle size of ESP on tensile and impact strengths. Therefore, ESP would possibly be an alternative filler for HDPE.

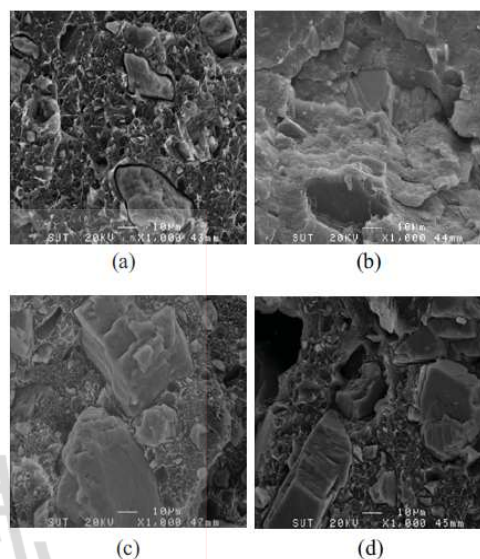


Figure 2. SEM micrographs (x1000) of cryo-fractured parts of filled HDPE: 20 wt% ESP (a); 20 wt% CaCO_3 (b); 40 wt% ESP (c); 40 wt% CaCO_3 (d)

5. Acknowledgement

The authors gratefully acknowledge Suranaree University of Technology for financial support and the SUT Farm for supplying chicken eggshell. The authors are very grateful to Sand and Soil Industry Co., Ltd. for providing calcium carbonate.

6. References

1. Peacock, A. J. *Handbook of polyethylene*, New York, Marcel Dekker: 534 (2000).
2. Rukchonlatee, S., Prasertwong, T. and Sangpakdee, T., "Effect of compatibilizer types on properties of CaCO_3 -filled high density polyethylene", *Suranaree Journal of Science and technology*, **9**: 253-260 (2002).
3. Stadelman, W.J., "Eggs and Egg Products", In: Francis, F.J. (ed.) *Encyclopedia of Food Science and Technology*, second ed. New York, John Wiley and Sons: 593-599 (2000).

BIOGRAPHY

Mr. Panuwat Pakdeechote was born on May 5, 1977 in Trang province, Thailand. He earned his Bachelor's Degree of Engineering (Chemical Engineering) from Suranaree University of Technology (SUT), Nakhon Ratchasima, in 2002. After graduation, he had worked at Sheico (Thailand) Co., Ltd., at MAXXIS International (Thailand) Co., Ltd., and at Extensive Research Polymers Co., Ltd., respectively. He continued his Master's degree in Polymer Engineering at School of Polymer Engineering, Institute of Engineering, Suranaree University of Technology. During his master degree study, he presented two poster presentations entitle: **“Preparation and characterization of heat-treated eggshell for HDPE composites: A preliminary study”** in the Pure and Applied Chemistry International Conference (PACCON2009) in Phitsanulok province, Thailand, **“Mechanical properties of HDPE filled with eggshell powder”** in the 11th Pacific Polymer Conference 2009 (PPC11) in Cairns, Australia. In addition, he has presented one oral presentation entitled of **“Rheological, mechanical and morphological properties of eggshell powder (ESP) filled high density polyethylene (HDPE)”** in the Sixth Thailand Materials Science and Technology Conference (MSAT-6) in Bangkok, Thailand. Moreover, he received a certificate of best paper award in material for environment session for the paper entitled **“Rheological, mechanical and morphological properties of eggshell powder (ESP) filled high density polyethylene (HDPE)”** from MSAT-6.